T.C. DOGUS UNIVERSITY

INSTITUTE OF SCIENCE AND TECHNOLOGY

ANALYSIS AND DESIGN OF A 3.5 GHz PATCH ANTENNA FOR WiMAX APPLICATIONS

M. Sc. Thesis

FUNDA CIRIK

201192002

Thesis Supervisor: Assoc. Prof. Bahadır YILDIRIM

Istanbul , January 2014

FOREWORD

I would like to express my deepest sincere gratitude to my advisor, Assoc. Prof. Bahadır Süleyman YILDIRIM, for his wide knowledge and efforts. His personal guidance have provided a great basis during this hard period. He supported from the initial to the final level enabled me to develop every parts of this thesis.

I also thank to my family for always having their belief in me, motivating and supporting me throughout my academic career.

Finally, I would like to thank to my very special thanks Halil Acıkaya for his endless love and patience. Without his encouragement and endurance, this work would not have been possible.

Istanbul, January, 2014 FUNDA CIRIK

ABSTRACT

In 1953, the microstrip antenna approach was firstly proposed by Deschamps. However, two years later, Gutton and Bassinot received the first microstrip antenna patent in France. After twenty years from this patent, the first microstrip antenna was built by Munson, and Howell, and they published a paper announcing their design and realization of the first microstrip antenna, which was first proposed by Deschamps. With this realization, the microstrip antenna and its applications gained widespread importance.

In recent years, the study of microstrip patch-type antennas has gained good momentum. Compared to conventional antennas, microstrip antennas are low-cost, low-profile, conformal, easier to fabricate, and have smaller dimensions. Because of these advantages, microstrip antennas attract many researchers in the field of wireless communications. Furthermore, the microstrip antennas can provide dual polarizations, multiband operation, feedline flexibility, and directional radiation patterns.

This thesis presents a patch-type microstrip WiMAX antenna operating at 3.5 GHz with a parasitic radiator and a raised ground plane. This high gain antenna has been designed through extensive 3-D electromagnetic simulations. The patch itself provides a realized gain of about 3.5 dBi at 3.5 GHz. When a parasitic radiator, side walls and upper dielectric layer are placed on top of the patch, the gain increases from 3.6 dBi to about 8.8 dBi that's about an improvement of 5.2 dB without the need of an amplifier.

ÖZET

1953'de, ilk olarak Deschamps, mikroşerit anten yaklaşımını ortaya koydu. Fakat Deschamps'tan 2 yıl sonra Fransa'da bilim adamları Gutton ve Bassinot, mikroşerit anten patentini aldılar. Patentin alınmasından 20 yıl sonra ise ilk mikroşerit anten Munson, ve Howell tarafından üretildi. Bu yazarlar daha sonra fikir olarak Deschamps tarafından ortaya konulan, üretilen bu ilk mikroşerit antenin tasarımını ve gerçeklemesini anlatan bir çalışma yayımladılar. Bu gerçeklemenin ardından mikroşerit anten uygulamaları daha da önem kazanmaya başladı.

İlerleyen yıllarda, mikroşerit yama anten çalışmaları iyi bir ivme gösterdi. Mikroşerit anten yapısı alışılagelmiş antenlere kıyasla, düşük maliyet, düşük profil, daha küçük boyutlar, kolay fabrikasyon aşaması ve uyumluluk özelliklerine sahipti. Getirdiği bu avantajlar dolayısıyla bir çok araştırmacıyı kablosuz haberleşme alanında çalışmalar yapmaya sevk etmiştir. Bunun yanında mikroşerit yama anten, çift kutuplanma, çok bantlı frekanslarda çalışabilme yeteneği, besleme kolaylığı ve çok yönlü anten örüntüsü gibi kolaylıklar da sağlamaktadır.

Bu tezde 3.5 GHz frekansında çalışan parazitik radyatörlü ve yükseltilmiş yer düzeyi üzerinde bulunan yama tipli mikroşerit WIMAX anten yapısı incelenmiştir. Bu yüksek kazançlı anten yapısı, kapsamlı üç boyutlu elektromanyetik simülasyonlar aracılığıyla tasarlanmıştır. Yama yapısı ile 3.5 GHz frekansında yaklaşık 3.5 dBi'lik bir kazanç elde edilmiştir. Yamanın üzerine eklenen parazitik radyatör, yan duvarlar ve üst dielektrik kapak ile 3.6 dBi'dan yaklaşık olarak 8.8 dBi kazanca ulaşılmıştır. Bu demektir ki; herhangi bir yükseltece ihtiyaç duyulmadan 5.2 dB' lik bir kazanç artımı elde edilmiştir.

CONTENTS

LIST OF FIGURES

LIST OF TABLES

ABBREVIATIONS

WiMAX	Worldwide Interoperability for Microwave Access
IEEE	Institute of Electrical and Electronics Engineers
Eq.	Equation
Fig.	Figure
3D	Three Dimensional
Hz	Hertz
GHz	Gigahertz
MHz	Megahertz
ε_r	Relative electrical permittivity
UWB	Ultra-Wideband
SMA	Sub-Miniature Version A
RF	Radio Frequency
PEC	Perfect Electric Conductors (PEC)
VNA	Vector Network Analyzer
FR4	Flame Resistant 4

1. INTRODUCTION

WiMAX (Worldwide Interoperability for Microwave Access) is a wireless communication standard created by the companies Intel and Alvarion in 2002 and approved by the IEEE (Institute of Electrical and Electronics Engineers) under the name IEEE-802.16. The IEEE 802.16 WiMAX standard allows data transmission using multiple broadband frequency ranges [1]. The aim of WiMAX is to supply, high-speed data rates and internet access in a coverage range several kilometres in radius. Different bands are available for WiMAX applications in different parts of the world. There is no uniform global licensed spectrum for WiMAX, however the WiMAX Forum has published three licensed spectrum profiles: the low band 2.3-2.69 GHz, the middle band 3.2-3.8 GHz and the upper band 5.2-5.8 GHz. Different WiMAX frequencies are used in different countries as outlined in Table 1. As can be seen, the frequencies commonly used are 3.5 and 5.8 GHz for 802.16d and 2.3, 2.5 and 3.5 GHz for 802.16e but the exact use depends upon the countries [2].

One of the significant advantages of advanced wireless systems such as WiMAX is the link spectral efficiency. For example, IEEE 802.16.d WiMAX has a spectral efficiency of 4.8 (bit/s)/Hertz. IEEE 802.11.n Wi-Fi and IEEE 802.11.n a/g Wi-Fi link spectral efficiencies are maximum 3.6 (bit/s)/Hertz and 2.7(bit/s)/Hertz, respectively. Wi-Fi works at 2.7 bps/Hz and can peak up to 54 Mbps in a 20 MHz channel. But WiMAX works at about 5 bps/Hz and can peak up to 100 Mbps in a 20 MHz channel [3].

The WiMAX physical layer is based on orthogonal frequency division multiplexing (OFDM), which enables high-speed data, video, and multimedia communications and besides WiMAX is used by a variety of commercial broadband systems, including DSL, Wi-Fi, and Digital Video Broadcast-Handheld (DVB-H). WiMAX supports a variety of modulation types and coding schemes. These are BPSK, QPSK, 16-QAM, and 64-QAM. Depending on channel conditions, WiMAX allows for the scheme to change on a burst-by-burst basis per link [4]. The mobile can provide the base station with feedback on the downlink channel quality using the channel quality feedback indicator.

Table 1.1 Current major spectrum allocations for WiMAX worldwide [5].

Region	Frequency Bands (GHz)	Comments
Canada	2.3, 2.5 3.5 5.8	
USA	2.3, 2.5 5.8	
Central and South America	2.5 3.5 5.8	The spectrum is very fragmented and allocations vary from country to country
Europe	2.5 3.5 5.8	The 2.5 GHz allocation is currently allocated to IMT 2000. 5.8 GHz is also not available in most European countries.
Middle East and Africa	3.5 5.8	The spectrum is very fragmented.
Russia	2.5 3.5 5.8	The 2.5 GHz allocation is currently allocated to IMT 2000.
Asia Pacific (China, India, Australia, etc)	2.3, 2.5 3.3, 3.5 5.8	The spectrum is very fragmented and varies between countries.

In this thesis, a microstrip patch-type WiMAX antenna with a parasitic radiator, two metallic side walls and an upper dielectric layer have been analyzed, designed, and fabricated for 3400 – 3600 MHz WiMAX applications. This band is also used in Europe and primarily allocated to radiolocation (radar and navigation) services.

The parasitic radiator is placed on top of the microstrip patch antenna to increase the antenna gain. It is observed that the gain increase is maximum when the distance between the parasitic patch and the main patch is about 15 mm. Further improvement of gain has been achieved by adding metallic side walls that are shorted to RF ground. Therefore, a total gain improvement of about 5.2 dB has been achieved without the need of an RF amplifier. The patch antenna has been built on low-cost and easily available 1.6 mm thick

FR4-type substrate with a relative permittivity of 4.4 and a loss tangent of 0.02. RF ground plane has an area of 100×100 mm^2.

The patch antenna is driven by a 50-Ω microstrip line. Impedance matching between the driving port (SMA connected port) and the antenna has been realized using a quarter-wave long transformer. Antenna VSWR is about 1.2 dB at the operating frequency. A foam-type material whose relative permittivity is very close to that of the air ($\varepsilon_r \cong 1.0006$ at standard temperature and pressure as a temperature of 273.15 K (0 °C, 32 °F) and an absolute pressure of 100 kPa (14.504psi, 0.987 atm, 1 bar), for 0.9 MHz) [6] has been placed between the patch antenna and the parasitic radiator as mechanical support. Antenna analysis has been carried out using HFSS [7] and SEMCAD [8].

The interest in microstrip antennas dates back to the 1950's, but it was not until the 1970's that greater emphasis was given to develop this technology. In recent years, microstrip antennas have been one of the most innovative topics in antenna theory and design. The basic idea came from utilizing printed circuit technology for the circuit components, transmission lines and the radiating elements of an electronic system. Compared to conventional antennas, microstrip antennas are low-cost, low-profile, conformal, and easy to fabricate. They have small volumes, provide good performance and can easily be integrated with the RF/microwave circuitry on the same board. Furthermore, the microstrip antennas can provide dual polarizations, multiband operation, feedline flexibility, and directional radiation patterns. Because of these advantages, microstrip antennas attract many researchers in the field of wireless communications [9].

In 1953, the microstrip antenna approach was firstly proposed by Deschamps [10]. However, two years later, in 1955, Gutton and Bassinot [11] received the first microstrip antenna patent in France. After nearly twenty years from this patent, first microstrip antennas were built physically by Munson [12], [13], [14] and Howell [15], and they published a paper entitled "Single Slot Cavity Antennas Assembly" announcing their design and realization of the first microstrip antenna. In addition, Bahl and Bhartia [16], [17] and James, Hall and Wood [18], [19] published some research articles and boks about the development of the microstrip antenna theory. In 1979, the first international meeting

about practical design, configuration and theoretical models of microstrip antennas was organized in New Mexico State University under the sponsorship of USA Military Research Office and New Mexico State University's Physical Laboratory [20]. With these investigations and realizations, the microstrip antenna and its applications gained widespread importance. In later years, various authors all over the world proposed microstrip patch antennas.

It is mentioned in [21] that the gain of a conventional microstrip patch antenna can be increased by about 3 dB by placing a rectangular loop shaped parasitic radiator which is placed at a specific distance away from the patch antenna surface. The antenna developed in this thesis was inspired by [21]. However, in this work the antenna operates at 3.5 GHz, the parasitic element that increases the gain is a copper plate instead of a rectangular loop shaped element, and two metallic side walls that are shorted to RF ground. In addition, an upper dielectric layer has been placed to protect the antenna.

Another work about the patch antenna is presented [22] in crisscross shape operating at 3.5 GHz. To design a broad band antenna, a shorting pin is embedded in each arm of the crisscross and two triangles are cut out from the end of each arm. The shorting pin also helps the reduction of resonant frequency. The measured S11 of this antenna is less than -15 dB when the operation frequency band is in the range of 3.4 GHz to 3.6 GHz.

2. ANTENNA DESIGN PARAMETERS

An antenna is a device for radiating and receiving electromagnetic waves. By transmitting a signal into radio waves the antenna transforms electric current into electromagnetic waves and vice versa by receiving. A transmitting antenna is used to transport electromagnetic energy from a transmitting source to a receiver. A receiving antenna is used to capture a part of the incident electromagnetic energy from the transmitting antenna and transport the received power to a receiver. Moreover an antenna has a transitional structure between free-space and a guiding device (e.g. waveguide, transmission line) [9].

The IEEE defines of an antenna as " That part of a transmitting or receiving system that is designed to radiate or receive electromagnetic waves " [23].

Antenna parameters that are used in the analysis and design of 3.5 GHz WiMAX patch antenna are as follows:

- Input impedance and return loss
- Bandwidth
- Radiation pattern and beamwidth
- Radiation intensity and directivity
- Efficiency
- Gain and realized gain

The basis for electromagnetic radiation from an antenna is mainly related to time-varying electric and magnetic fields. To create time-varying fields, conducting wires must be curved, bent, discontinuous, terminated or truncated so that the velocity of charges are not constant. In addition, the source should be time-varying. Radiation will not occur even if charges are moving with uniform velocity along a straight wire. If the charges are accelerating or decelarating, or oscillating with time, radiation will take place [25].

2.1 Near and Far Field Regions

The power at the input terminals of an antenna is distributed as the power dissipated by the antenna, power stored in the near field of the antenna, and the radiated power in the far field of the antenna. Thus, the definition of near and far field of an antenna is important. There are three regions around the antenna. These are reactive near-field region, radiating near field region, and the far field region [9].

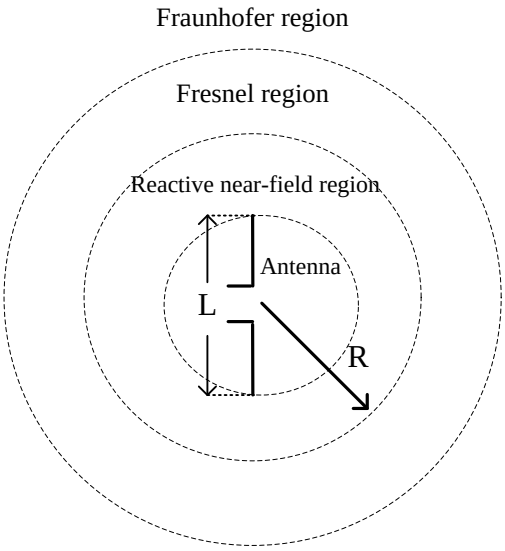

Figure 2.1 Antenna field regions.

- In reactive near field region the reactive energy oscillates towards and away from the antenna. In this region

$$R \leq 0.62\sqrt{D^3/\lambda} \tag{2.1}$$

where R is the distance from the antenna surface, D is the largest dimension of the antenna, and λ is the wavelength.

- Radiating near field region, named as Fresnel region, is located between the reactive near field region and the far field region. In this region

$$0.62\sqrt{D^3/\lambda} \leq R \leq 2\,D^2/\lambda \tag{2.2}$$

- In the far field region, also called as Fraunhofer region, the only fields are the radiated fields.

$$R \geq \frac{2D^2}{\lambda} \tag{2.3}$$

2.2 Input Impedance, Return Loss

The impedance presented by an antenna at its terminals is defined as the ratio of the voltage to the current (in frequency domain) at the antenna terminals. The mathematical formula of input impedance at the antenna terminals is defined as

$$Z_{in} = R_{in} + jX_{in} \tag{2.4}$$

Z_{in}= Antenna impedance (Ω)
R_{in}= Antenna resistance (Ω)
X_{in}= Antenna reactance (Ω)

The power stored in the near field of an antenna is represented in the imaginary part of the input impedance which is X_{in}. There are two components, R_r and R_L in the resistive part of R_{in} . R_r and R_L are referred as radiation and loss resistances, respectively.

The Return Loss (RL) is a parameter of the antenna which defines the amount of power that is " lost " to the load and does not return as a reflection. When the transmitter and antenna impedances do not match, waves are reflected leading to the formation of standing waves [9]. So the Return Loss indicates how well the matching between the transmitter and antenna is, and it's expressed as

$$RL = -20log_{10}|\Gamma| \tag{2.5}$$

For a perfect matching between the transmitter and the antenna, Γ = 0 and $RL = \infty$. This means no power would be reflected back. For full reflection Γ = 1 and $RL = 0$ dB.

2.3 Bandwidth

An antenna bandwith is defined as "the range of usable frequencies within which the performance of the antenna, with respect to some characteristic, conforms to a specified standard". The bandwidth can be the range of frequencies on either side of the center frequency where the antenna characteristics like input impedance, radiation pattern, beamwidth, polarization, side lobe level or gain, are close to those values which have been obtained at the center frequency. The bandwidth of a broadband antenna can be defined as the ratio of the upper to lower frequencies of acceptable operation. The bandwidth of a narrowband antenna can be defined as the percentage of the frequency difference over the center frequency [23]. The bandwith equation can be written as

$$BW_{broadband} = \frac{f_H}{f_L} \tag{2.6}$$

$$BW_{narrowband}(\%) = [\frac{f_H - f_L}{f_C}] \times 100 \tag{2.7}$$

where

f_H = upper frequency
f_L = lower frequency
f_C = center frequency

Impedance bandwidth is the frequency range where in the structure has a usable bandwidth compared to a certain impedance, usually 50-Ω. The impedance bandwidth depends on a large number of parameters related to the patch antenna element itself (e.g., quality factor) and the type of feed used. The bandwidth is typically limited to a few percent. This is the major disadvantage of basic patch antennas.

Directivity/gain bandwidth is the frequency range where in the antenna meets a certain directivity/gain requirement (e.g., 1 dB gain flatness).

2.4 Radiation Pattern and Beamwidth

Antenna radiation pattern is defined as "a mathematical function or a graphical representation of the radiation properties of the antenna as a function of space coordinates". In most cases, the radiation pattern is determined in the far-field region and is represented as a function of directional coordinates." In other words, radiation properties of the antenna are represented in the radiation pattern as a function of space coordinates. Radiation intensity, field strength, phase or polarizations are defined as radiation properties [23]. The spherical coordinate system which is used for antenna radiation pattern calculations is shown in Figure 2.2.

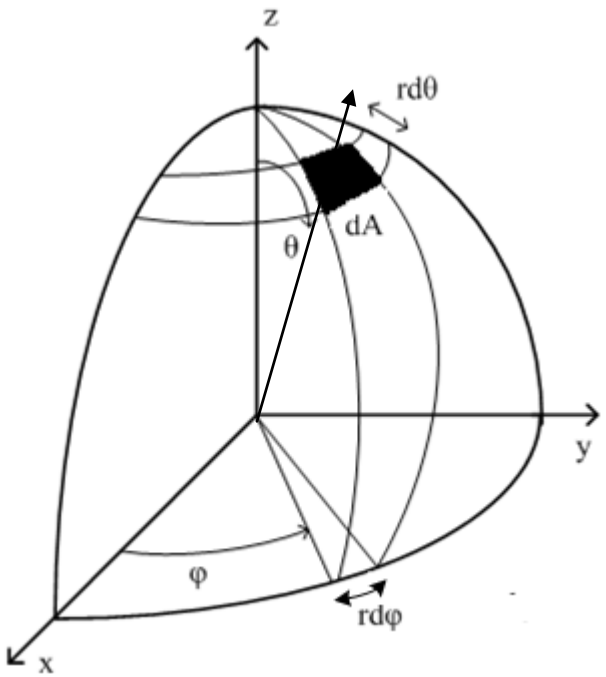

Figure 2.2 Spherical coordinate system.

Radiation patterns are conveniently represented in spherical coordinates, and expressed as E field pattern $E(\theta, \varphi)$ or power pattern $P(\theta, \varphi)$. The differential surface element dA is defined as

$$dA = r^2 \sin\theta d\theta d\varphi \tag{2.8}$$

The angles φ and θ are defined as azimuth and elevation angles, respectively. There are three types of radiation patterns:

- Isotropic pattern produced by an isotropic source. This type of pattern has equal radiation in all directions.
- Directional pattern produced by a directional antenna which radiates (or receives) more power in some direction than others.
- Omnidirectional pattern which is a special form of directional pattern. This type of pattern is non-directional in azimuth plane and directional in elevation plane [3].

Another important aspect of the radiation pattern is the beamwidth. The beamwidth of the antenna is also used to describe the resolution capability of an antenna to distinguish between two adjacent radiating sources. There are two beamwidth definitions. These are Half Power Beamwidth (HPBW) and First Null Beamwidth (FNBW), as shown in Figure 2.3 and Figure 2.4.

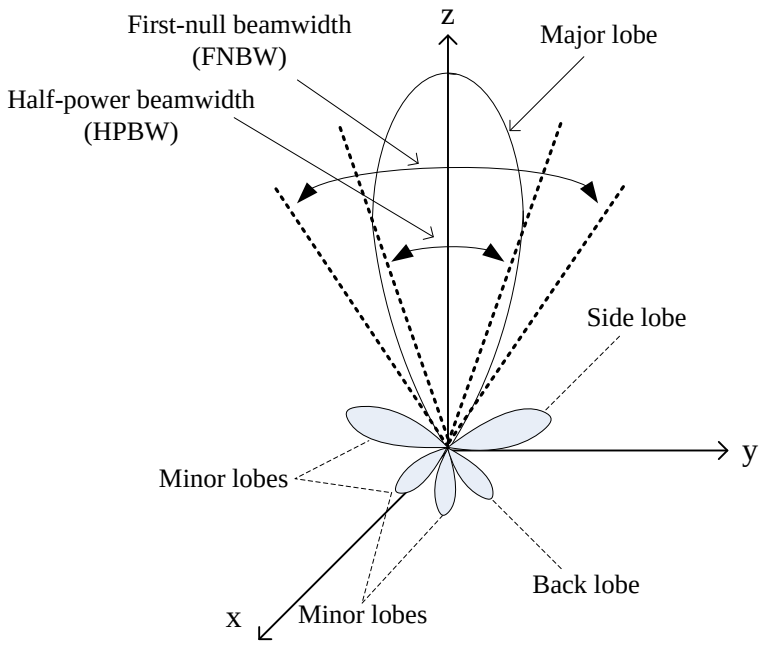

Figure 2.3 Radiation lobes and beamwidths of an antenna.

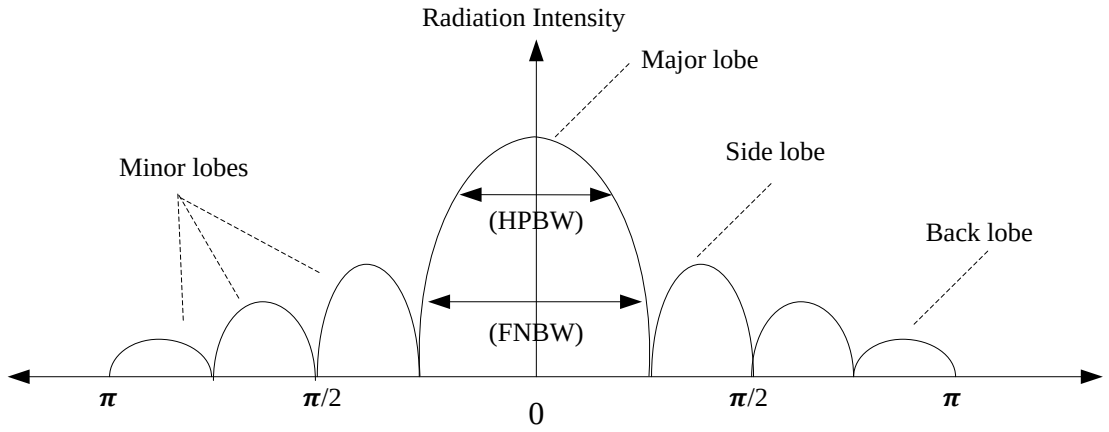

Figure 2.4 Linear plot of power pattern, its lobes, and beamwidths.

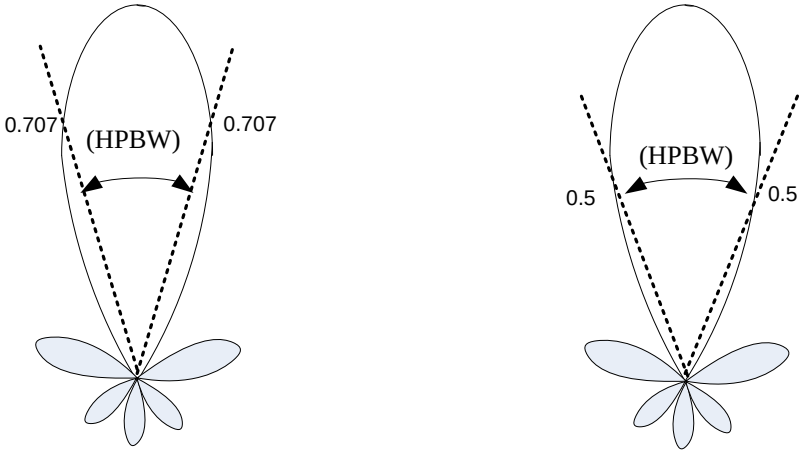

Figure 2.5 Field and power patterns in linear scale.

2.5 Radiation Intensity and Directivity

Radiation intensity is defined as "the power radiated from an antenna per unit solid angle". The radiation intensity is a far-field parameter, and it is obtained by simply multiplying the radiation density by the square of the distance [26]. In mathematical form

$$U(\theta, \varphi) = r^2 W_{rad} \tag{2.9}$$

where

$U(\theta, \varphi)$ = radiation intensity (W/unit solid angle)
W_{rad} = radiation density (W/m^2)

The directivity of an antenna is defined as "the ratio of the radiation intensity in a given direction from an antenna to the radiation intensity averaged over all directions". Directivity of an antenna is a measure of how directive an individual antenna is relative to an isotropic antenna radiating the same power. The units of directivity is dBi. The average radiation intensity is defined as the total power radiated by an antenna divided by 4π. Therefore directivity of an antenna can be expressed as

$$D(\theta, \varphi) = \frac{U(\theta, \varphi)}{U_0} = \frac{4\pi U(\theta, \varphi)}{P_{rad}} \tag{2.10}$$

If direction is not specified, maximum directivity is implied and the direction of maximum radiation intensity is taken to calculate the maximum directivity.

$$D_{max} = D_0 = \frac{U\big|_{max}}{U_0} = \frac{U_{max}}{U_0} = \frac{4\pi U_{max}}{P_{rad}} \tag{2.11}$$

where

D = directivity (dimensionless)

D_0 = maximum directivity (dimensionless)

$U(\theta, \varphi)$ = radiation intensity (W/unit solid angle)

U_{max} = maximum radiation intensity (W/unit solid angle)

U_0 = radiation intensity of isotropic source (W/unit solid angle)

P_{rad} = total radiated power (W)

2.6 Efficiency

The total antenna efficiency e_0 is a measure of the amount of radiated by an antenna when it's driven by a specific input power [9]. Total antenna efficiency e_0 is a combination of three efficiencies:

$$e_0 = e_r\, e_c\, e_d \tag{2.12}$$

$e_r =$ reflection efficiency

$e_c =$ conduction efficiency

$e_d =$ dielectric efficiency

The conduction and dielectric efficiencies can be written as a single term

$$e_{cd} = e_c\, e_d \tag{2.13}$$

where e_{cd} is the antenna radiation efficiency due to conductor and dielectric losses. Reflection efficiency can be written as

$$e_r = 1 - |\Gamma^2| \tag{2.14}$$

The total antenna efficiency e_0 can be written as

$$e_0 = e_{cd}(1 - |\Gamma^2|) \tag{2.15}$$

Where Γ is the voltage reflection coefficient at the input terminals of the antenna and it's expressed as

$$\Gamma = \frac{Z_{in} - Z_0}{Z_{in} + Z_0} \tag{2.16}$$

Z_{in} = antenna input impedance (Ω)
Z_0 = characteristic impedance of the transmission line (Ω)

Efficiency bandwidth is the frequency range where in the antenna has reasonable (application dependent) radiation (or total) efficiency.

2.7 Gain and Realized Gain

Antenna gain is defined as antenna directivity times a factor representing the radiation efficiency which is defined as the ratio of the radiated power (P_r) to the input power (P_i). Antenna gain can also be specified using the total efficiency instead of the radiation efficiency [9]. Gain is a measure of the ability of an antenna to direct the input power into radiation in a particular direction and is measured at the peak radiation intensity.

$$\text{Gain} = 4\pi \frac{radiation\ intensity}{total\ input\ accepted\ power} \tag{2.17}$$

$$G = \frac{4\pi U(\theta, \varphi)}{P_{in}} \tag{2.18}$$

Total radiated power (P_{rad}) is related to the total input power (P_{in}) by

$$P_{rad} = e_{cd} P_{in} \tag{2.19}$$

$$Gain = G = e_{cd} \frac{4\pi U(\theta, \varphi)}{P_{rad}} \tag{2.20}$$

The maximum value of gain is related to directivity as follows

$$Gain = G(\theta, \varphi) = e_{cd} D(\theta, \varphi) \tag{2.21}$$

while

$$P_{rad} = e_{cd} P_{in} \tag{2.22}$$

takes into account the loss of the antenna element itself, it does not take into account the loss when the antenna element is connected to a transmission line, shown in Figure 2.7. This loss is usually referred to as reflection (mismatch) loss, and it is taken into account by introducing the reflection (mismatch) efficiency (from equation 2.14) e_r which is related to the reflection coefficient. Thus we can introduce an absolute gain G_{abs} (also referred as realized gain) that takes into account the reflection/mismatch, and it can be written as

$$G_{abs}(\theta, \varphi) = e_r G(\theta, \varphi) \tag{2.23}$$

$$G_{abs}(\theta, \varphi) = (1 - |\ \Gamma^2|\ ) G(\theta, \varphi) \tag{2.24}$$

$$G_{abs}(\theta, \varphi) = e_r e_{cd} D(\theta, \varphi) = e_0\ D(\theta, \varphi) \tag{2.25}$$

If the antenna is matched to the transmission line, that is, the antenna input impedance Z_{in} is equal to the characteristic impedance Z_0 of the line ($|\Gamma| = 0$), then the two gains are equal $G_{abs} = G$. In this thesis, the absolute gain will be referred as the realized gain.

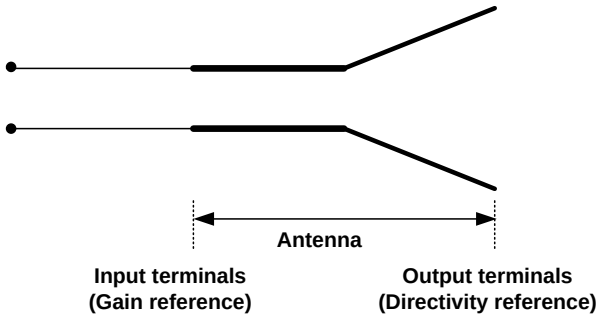

Figure 2.6 Antenna reference terminals.

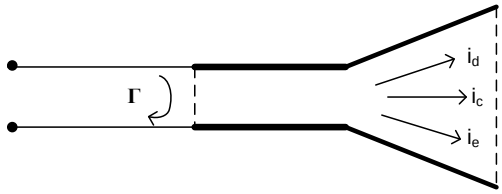

Figure 2.7 Antenna reference terminals and losses.

2.8 Simulation Tools

A large number of electromagnetic (EM) simulation software packages are available for use in antenna design. In this project, four software packages have been used. The patch antenna is simulated using Ansoft's High Frequency Structure Simulator (HFSS) based on finite-element method [27]. HFSS calculates electromagnetic fields at each frequency point. The patch antenna is also simulated with SEMCAD to verify HFSS simulations. SEMCAD is based on a finite-difference time-domain technique and a Gaussian pulse is used to excite the computational domain [8]. Frequency domain electric and magnetic fields are obtained by fast Fourier transforming the transient data. In some applications such as the analysis of wide band devices FDTD based simulators can be advantageous. Ansoft Designer is used to calculate the width and the length of the microstrip lines. Moreover Smith Software is used for the impedance matching of the antenna.

3. MICROSTRIP ANTENNA DESIGN

3.1 Introduction

A microstrip patch antenna is one of the most useful antennas at microwave frequencies ($f > 1$ GHz). As shown in Figure 3.1, the basic configuration of a microstrip antenna is a metal radiating patch on one side of a dielectric substrate which has a ground plane on the other side of the substrate. This configuration is also called as the "patch antenna". The metallic patch is made of conducting material such as copper or gold and it is fed with either a coaxial line through the bottom of the substrate, or by a microstrip line. The antenna patch can have a variety of shapes, but rectangular and circular shapes are widely used [28].

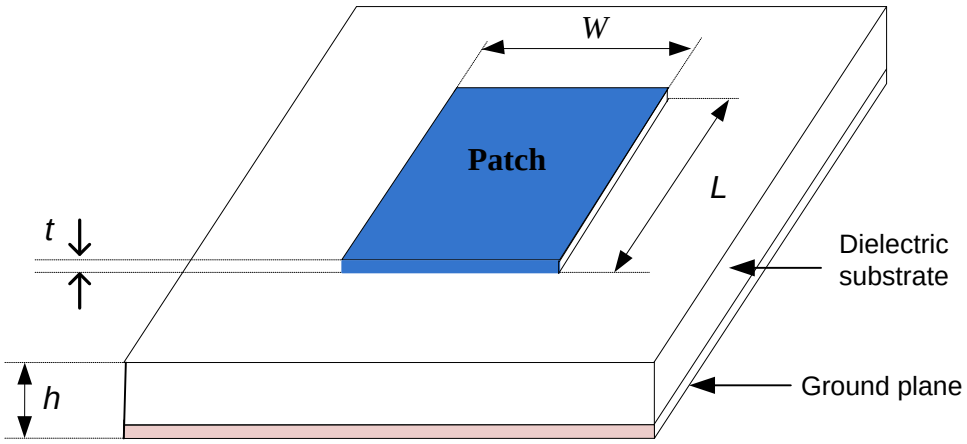

Figure 3.1 Structure of a microstrip patch antenna.

As can be seen in Figure 3.1, L is the resonant dimension. The patch width W is usually chosen to be larger than L to get a higher bandwidth. However, usually $W < 2\,L$ because of geometry constraints and $W = 1.5\,L$ is typical. Some general properties of the patch antenna are listed as follows.

- The bandwidth is directly proportional to substrate thickness h. If h is greater than about $0.05\,\lambda_0$ where λ_0 is the free-space wavelength, the probe inductance becomes large enough and matching becomes difficult.
- The bandwidth is inversely proportional to ε_r .
- The bandwidth is directly proportional to width W.
- The directivity is fairly insensitive to substrate thickness.

The length of the patch antenna is slightly less than $\lambda/2$. When the length is equal to $\lambda/2$, the antenna is said to be at resonance.

3.2 Advantages and Disadvantages of a Microstrip Patch Antenna

Microstrip patch antennas are widely used in wireless applications owing to their low-profiles. Patch antennas are usually employed in GPS receivers, speed control radars, closed circuit video systems, radio altimeters and biomedical systems. Also they are extremely suitable for embedded antennas in handheld wireless devices such as cellular phones. Patch antennas are often used as telemetry and communication antennas on missiles, since they can be very thin and have conformal structures. Another area is satellite communication [26].

The microstrip patch antenna has advantages as well as disadvantages. The advantages of patch antennas have been discussed in [26].

Microstrip antenna can be fabricated using (printed circuit) photolithographic techniques at low cost. They can even be made conformable, and lightweight. They can be fed by coaxial cables, microstrip lines, etc. Another interesting feature is that microstrip antennas can be easily used in an array or microwave integrated circuits (MICs). They can support both, linear as well as circular polarization, and capable of multiband operation. They are mechanically robust when mounted on rigid surfaces.

Microstrip patch antennas have some disadvantages as compared to conventional antennas. Some of their major disadvantages have been discussed by [26] and Garg et al [17]. These

advantages can be listed as follows. Microstrip antennas usually have narrow bandwidths and low efficiencies due to conductor and dielectric losses, and surface-wave loss due to surface wave excitation. Conductor and dielectric losses become more severe for thinner substrates. A single-patch microstrip antenna with a thin substrate (thickness less than 0.02 free-space wavelength) generally has a narrow bandwidth of less than 5%. Also surface-wave losses become more severe for thicker substrates. Another disadvantage is lower power handling capacity (can be overcome by using an array configuration for the elements) due to the small separation between the radiating patch and its ground plane. Generally, a few tens of watts of average power or less can be handled safely [9].

3.3 Q Factor (Quality Factor)

The antenna quality factor (Q) of microstrip patch antennas is usually very high. A large Q corresponds to narrow bandwidth and low efficiency [9]. Q can be reduced by increasing the thickness of the dielectric substrate. But when the thickness increases, an increasing part of the total power delivered by the source goes into surface waves which results in unwanted power loss. The equation of Q is given by:

$$Q = 2\pi \frac{stored\ energy}{dissipated\ power} \tag{3.1}$$

3. 4 Feeding Methods

Microstrip patch antennas can be fed by a variety of methods. These are contacting and non-contacting methods. In the contacting method, the RF power is fed directly to the radiating patch using a connecting element such as a microstrip line or a coaxial cable. In the non-contacting scheme, such as aperture or proximity coupling, electromagnetic field coupling is done to transfer power between a microstrip line and a radiating patch [24]. In this design, microstrip line feed method is used.

As shown in the Figure 3.2 the feed line is directly connected to the patch antenna. The width of the microstrip feed line is selected such that the characteristic impedance of the

line is 50-Ω. When designing the feed line, this must be along the side of the length, as the current flow is along the direction of the feed line.

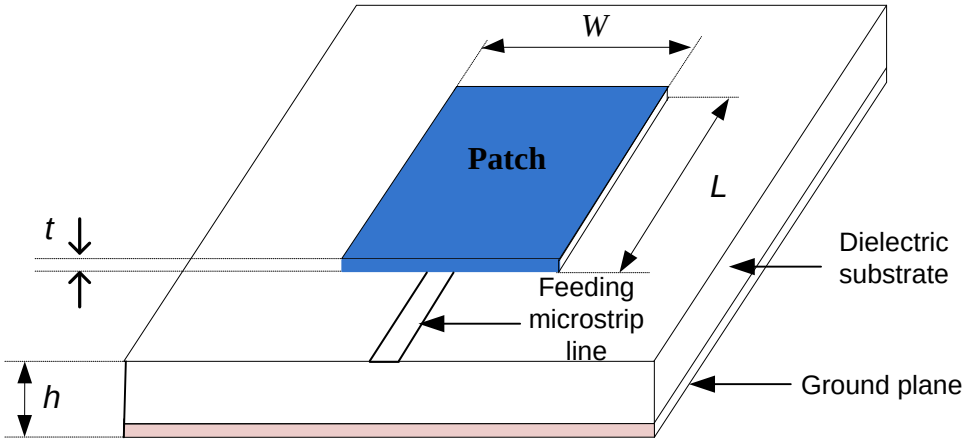

Figure 3.2 Microstrip line feed.

The selected model to design and analyze the patch antenna is the transmission line model because it is simple and gives good physical insight. This model represents the microstrip antenna by two slots of width *W* and height *h* , separated by a transmission line of length *L*. The microstrip is essentially a nonhomogeneous line of two dielectrics, typically the substrate and air.

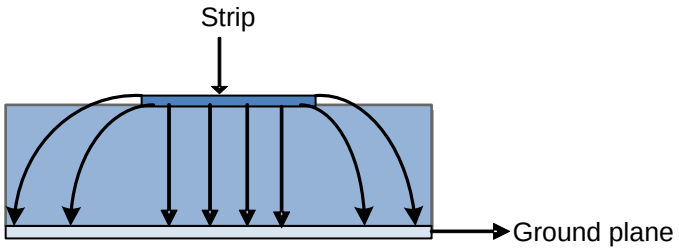

Figure 3.3 Electric field lines.

A microstrip patch, operating at its fundamental mode, is essentially a $1/2$ λ-long. For a rectangular or square patch, radiation is basically generated from its two edges with two equivalent slots along the resonating dimension. As shown in Figure 3.3 the electric field lines are moving into the air before entering the dielectric substrate. For low frequencies

the effective dielectric constant is essentially constant. At intermediate frequencies its values begin to monotonically increase and eventually approach the values of the dielectric constant of the substrate for this purpose the ε_r is replaced by ε_{reff} which is slightly less than ε_r [9]. The equation of ε_{reff} is given in by

$$\varepsilon_{reff} = \frac{\varepsilon_r + 1}{2} + \frac{\varepsilon_r - 1}{2}\left[1 + 12\frac{h}{W}\right]^{-\frac{1}{2}} \tag{3.2}$$

where

ε_r= dielectric constant of the substrate
h = height of the the dielectric substrate
W = width of the patch

Since fringing electric field lines exist in air, the length of the patch is extended on both sides to include this effect. Figure 3.4 shows the two radiating slots along the length of the patch [29].

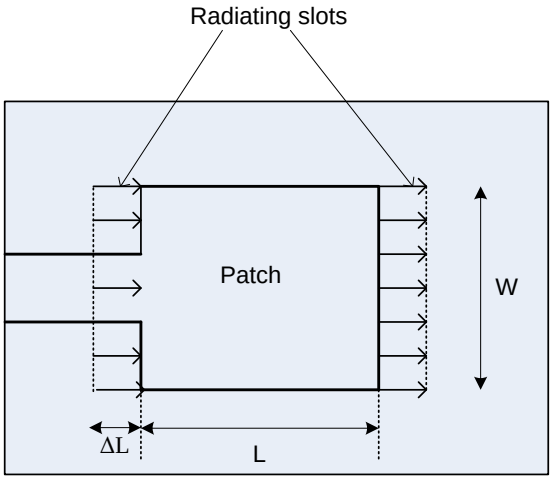

Figure 3.4 Radiating slots of the line fed patch antenna.

From Figure 3.4 it can be seen that along the width the voltage is at a maximum and the current is at a minimum due to the open ends. Since the electric field lines at the two edges

of the width are in opposite directions, they are out of phase and thereby cancel each other out. The two components which are in phase, give the maximum radiated field by combining the resulting fields. It is said that the radiation is produced by these two radiating slots. The extended length ΔL can now be calculated by the following equation.

$$\Delta L = 0.412h \frac{\left(\varepsilon_{reff} + 0.3\right)\left(\frac{W}{h} + 0.264\right)}{\left(\varepsilon_{reff} - 0.258\right)\left(\frac{W}{h} + 0.8\right)} \tag{3.3}$$

The width W can be calculated by the following equation.

$$W = \frac{1}{2f_0\sqrt{\mu_0\varepsilon_0}}\sqrt{\frac{2}{\varepsilon_r + 1}} = \frac{c}{2f_0}\sqrt{\frac{2}{\varepsilon_r + 1}} \tag{3.4}$$

where,

c = the speed of light.
f_0 = operation frequency
ε_r = relative dielectric constant of the substrate

The effective length L_{eff} can be calculated by the following equation.

$$L_{eff} = \frac{c}{2f_0\sqrt{\varepsilon_{reff}}} \tag{3.5}$$

The actual length of the patch can be calculated by the following equation.

$$L = L_{eff} - 2\Delta L \tag{3.6}$$

Essentially the transmission line model is applicable to an infinite ground plane only. For practical designs, reasonably large ground planes are used.

3.5 Design Specifications

Microstrip patch antenna has three important design parameters [28].

- Frequency of operation (f_0): The resonant frequency of the antenna must be selected appropriately. The WiMAX system uses the frequency range from 3.4 GHz to 3.6 GHz. Hence the antenna designed must be able to operate in this frequency range. The central frequency of operation is selected as 3.5 GHz.
- Relative dielectric constant of the substrate (ε_r): The dielectric material selected for this work is FR4 which has a relative dielectric constant of 4.4 .
- Height of dielectric substrate (h): Height of the dielectric substrate is selected as 1.59 mm which is one of the standard substrate thicknesses available in the industry.

FR4 is made of woven fiberglass with an epoxy resin binder (binds the copper clad to the dielectric substrate) that is flame resistant.

For the width of the patch

$$W = \frac{1}{2f_0\sqrt{\mu_0\varepsilon_0}}\sqrt{\frac{2}{\varepsilon_r+1}} = 26.07 \text{ mm} \tag{3.7}$$

For the effective dielectric constant

$$\varepsilon_{reff} = \frac{\varepsilon_r+1}{2} + \frac{\varepsilon_r-1}{2}\left[1+12\frac{h}{W}\right]^{-\frac{1}{2}} = 4 \tag{3.8}$$

For the effective length of the patch

The resonant length determines the resonant frequency and is about $\lambda/2$ for a rectangular patch excited in its fundamental mode. The patch is, in fact, electrically a bit larger than its physical dimensions due to fringing fields. The deviation between electrical and physical

size is mainly dependent on the circuit board thickness and dielectric constant. A better approximation for the resonant length is:

$$\lambda = \frac{c}{f_0} = 0.0857 \text{ m} \tag{3.9}$$

$$L_{eff} = \frac{c}{2f_0\sqrt{\varepsilon_{reff}}} = \frac{\lambda \times f_0}{2f_0\sqrt{\varepsilon_{reff}}} = \frac{1}{2}\frac{\lambda}{\sqrt{\varepsilon_{reff}}} \tag{3.10}$$

$$L_{eff} = 0.5\lambda_d \tag{3.11}$$

$$\lambda_d = \frac{\lambda}{\sqrt{\varepsilon_{reff}}} = 0.043 \text{ m} \tag{3.12}$$

$$L_{eff} = 0.5\lambda_d = 21.53 \text{ mm} \tag{3.13}$$

where

L = resonant length of element
λ_d= wavelength in substrate
λ_0= wavelength in free space
ε_r= relative dielectric constant of the substrate

This formula includes a first order correction for the edge extension due to fringing fields.

For the delta length

$$\Delta L = 0.412h\,\frac{\left(\varepsilon_{reff} + 0.3\right)\left(\frac{W}{h} + 0.264\right)}{\left(\varepsilon_{reff} - 0.258\right)\left(\frac{W}{h} + 0.8\right)} \tag{3.14}$$

$$\Delta L = 0.7\ \mu m \tag{3.15}$$

For the actual length

$$L = L_{eff} - 2\Delta L = 20.11 \text{ mm} \tag{3.16}$$

3.6 Simulations

3.6.1 Design of the Basic Patch Antenna

A patch antenna has been simulated by Ansoft HFSS using the theoretical calculations from the previous section. The ground plane dimensions are selected as 100×100 mm^2. The width of the patch is 26.07 mm and the length of the patch is 20.11 mm. On a 1.59 mm thick FR4 substrate ($\varepsilon_r = 4.4$, $\tan\delta = 0.002$), a 50-Ω line should be about 3 mm wide as calculated by Ansoft Designer. As seen from Figure 3.5 there is a $l_t = 42$ mm long transmission line that is connected to the patch and its width is $w_t = 2.8$ mm. The reason that 2.8 mm has been used as the width of the microstrip instead of 3 mm, because HFSS simulation gave about 50-Ω characteristic impedance for $w_t = 2.8$ mm. Figure 3.6 shows the S11 simulation of the patch antenna.

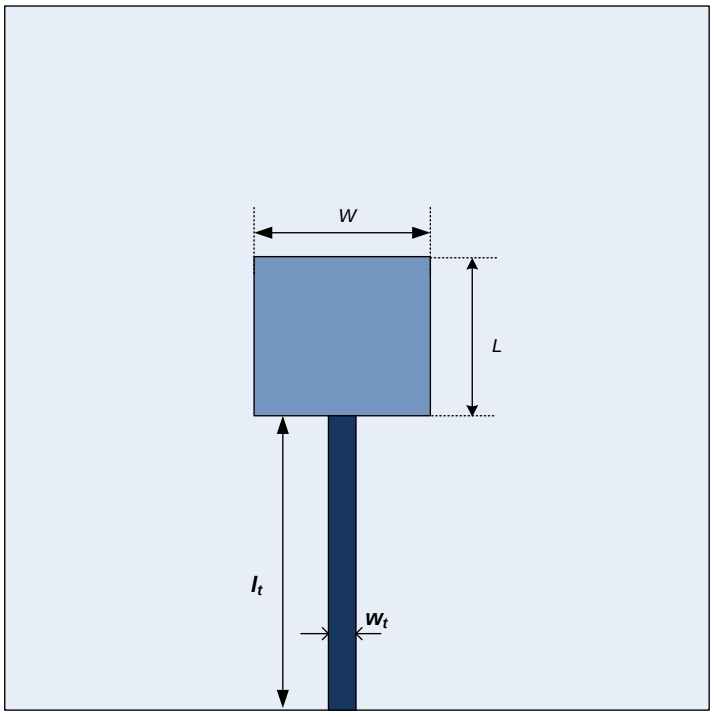

Figure 3.5 Geometry of the basic patch antenna.

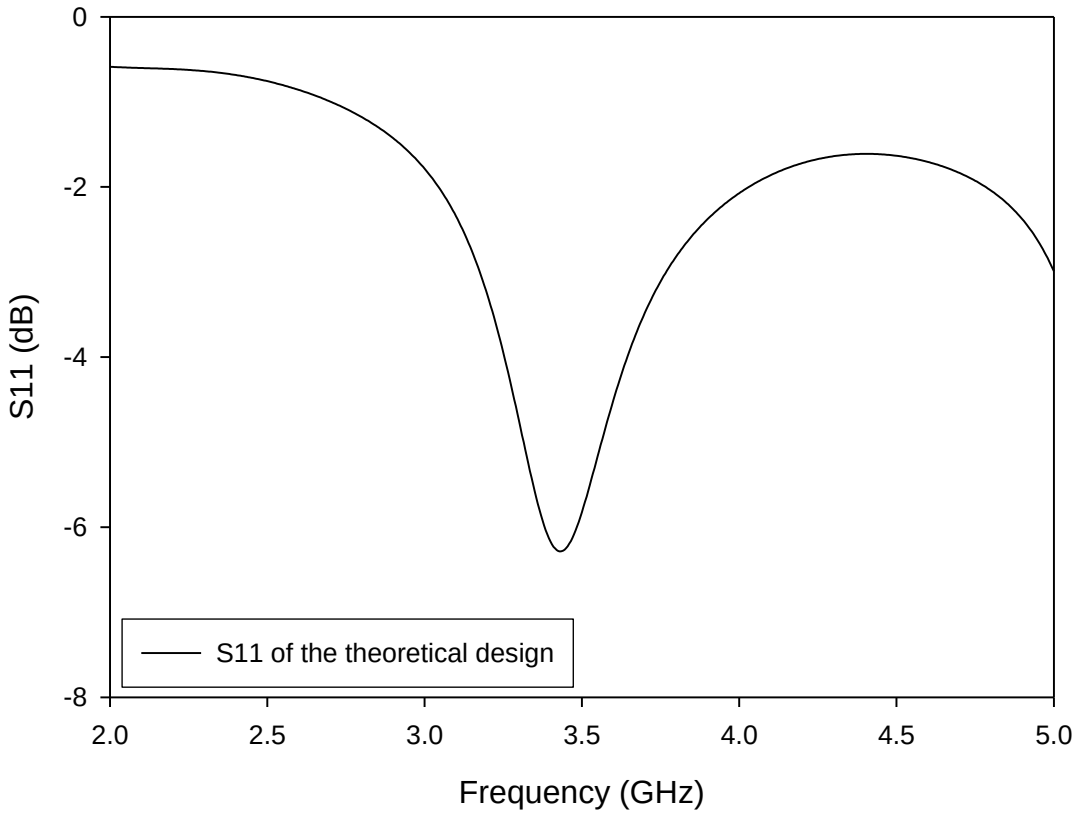

Figure 3.6 S11 simulation of the theoretical patch antenna ($W = 26.07, L = 20.11$).

Instead of a rectangular patch as calculated from theoretical calculations we aim to use a square patch because it turns out that by using a nearly square patch it is possible to reduce the footprint of the antenna. The dimensions of the nearly square patch have been selected as $W = 22$ mm and $L = 19.5$ mm. The area of the theoretical patch is the $26.07 \times 20.11 = 524.27$ mm^2 while the area of the nearly square patch is $22 \times 19.5 = 429$ mm^2. So the patch size can be reduced by about $\%\,18$ if it is made nearly square. Figure 3.7 shows S11 of the nearly square patch.

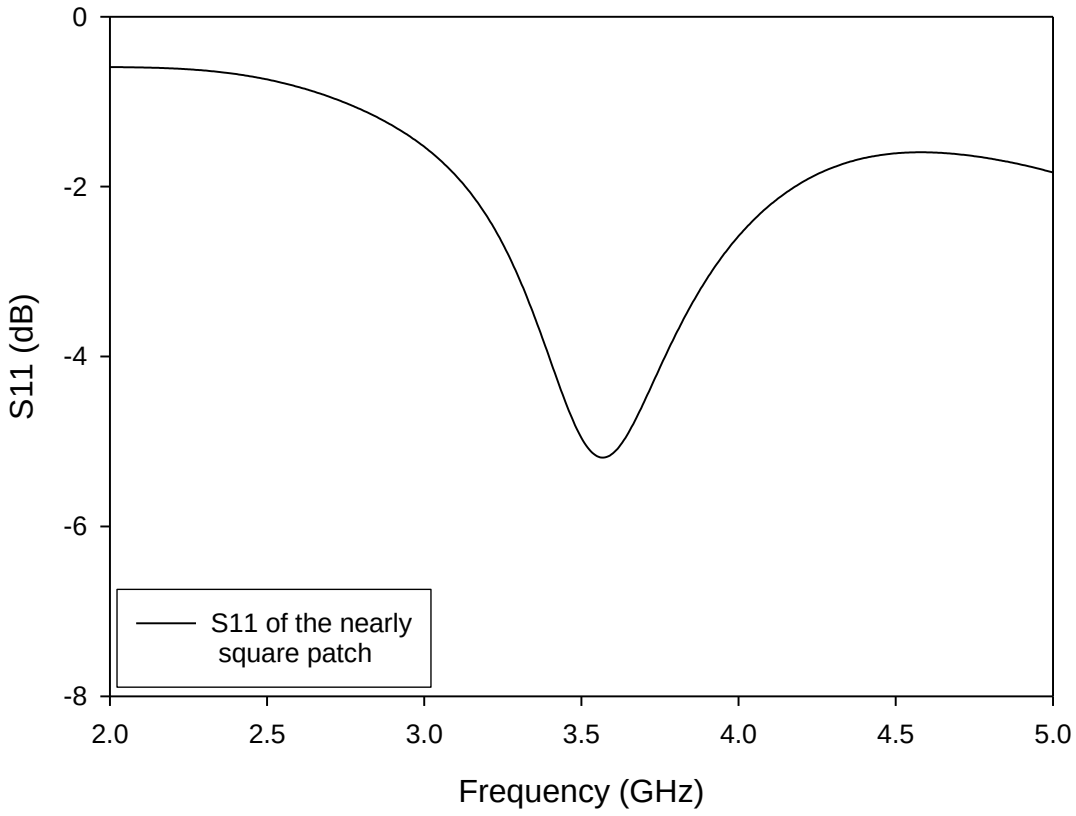

Figure 3.7 S11 simulation of the patch antenna ($W = 22,\ L = 19.5$).

By looking at the S11 of this antenna it is observed that S11 is about -5 dB at 3.5 GHz, which implies that the antenna is not well-matched. In order to match the antenna impedance to 50-Ω, a matching circuit is needed. This circuit has been designed using a $\lambda/4$ transformer section.

The location of the normalized input impedance as seen from the driving port is shown with marker m3 in Figure 3.8.

Name	Freq	Ang	Mag	RX
m3	3.5000	75.4652	0.5651	0.6572 + 1.0563i

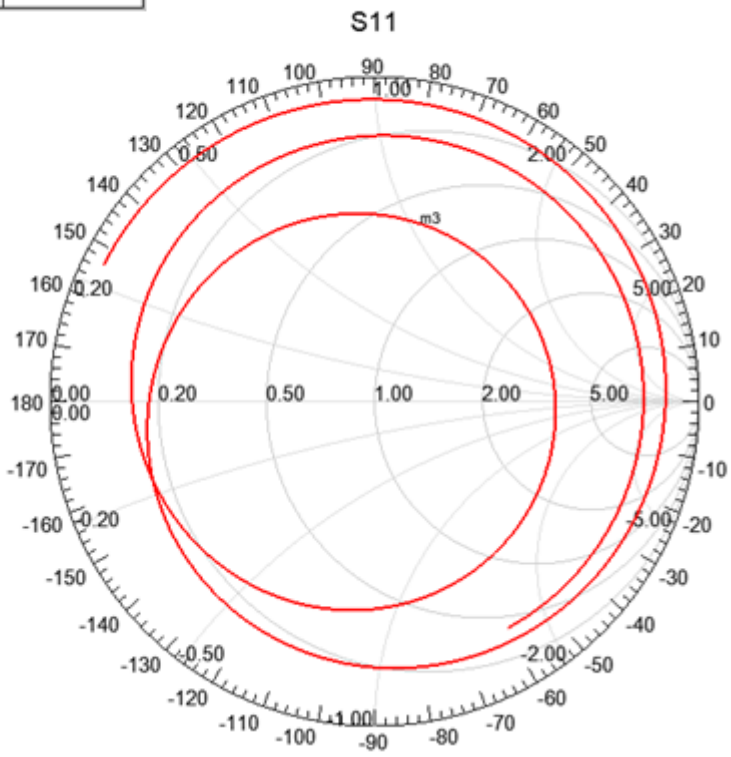

Figure 3.8 S11 of the patch antenna on Smith Chart.

At 3.5 GHz

$\overline{Z_{in}} = 0.6572 + j1.0563$ (from m3 data point on Smith Chart)

$\Gamma = 0.5651\angle 75.47°$

$Z_{in} = \overline{Z_{in}} \times 50$

$Z_{in} = 32.86 + j52.815$

There is a 42 mm long transmission line after the patch. So the antenna input impedance has to be transformed to Z_{in} through this length. Using Ansoft Designer [31], the amount of phase shift introduced by the 42 mm long line is found as 326º which is the electrical length βl.

$\beta l = 326°$

Now on the Smith Chart [30], we move $2\beta l$.

$2\beta l = 652°$

Since $652° > 360°$, $360°$ is subtracted from $652°$.

$652° - 360° = 292°$

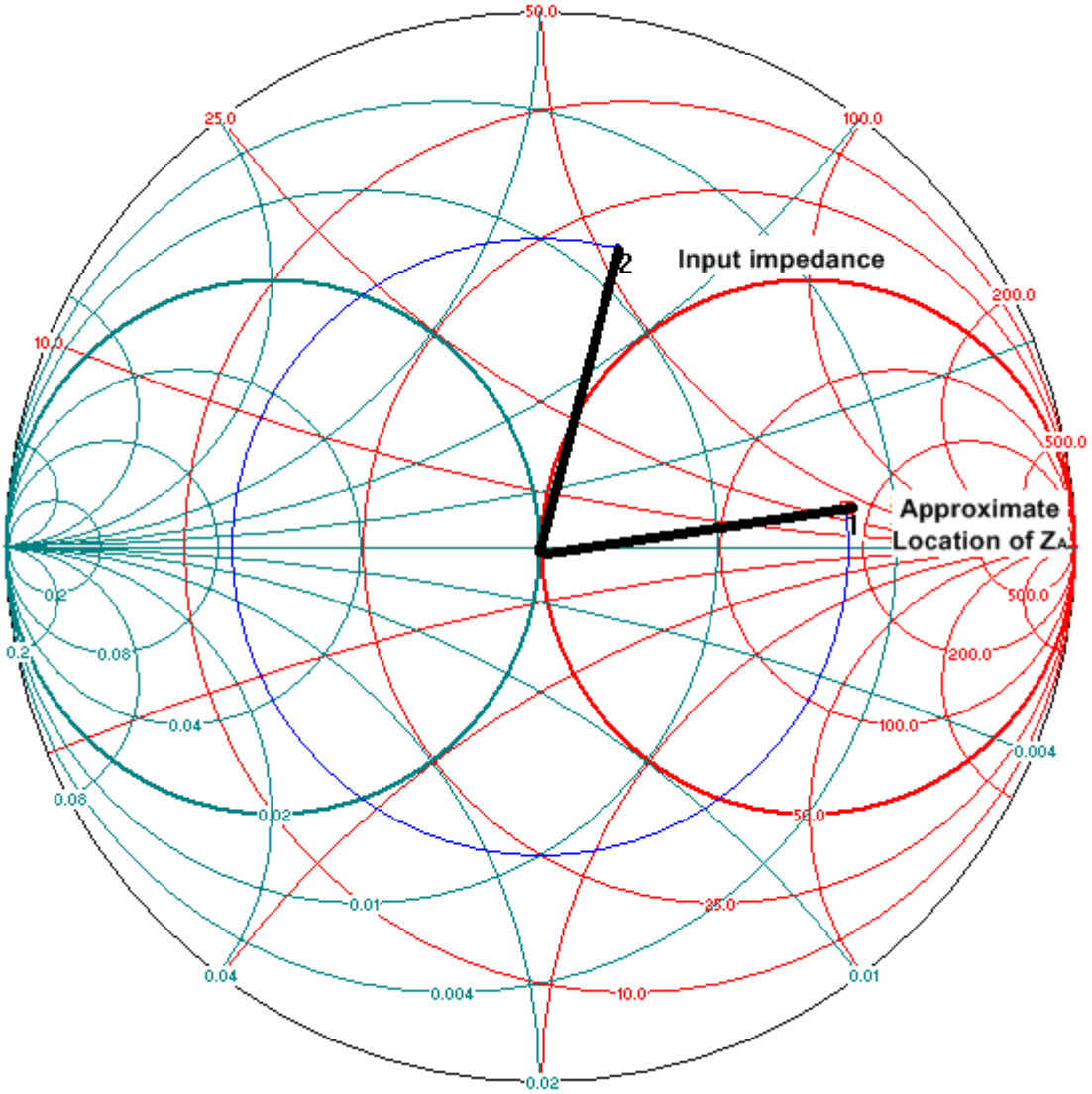

Figure 3.9 Input impedance of the antenna on Smith Chart.

This implies that to move from some point $\overline{Z_A}$ (approximate location of Z_A, on the Smith Chart point 1) to $\overline{Z_{in}}$ (input impedance, on the Smith Chart point 2) a $292°$ rotation in clock wise direction is needed. The Γ at the location of the normalized imput impedance is

$\Gamma = 0.5651\angle 75.47°$

$Z_A\big|_{Phase} = Z_{in}\big|_{Phase} + 292° = 76° + 292° = 368°$

Again $368° > 360°$, we subtract $360°$ from this number since it is one full rotation.

$368° - 360° = 8°$

And we obtain $8°$ as the approximate angle of the antenna impedance Z_A.

Verification

Using Smith Software we move from point $\overline{Z_A}$ (which come point to $\Gamma = 0.5651\angle 8°$) to $\overline{Z_{in}}$. This rotation come point exactly to $292°$.

The $Z_A = 170 + j39.3\ \Omega$. Since this point is really close to $j0$ axis (horizontal axis) we assume Z_A to be about $170\ \Omega$. Next step is to use a $\lambda/4$ transmission line section to transform Z_A to $50\ \Omega$. Let's refer the characteristic impedance of $\lambda/4$ section as Z_X . Then

$Z_X = \sqrt{170 \times 50} = 92.2\ \Omega$

This corresponds to (from Ansoft Designer);

$w_q = 0.84$ mm

$l_q = 12.2$ mm

After some optimization, the following values have been obtained for best performance.

$w_q = 0.6$ mm

$l_q = 12.6$ mm

$w_t = 2.8$ mm

$l_t = 29.4$ mm

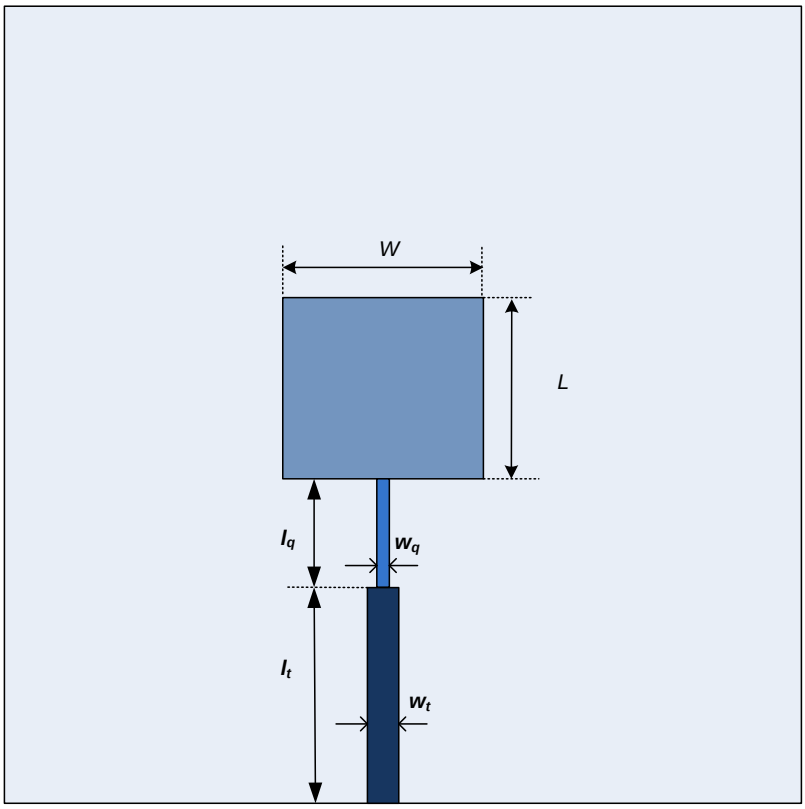

Figure 3.10 Geometry of the patch antenna with quarter wave long transformer section.

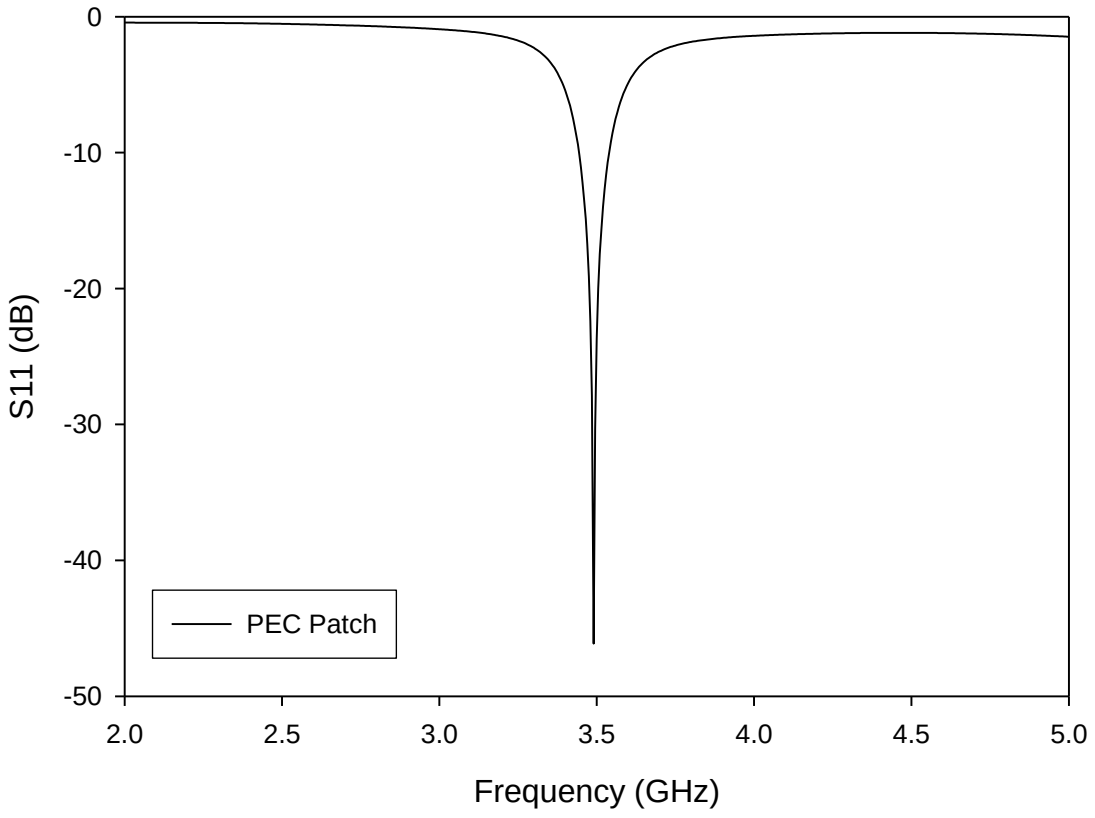

Figure 3.11 S11 of the PEC patch antenna.

Figure 3.11 shows the S11 simulation of the matched antenna by HFSS. For the simulation model, RF ground plane, patch, and microstrip transmission lines are assumed to be perfect electric conductors (PEC). A (PEC) is an idealized material that allows a completely free flow of electrons and exhibiting infinite electrical conductivity. A perfect conductor has zero resistance. Metals such as Cu, Ag, Al are closely approximated by the concept of a perfect electric conductor. For this antenna, the operation frequency is at 3.5 GHz. When the conducting elements are made of about 0.035 mm thick copper, the operating frequency is shifted down to 3.46 GHz as shown in Figure 3.12.

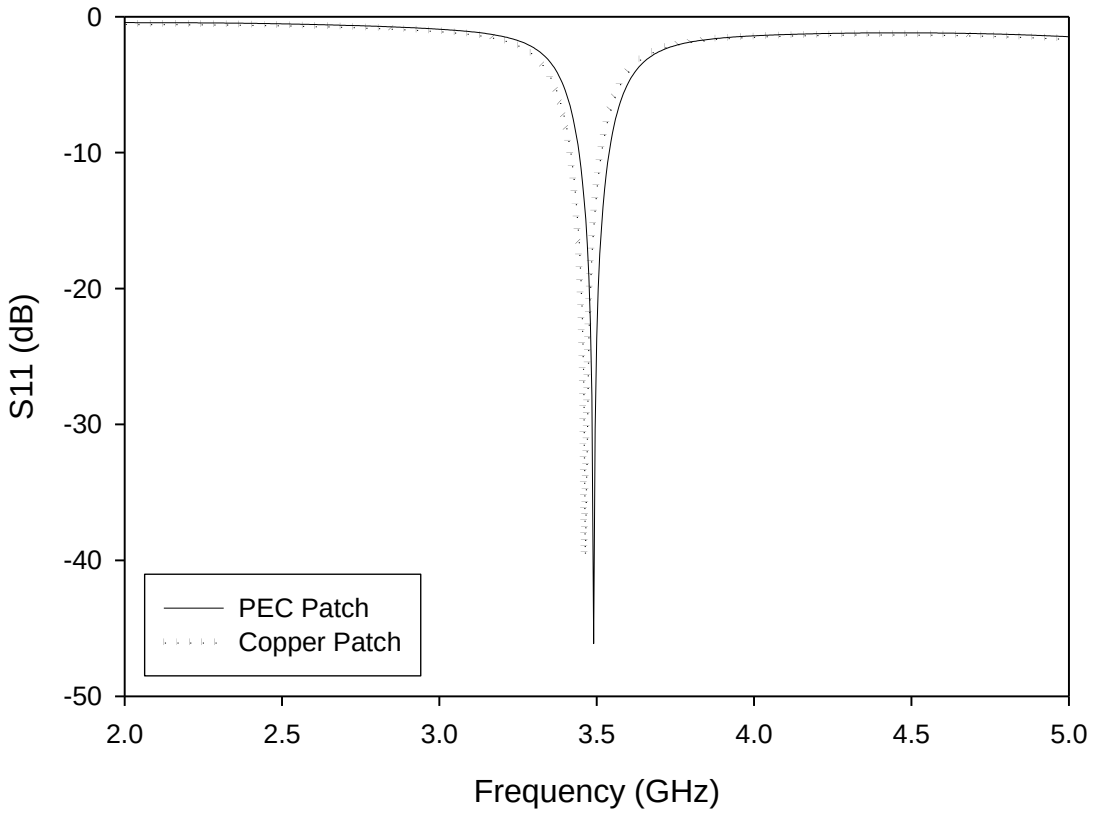

Figure 3.12 S11 of the PEC patch and the copper patch antenna.

To bring the frequency back to 3.5 GHz, the dimensions of the patch have been changed to 19.6×19.4 mm. Figure 3.13, shows the S11 measurement and HFSS simulation results of the antenna for this case. It can be seen from the Figure 3.13 that measurement and HFSS simulation are in excellent agreement. From now on, this design will be referred as the basic design. For this design, the RF ground plane dimensions are 100×100 mm^2. In addition, antenna S11 measurements have been performed at Tübitak BİLGEM Electromagnetic and Antenna Systems Division using an Anritsu MS2037C/2 Vector Network Analyzer (VNA. Figure 3.14 shows a photograph of the fabricated patch antenna with quarter wave long transformer section and SMA connector.

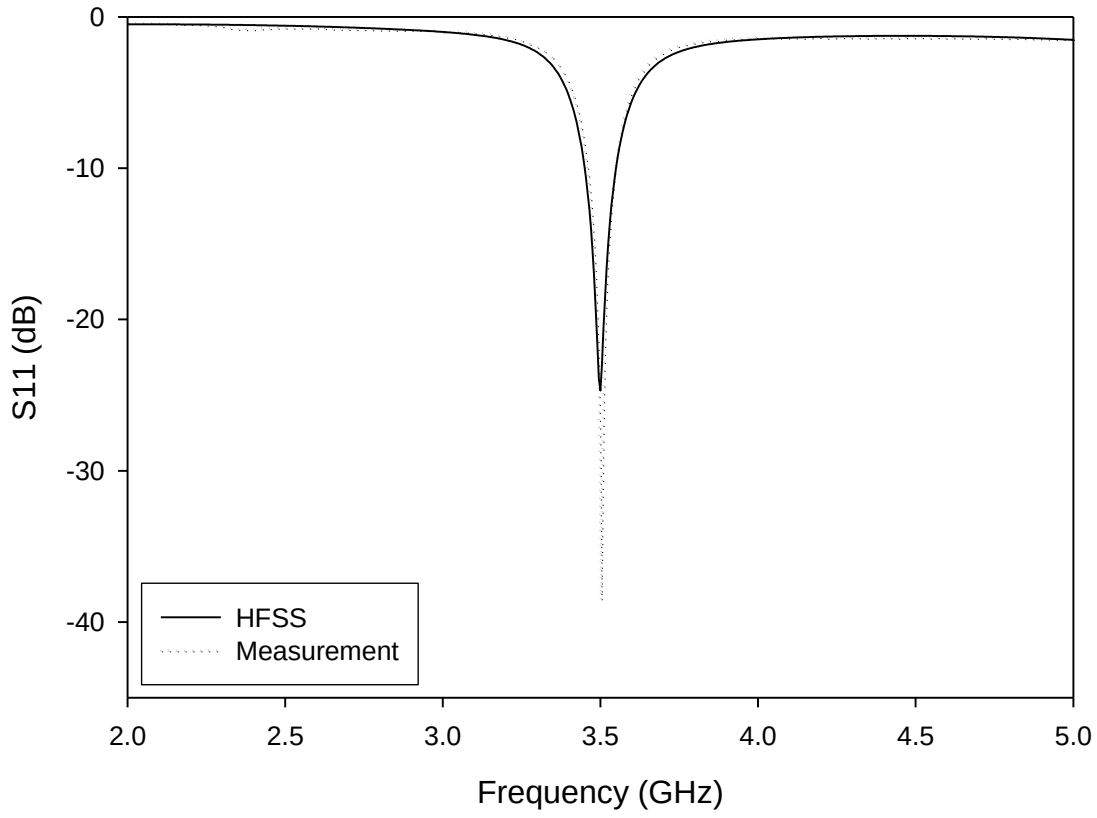

Figure 3.13 S11 of the optimized copper patch antenna.

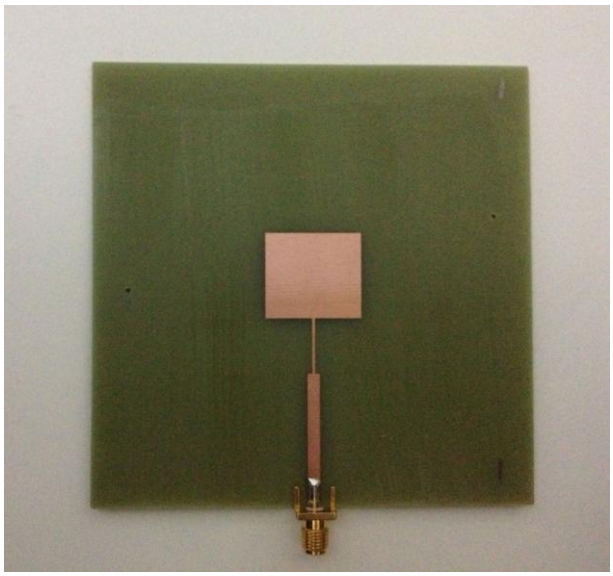

Figure 3.14 A photograph of the fabricated patch antenna with quarter wave long transformer section and SMA connector.

3.6.2 The Patch Antenna on 100 × 100 mm^2 Ground Plane with the Parasitic Patch

Now, a parasitic patch which is used to increase the realized gain is placed at difference height from the main patch. The size of the parasitic patch is about 23.6 × 23.4 mm^2.

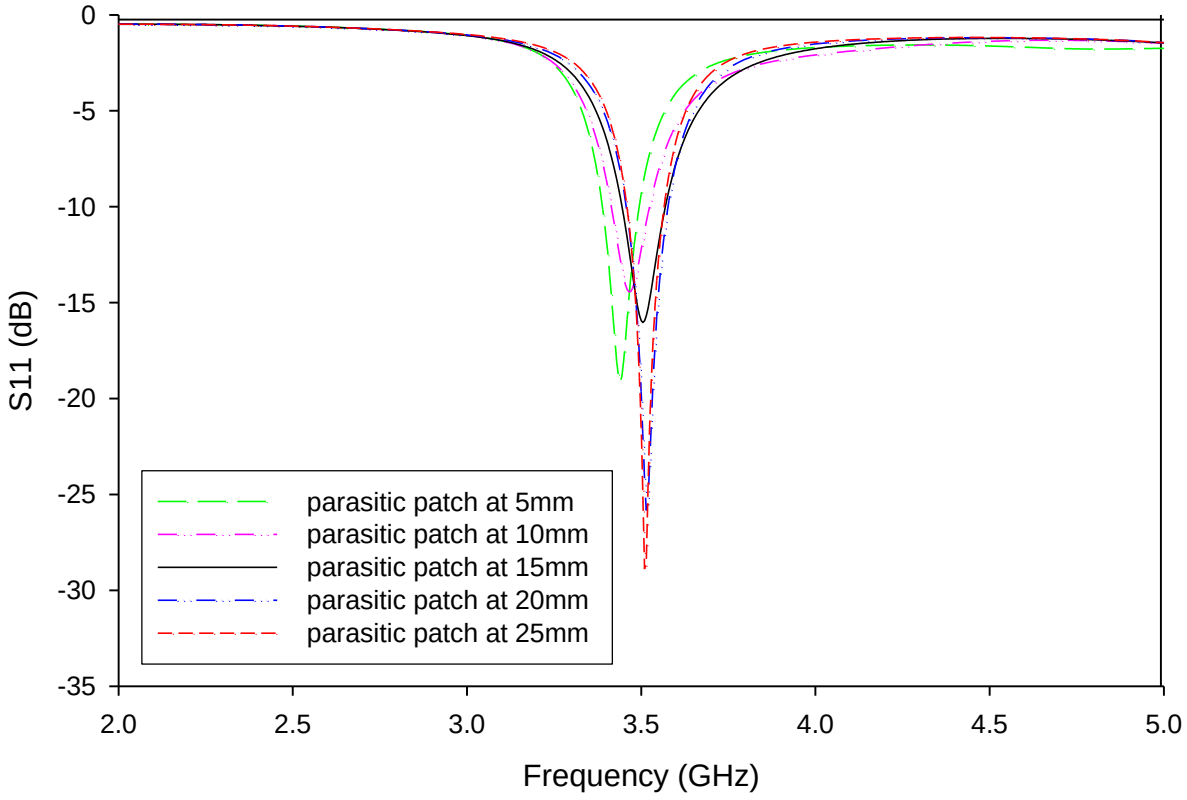

Figure 3.15 S11 of the patch antenna for different heights of the parasitic patch.

Figure 3.15 shows the variation of S11 with the frequency for different values of the height of the parasitic patch. The simulated S11 with the parasitic patch changes as the height of the parasitic patch is varied from 5 mm to 25 mm with 5 mm steps. The operating frequency fluctuates between 3.4 GHz and 3.5 GHz for these cases.

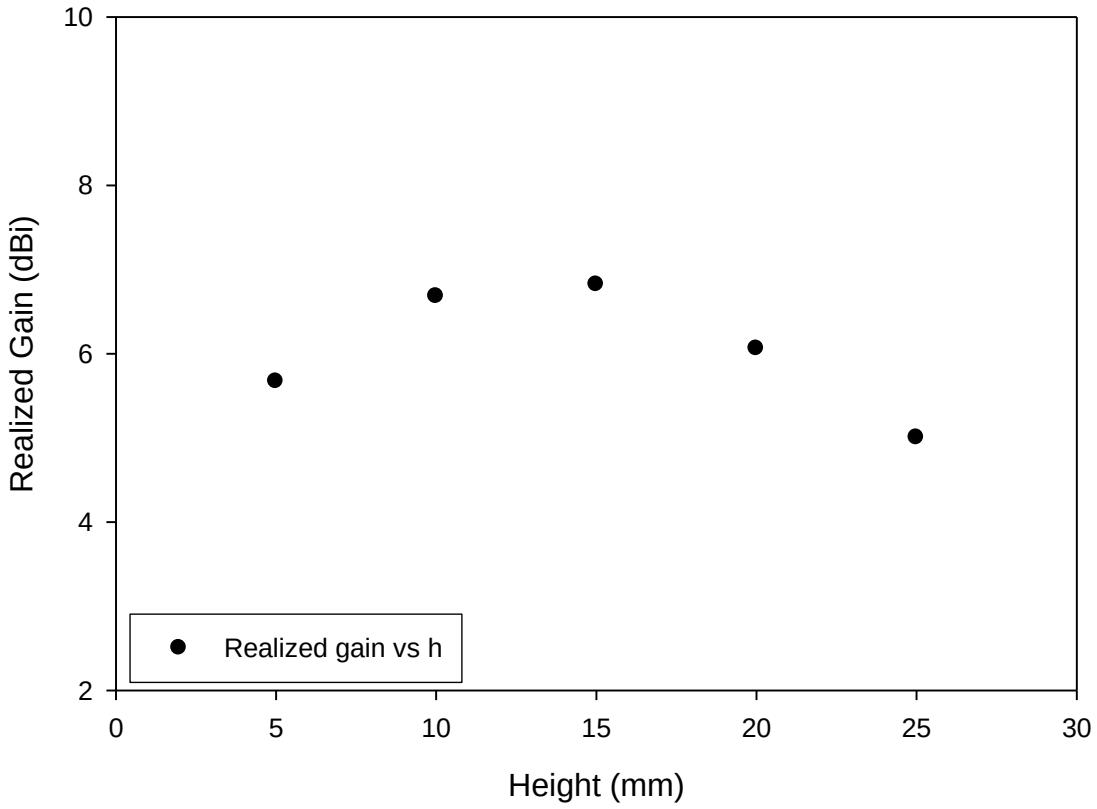

Figure 3.16 Realized gain values for different heights of the parasitic patch.

As seen in Figure 3.16 the simulated maximum realized gain with a parasitic patch increases for certain values of h, when the height of the parasitic patch is varied from 5 mm to 25 mm with 5 mm steps. The gain improvement is maximum for $h = 15$ mm. When $h = 15$ mm, the realized gain is 6.81 dBi whereas a distance 5 mm provides a realized gain of about 5.6 dBi.

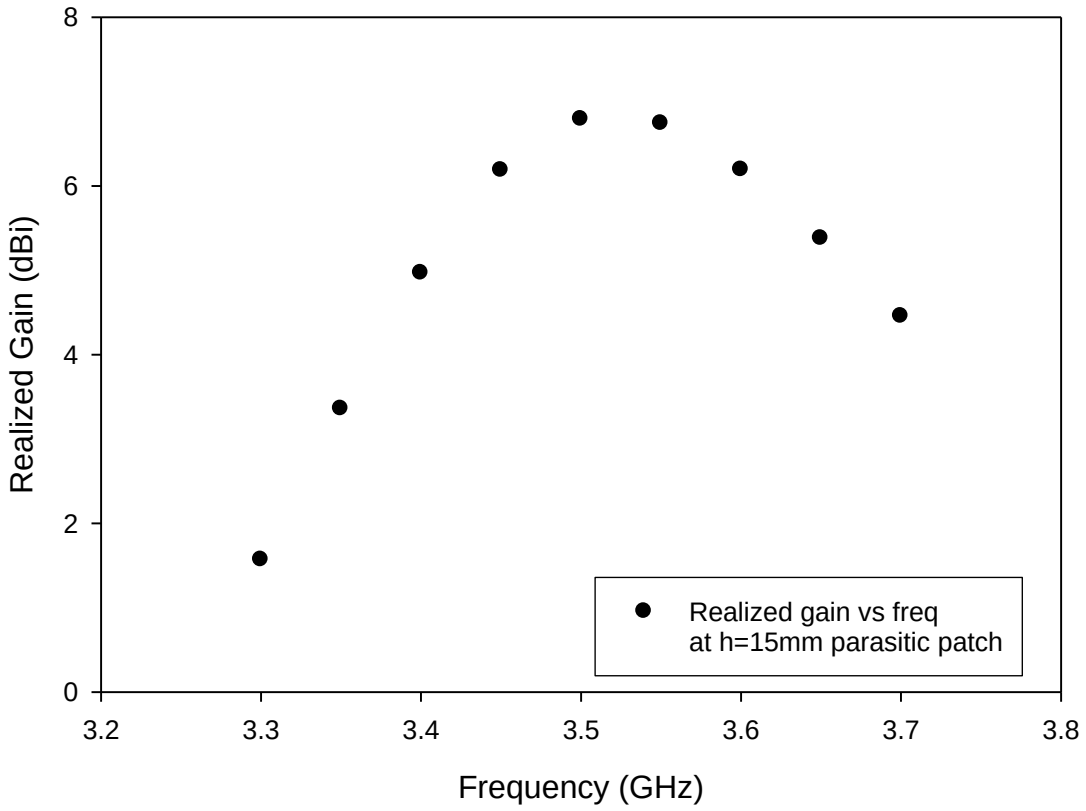

Figure 3.17 Realized gain as function of the frequency when the parasitic patch is 15 mm above the main patch.

As seen in Figure 3.17 the realized gain simulations for the parasitic patch at $h = 15$ mm give the best result at 3.5 GHz. At this frequency the value of the realized gain is approximately 7 dBi.

After determining the distance of the parasitic patch, $h = 15$ mm, which provided the maximum gain enhancement, the radiation patterns of the antenna at 3.5 GHz are taken in the principal cuts, which correspond to $yz\ (\varphi = 90°)$ and $xz\ (\varphi = 0°)$, $xy\ (\theta = 90°)$ planes.

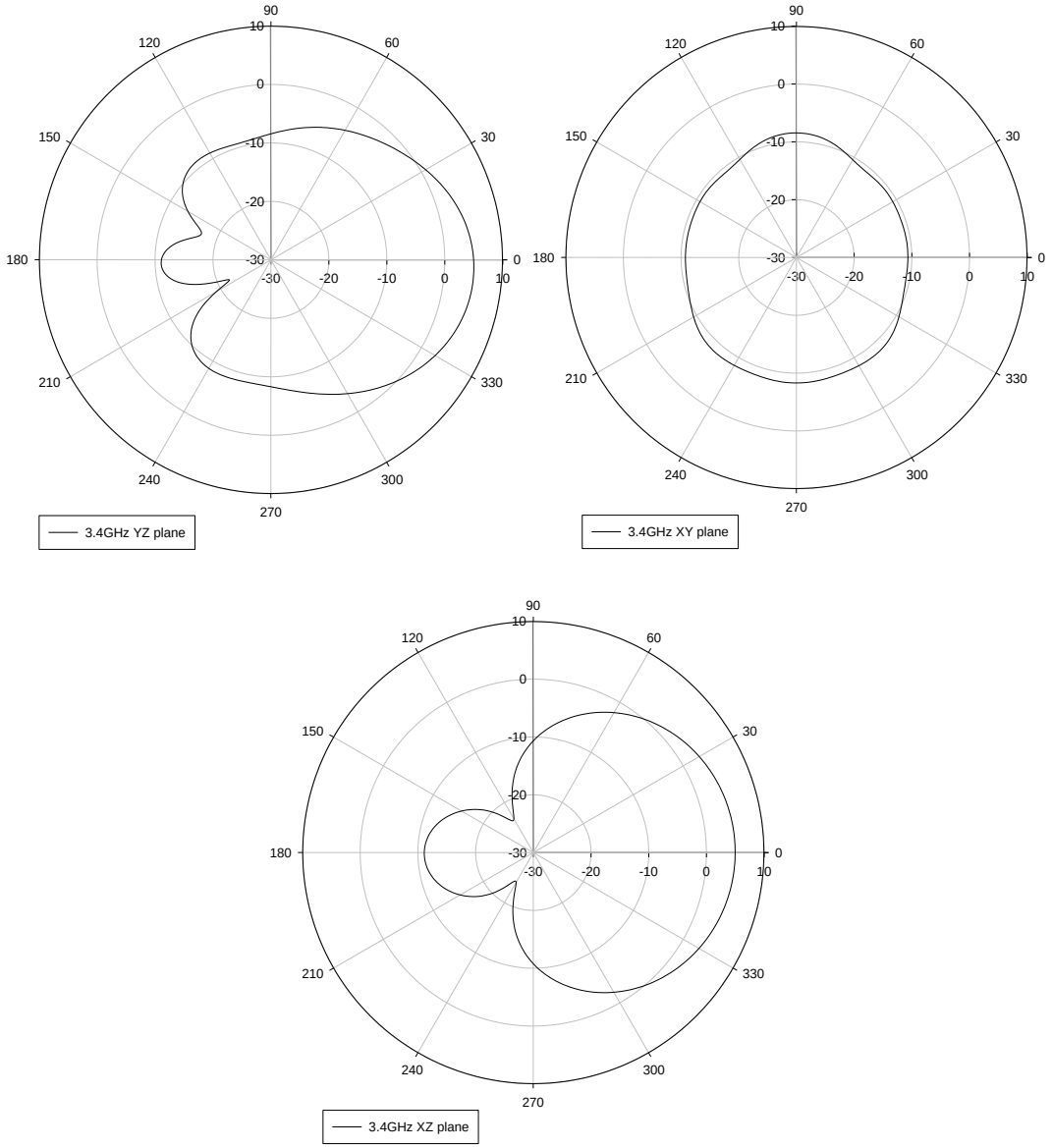

Figure 3.18 Radiation patterns at *yz*, *xy*, and *xz* planes at 3.4 GHz.

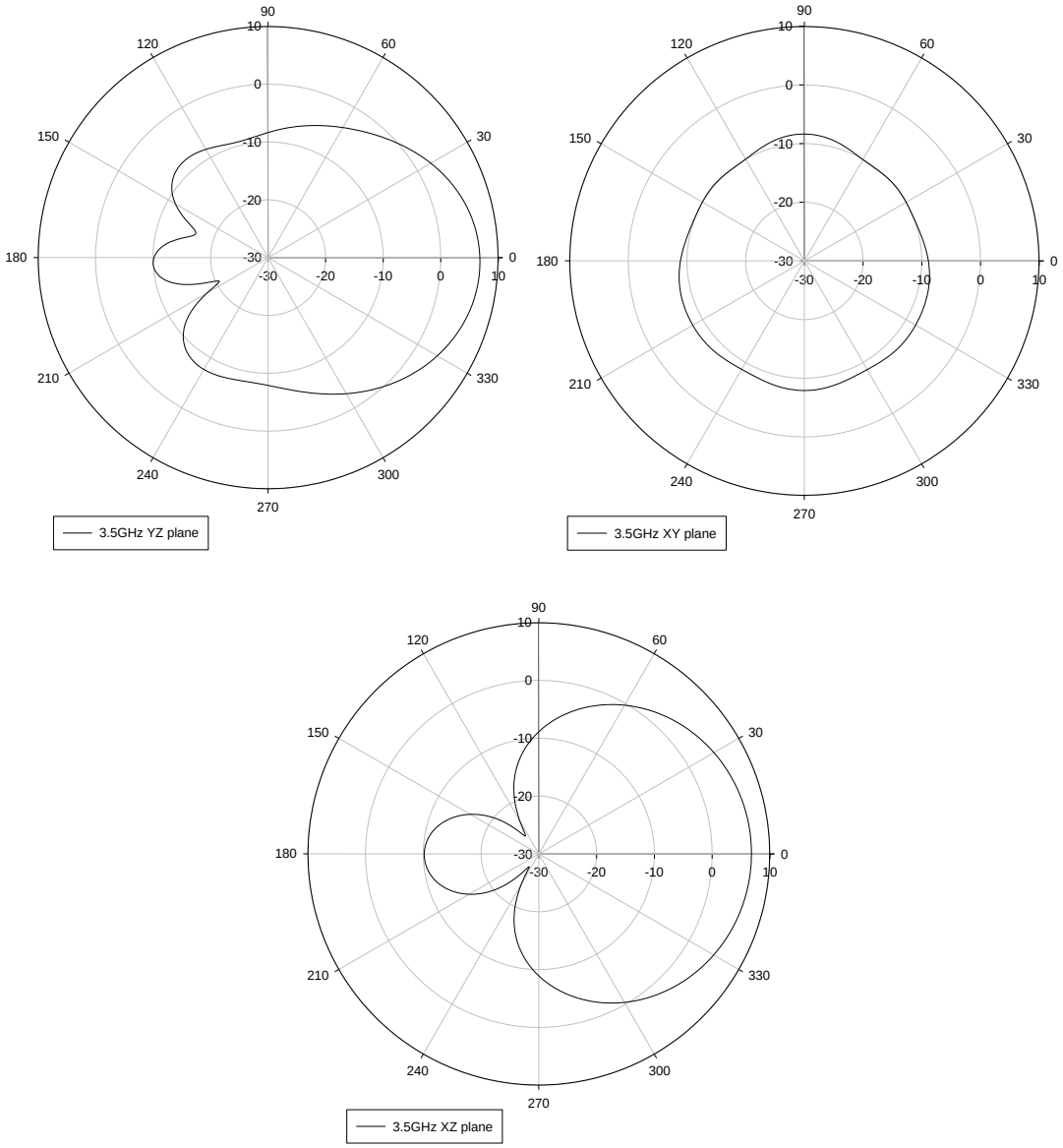

Figure 3.19 Radiation patterns at *yz*, *xy*, and *xz* planes at 3.5 GHz.

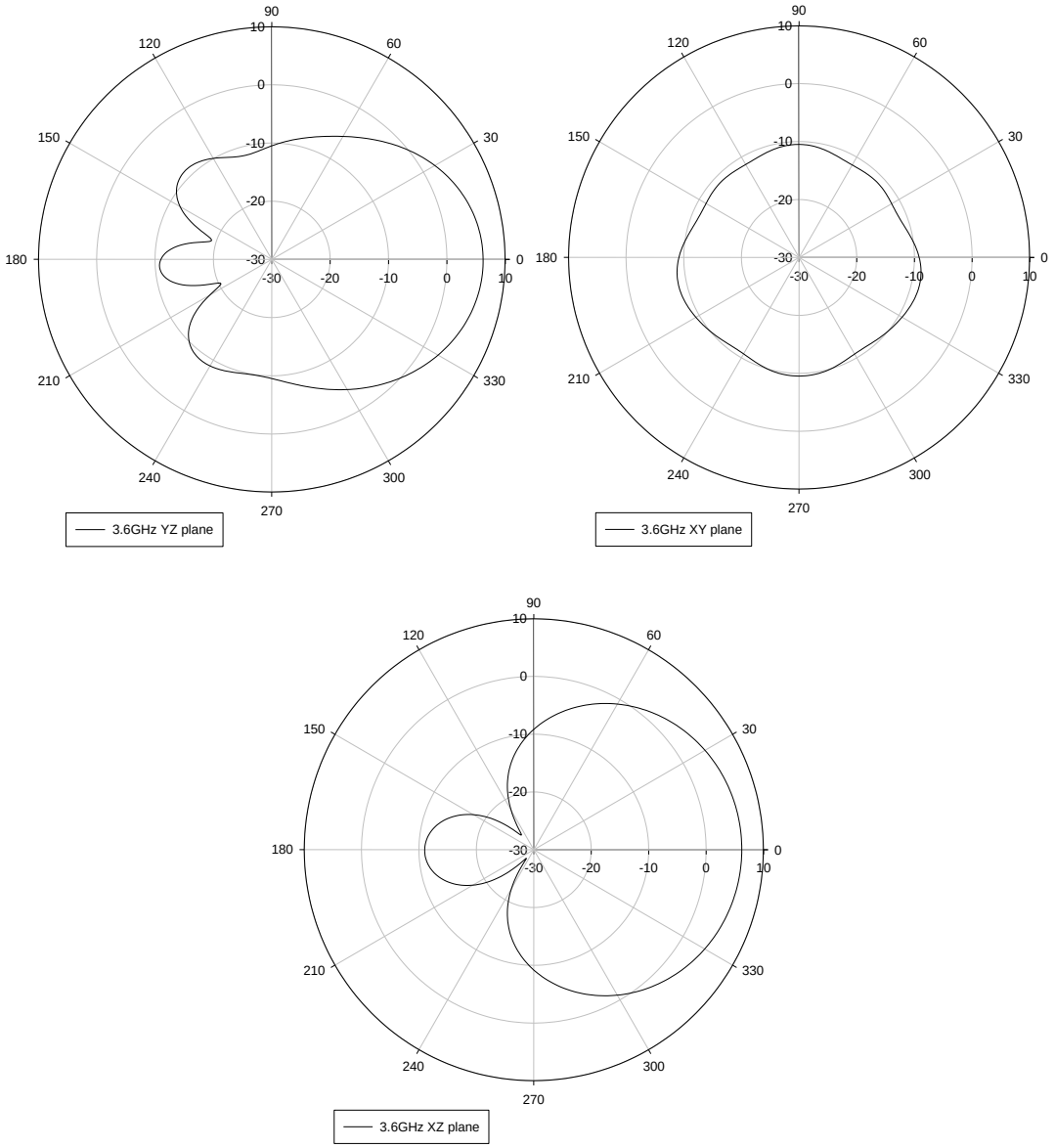

Figure 3.20 Radiation patterns at *yz*, *xy*, and *xz* planes at 3.6 GHz.

As can be seen from Figs. 3.18, 3.19, 3.20 the antenna has a peak gain at 3.5 GHz when the elevation angle is zero degrees. The radiation patterns do not vary significantly when the frequency is varied from 3.4 GHz to 3.6 GHz. There is not much radiation behind the ground plane. Beamwidth for 3.5 GHz is 78º at *xz* plane and 48º at *yz* plane.

3.6.3 Effect of the Size of the Parasitic Patch on the Realized Gain for 100×100 Ground Plane

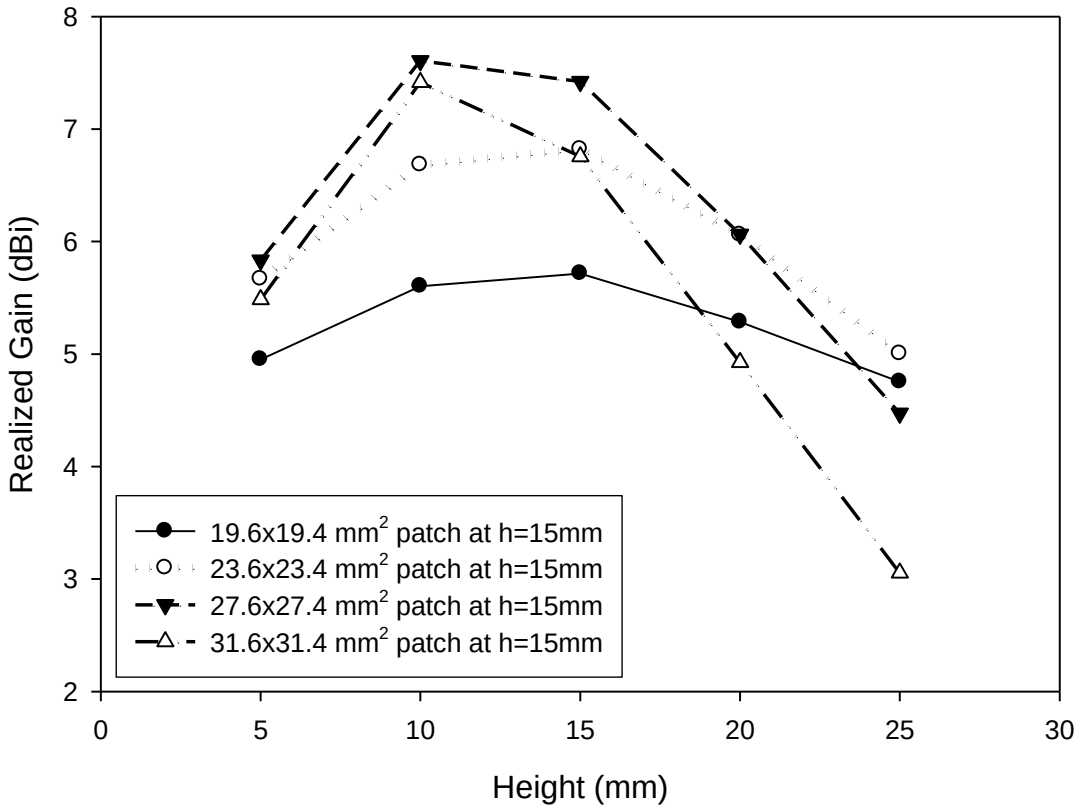

Figure 3.21 Comparison of realized gains for different sizes of the parasitic patch**.**

The effect of the size of the parasitic patch on the realized gain has also been studied and the results are shown in Figure 3.21. The patch sizes and the corresponding realized gains have been listed in Table 3.1.

When the parasitic patch size is 23.6×23.4 mm^2 (this is the reference parasitic patch), the realized gain is 6.82 dBi. When the reference patch size is increased 4 mm in x and y directions (the 27.6×27.4 mm^2 parasitic patch), the realized gain becomes about 7.43 dBi. When the reference patch size is increased 8 mm in x and y directions (the 31.6×31.4 mm^2 parasitic patch), the realized gain 6.75 dBi is obtained. If the size of the reference patch is decreased by 4 mm in x and y directions, the realized gain becomes about 5.72 dBi.

Table 3.1 Realized gain and the parasitic patch is at $h = 15$ mm and ground plane is 100×100 mm^2.

Patch size (mm^2)	Realized Gain (dBi)
23.6×23.4 (ref. design)	6.82
27.6×27.4 (+4 mm)	7.43
31.6×31.4 (+8 mm)	6.75
19.6×19.4 (-4 mm)	5.72

It can be seen that the maximum realized gain is achieved when the patch size is 27.6×27.4 mm^2 . The realized gain is about 7.5 dBi for this case.

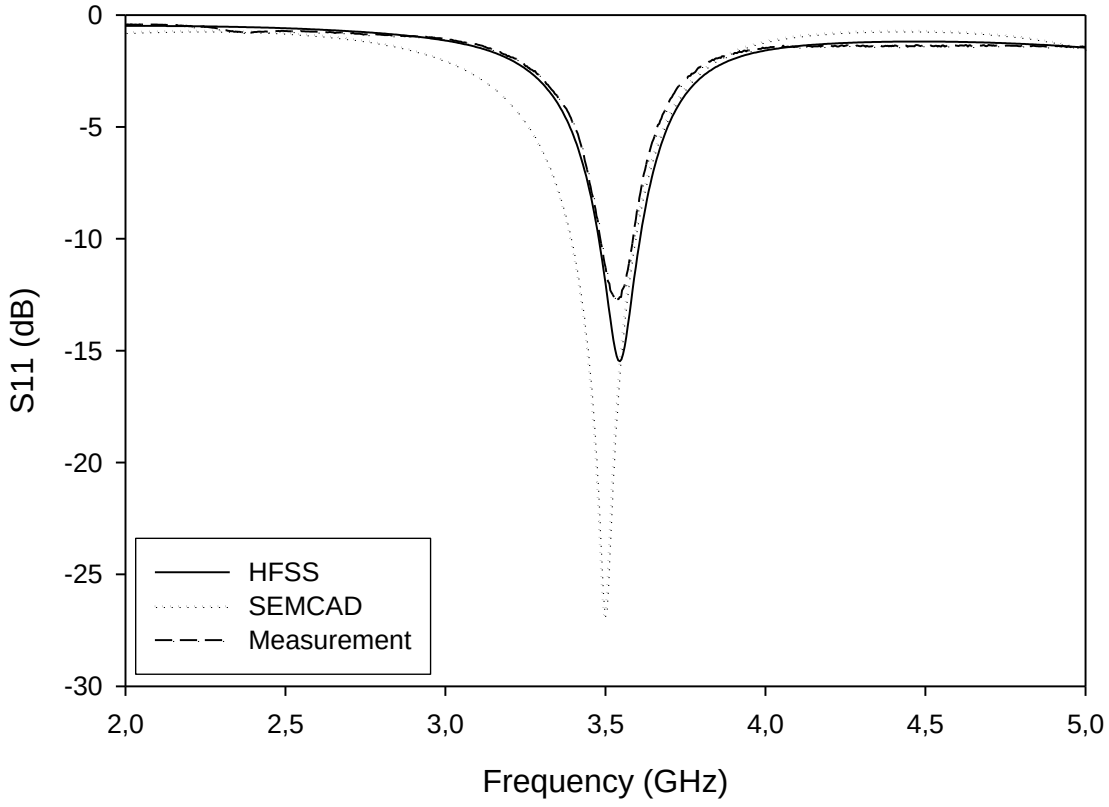

Figure 3.22 S11 of the patch antenna for $h = 15$ mm and 27.6×27.4 mm^2 parasitic patch.

Figure 3.22 shows S11 measurement, HFSS and SEMCAD simulated S11 of the patch antenna for $h = 15$ mm, when the parasitic patch size is 27.6×27.4 mm^2. It can be seen that the agreement between measurement and, HFSS simulation is excellent. Antenna S11

measurements have been performed at Tübitak BİLGEM Electromagnetic and Antenna Systems Division using an Anritsu MS2037C/2 Vector Network Analyzer (VNA).

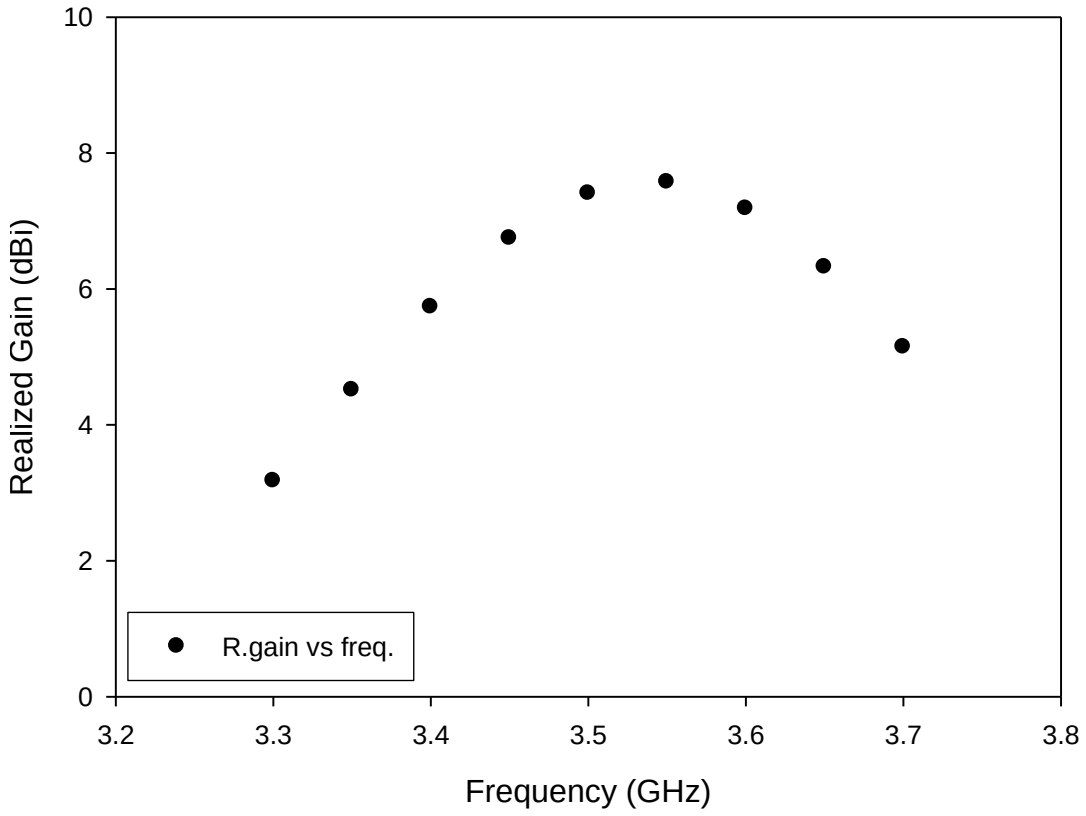

Figure 3.23 Realized gain as function of the frequency when the parasitic patch is 15 mm above the main patch and parasitic patch size is 27.6×27.4 mm^2.

Figure 3.23 shows realized gain as function of the frequency when the parasitic patch is 15 mm above the main patch and when the size of the parasitic patch is 27.6×27.4 mm^2. It can be seen from the Figure 3.23 that frequency dependent realized gain is maximum at about 3.55 GHz. The gain at 3.5 GHz is approximately 7.4 dBi.

Figure 3.24 and 3.25 shows the photographs of the top and side views of the fabricated patch antenna with the parasitic patch. The tape has been added on the parasitic patch to protect the antenna and there is no effect on the radiation pattern.

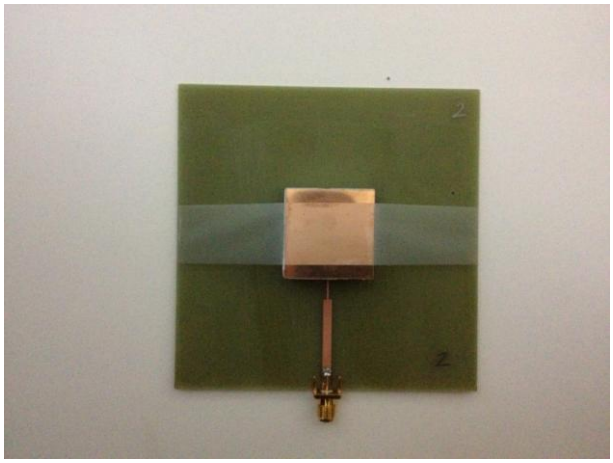

Figure 3.24 Top view of the fabricated patch antenna with the parasitic patch.

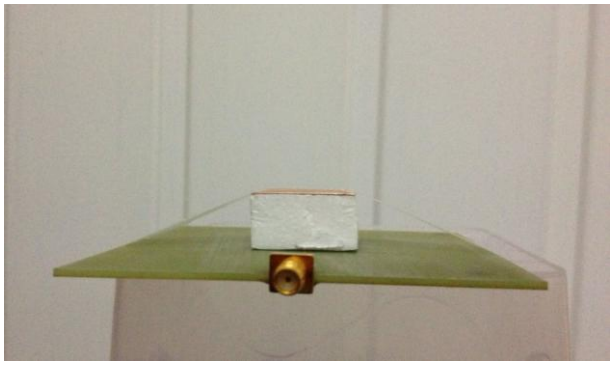

Figure 3.25 Side view of the fabricated patch antenna with the parasitic patch.

After fixing the distance of the parasitic patch at $h = 15$ mm which provided the maximum gain enhancement for the 100×100 mm^2 ground plane, the radiation patterns of the antenna at 3.5 GHz are taken in the principal cuts, which correspond to yz ($\varphi = 90°$) and xz ($\varphi = 0°$), xy ($\theta = 90°$) planes, respectively.

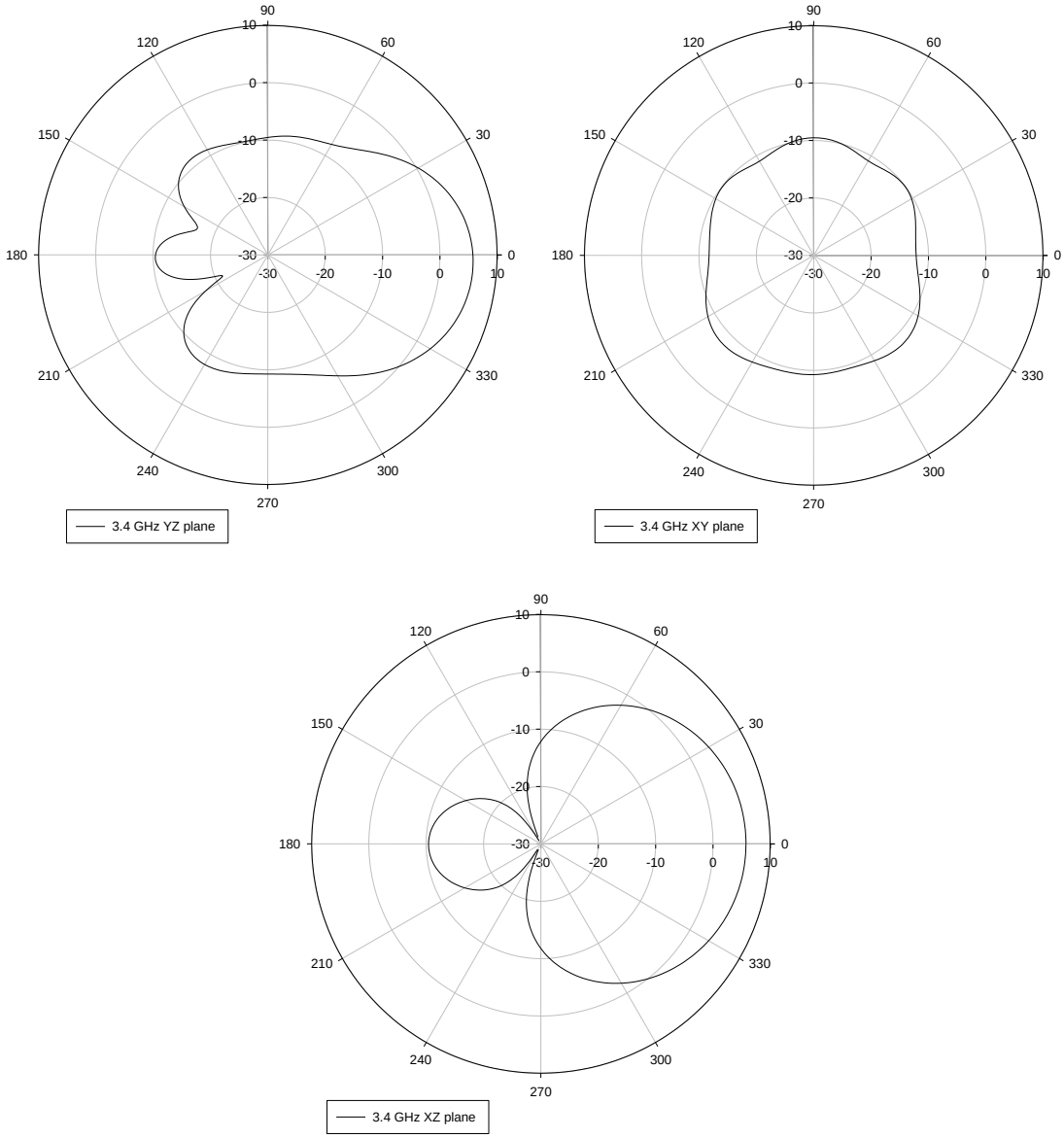

Figure 3.26 Radiation patterns at *yz*, *xy*, and *xz* planes at 3.4 GHz.

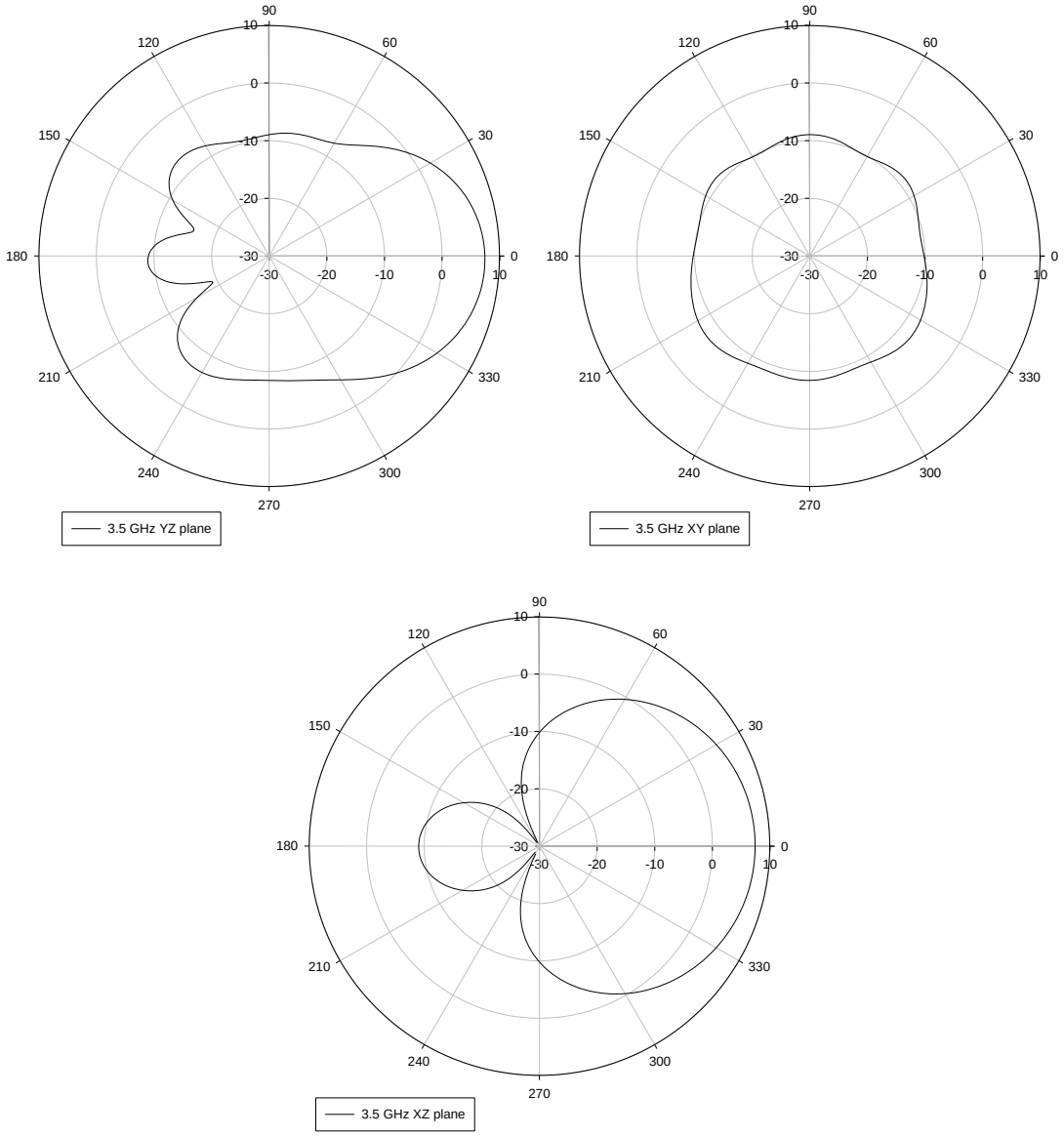

Figure 3.27 Radiation patterns at *yz*, *xy*, and *xz* planes at 3.5 GHz.

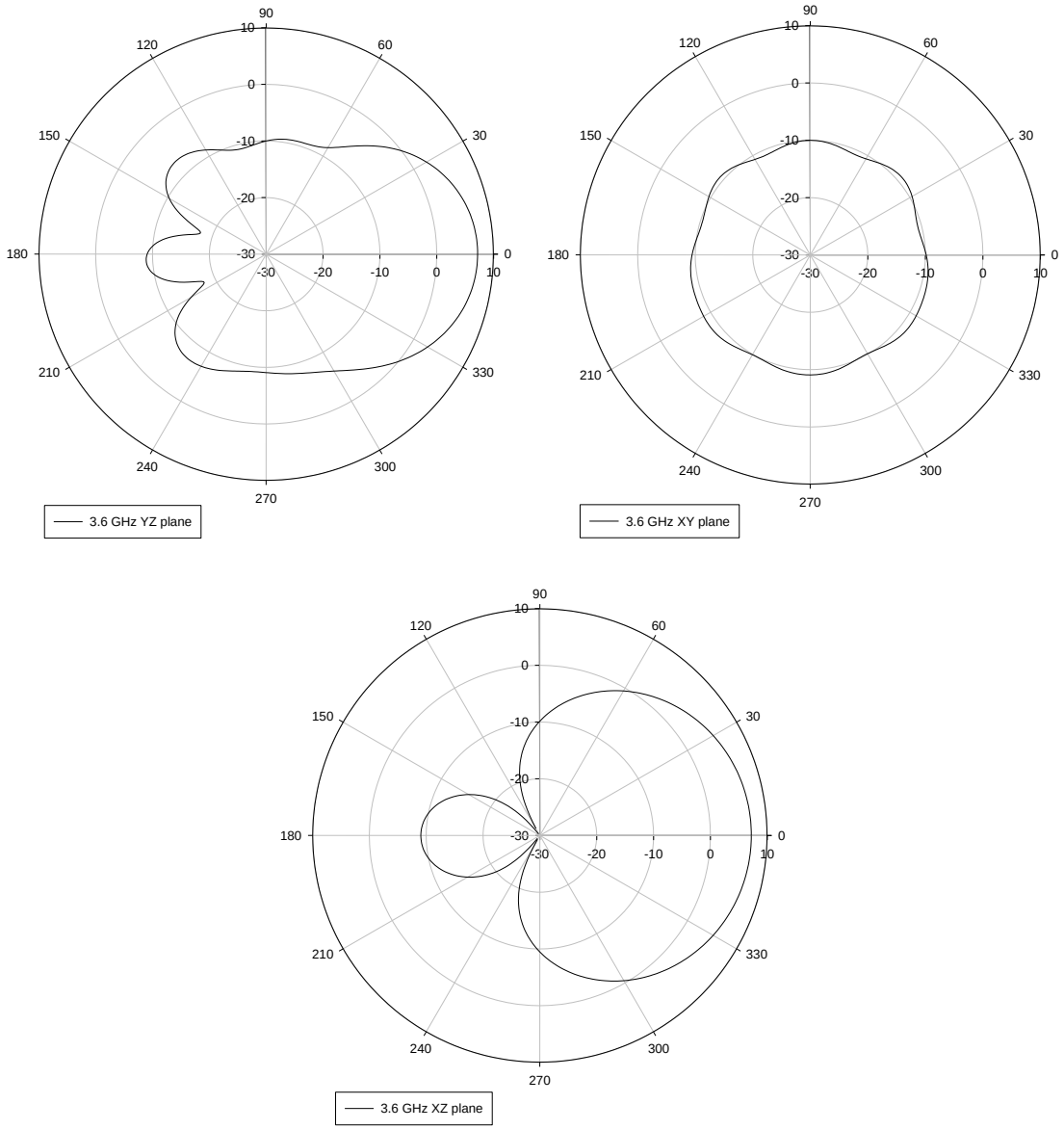

Figure 3.28 Radiation patterns at *yz*, *xy*, and *xz* planes at 3.6 GHz.

Figs. 3.26, 3.27, and 3.28 show the radiation pattern of the patch antenna for $h = 15$ mm and when the parasitic patch size is 27.6×27.4 mm^2. The antenna has a peak gain at 3.5 GHz when the elevation angle is zero degrees. The radiation patterns do not vary significantly when the frequency is varied from 3.4 GHz to 3.6 GHz. There is not much radiation behind the ground plane. Beamwidth for 3.5 GHz is 86º in *xz* plane and 52º in *yz* plane.

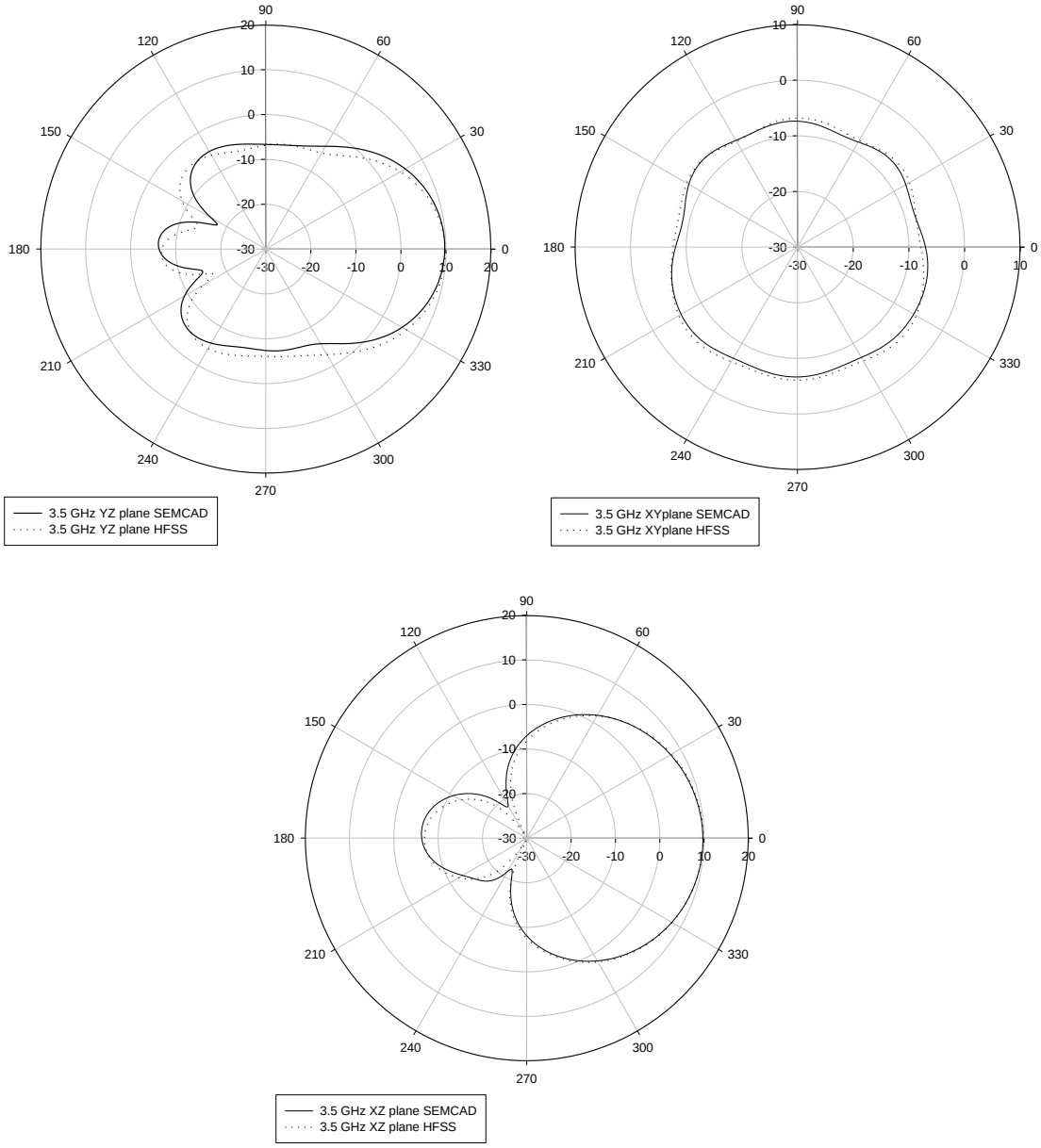

Figure 3.29 Directive pattern of the patch antenna at 3.5 GHz, for $h = 15$ mm and when the parasitic patch size is 27.6×27.4 mm^2**.**

Figure 3.29 shows that directive pattern of the patch antenna at 3.5 GHz, for $h = 15$ mm and 27.6×27.4 mm^2 parasitic patch size. It can be seen from the Figure 3.29 that SEMCAD and HFSS simulations are in excellent agreement.

3.6.4 The Patch Antenna on 80×80 mm^2 Ground Plane with the Parasitic Patch

The antenna has also been analyzed on 80×80 mm^2 ground plane to examine the effect of the ground plane dimensions on the performance of the patch antenna. The antenna gain is maximum when the parasitic patch is placed 10 mm above the main patch and the size of the parasitic patch is about 23.6×23.4 mm^2.

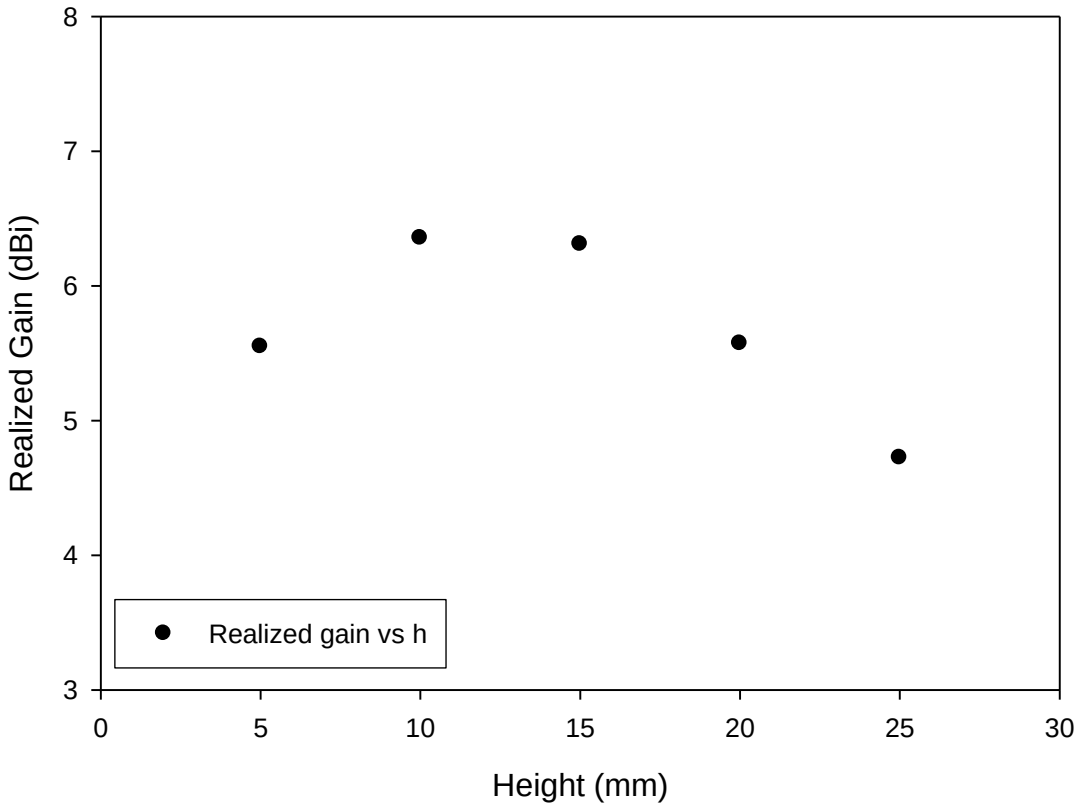

Figure 3.30 Realized gain values for different heights of the parasitic patch.

Similar to the simulations of the patch antenna on 100×100 mm ground plane, S11 and realized gain of the modified antenna have also been analyzed with HFSS for $h = 10$ mm. The simulated maximum realized gain with a parasitic patch increases for certain values of h. When the height of the parasitic patch is varied from 5 mm to 25 mm with 5 mm steps the realized gain varies as shown in Figure 3.30. The realized gain improvement is maximum for $h = 10$ mm. When $h = 10$ mm the realized gain is 6.4 dBi whereas a distance 5 mm provides a gain of about 5.5 dBi.

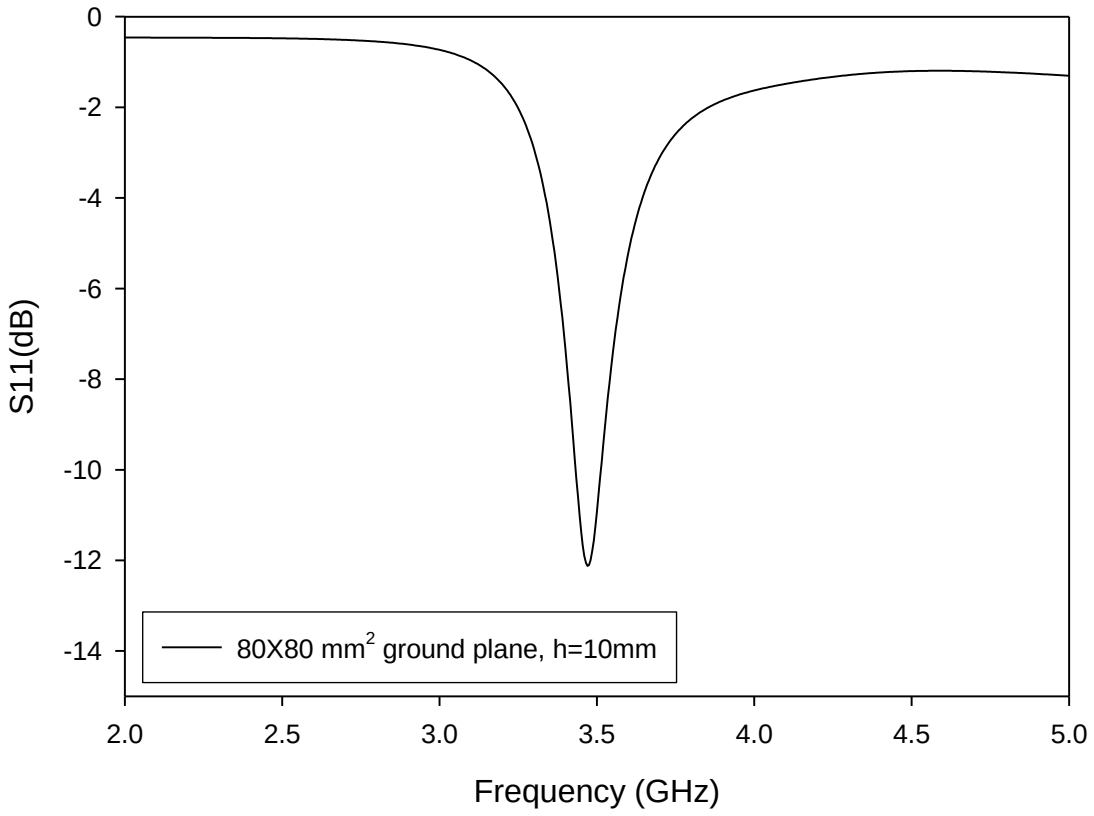

Figure 3.31 S11 of the patch antenna on 80 × 80 mm^2 ground plane when the parasitic patch is placed 10 mm above the main patch.

Figure 3.31 shows the variation of S11 when the parasitic path is placed 10 mm above the main patch for 80 × 80 mm^2 ground plane.

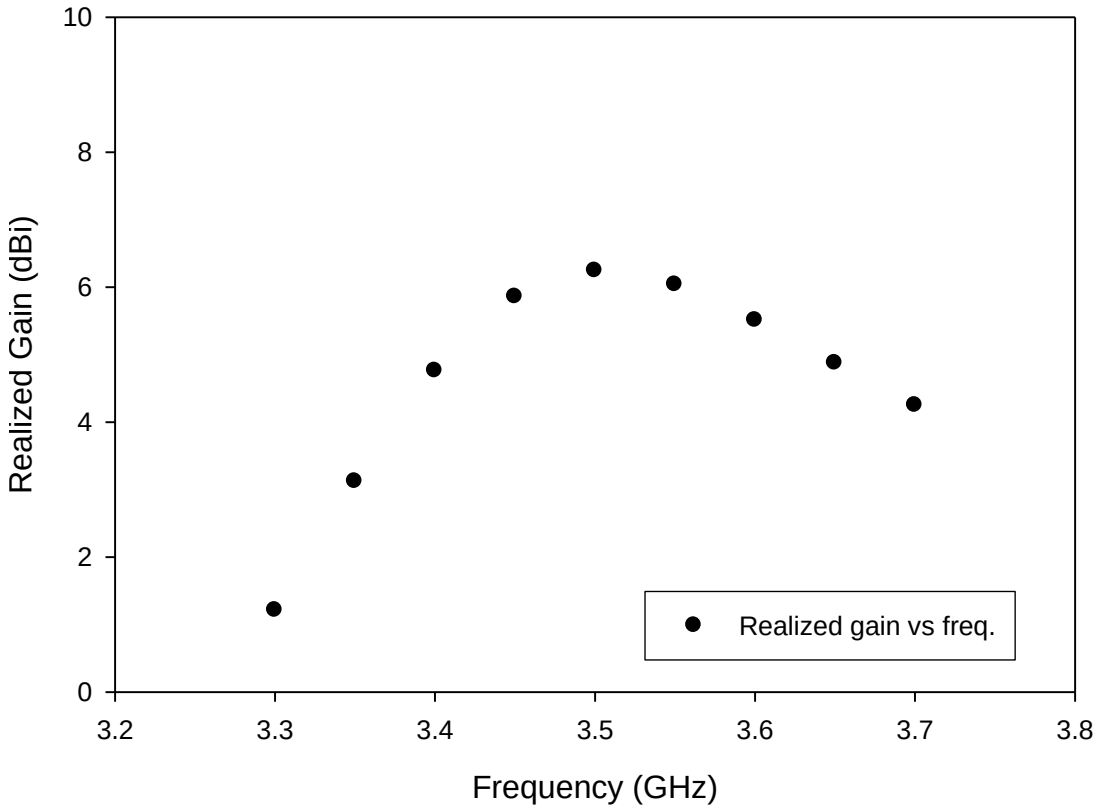

Figure 3.32 Realized gain values at different frequencies for 10 mm.

As seen in Figure 3.32 the realized gain simulations for the parasitic patch at $h = 10$ mm give the best result at 3.5 GHz. At this frequency the value of the realized gain is approximately 6.4 dBi.

After determining the optimum distance of the parasitic patch for the 80×80 mm^2 ground which provided the maximum gain enhancement, the radiation patterns of the antenna at 3.5 GHz are taken in the principal cuts, which correspond to yz ($\varphi = 90°$) and xz ($\varphi = 0°$), xy ($\theta = 90°$) planes, respectively.

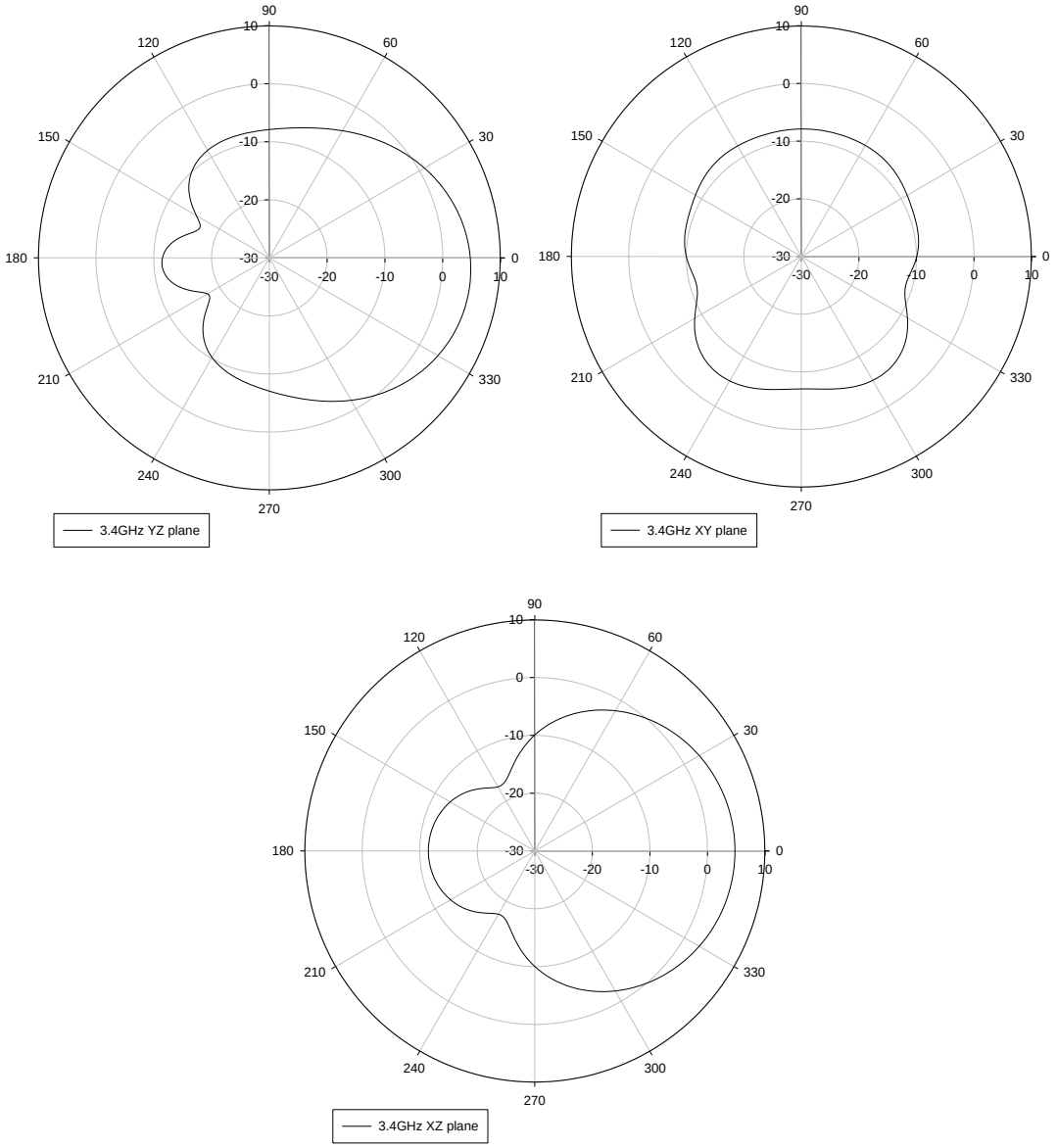

Figure 3.33 Radiation patterns at *yz*, *xy*, and *xz* planes 3.4 GHz.

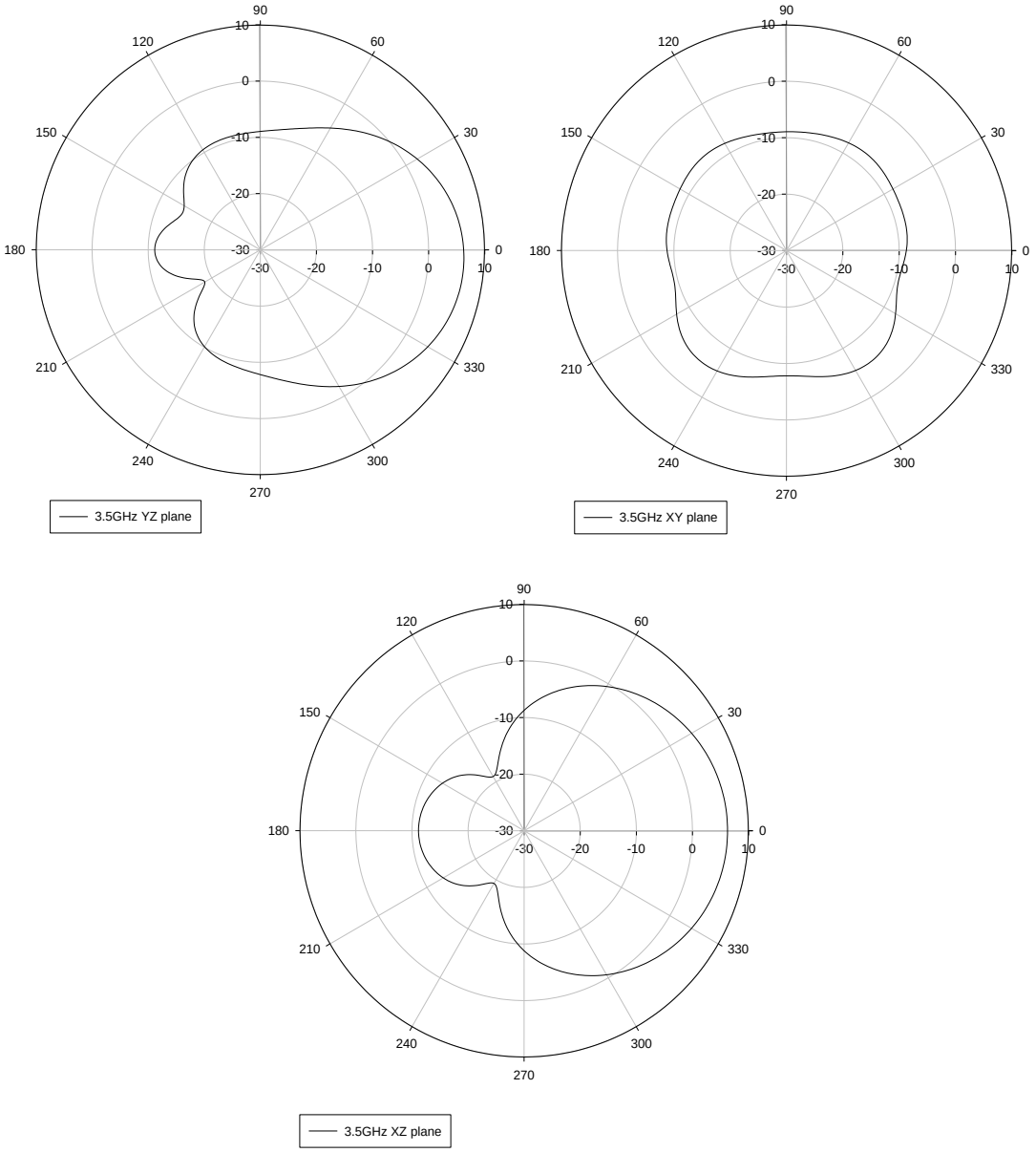

Figure 3.34 Radiation patterns at *yz*, *xy*, and *xz* planes 3.5 GHz.

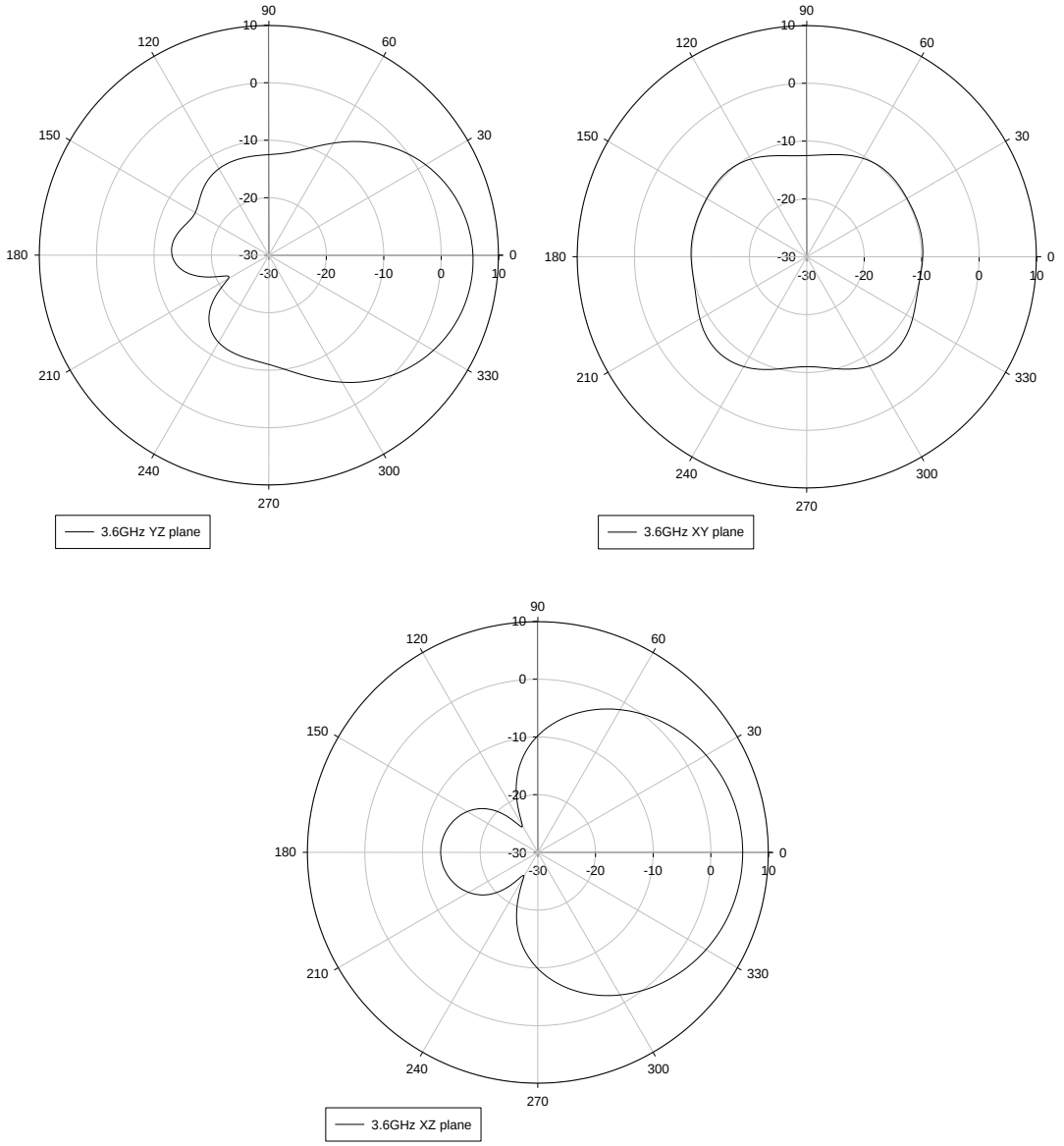

Figure 3.35 Radiation patterns at *yz*, *xy*, and *xz* planes 3.6 GHz.

As can be seen from Figs. 3.33, 3.34 and 3.35 again, the antenna has a peak gain at 3.5 GHz when the elevation angle is zero degrees. The radiation patterns do not vary significantly when the frequency is varied from 3.4 GHz to 3.6 GHz. There is not much radiation behind the ground plane. Beamwidth for 3.5 GHz is about 78º in *xz* plane and about 49º in *yz* plane.

3.6.5 Comparison of Patch Antennas on 100×100 mm^2 and 80×80 mm^2 Ground Planes

Figure 3.36 shows the comparison of the realized gains of the patch antennas on 100×100 mm^2 and 80×80 mm^2 ground planes. The maximum realized gain is achieved when $h = 15$ mm and $h = 10$ mm for the 100×100 mm^2 and 80×80 mm^2 ground planes, respectively. The patch antenna on the 80×80 mm^2 ground plane has less volume but it has about 0.5 dBi less gain than that of the 100×100 mm^2 ground plane. However the antenna is very well matched on 100×100 mm^2 ground plane. For this reason the 100×100 mm^2 ground plane has been selected over the 80×80 mm^2 ground plane for the rest of the design process.

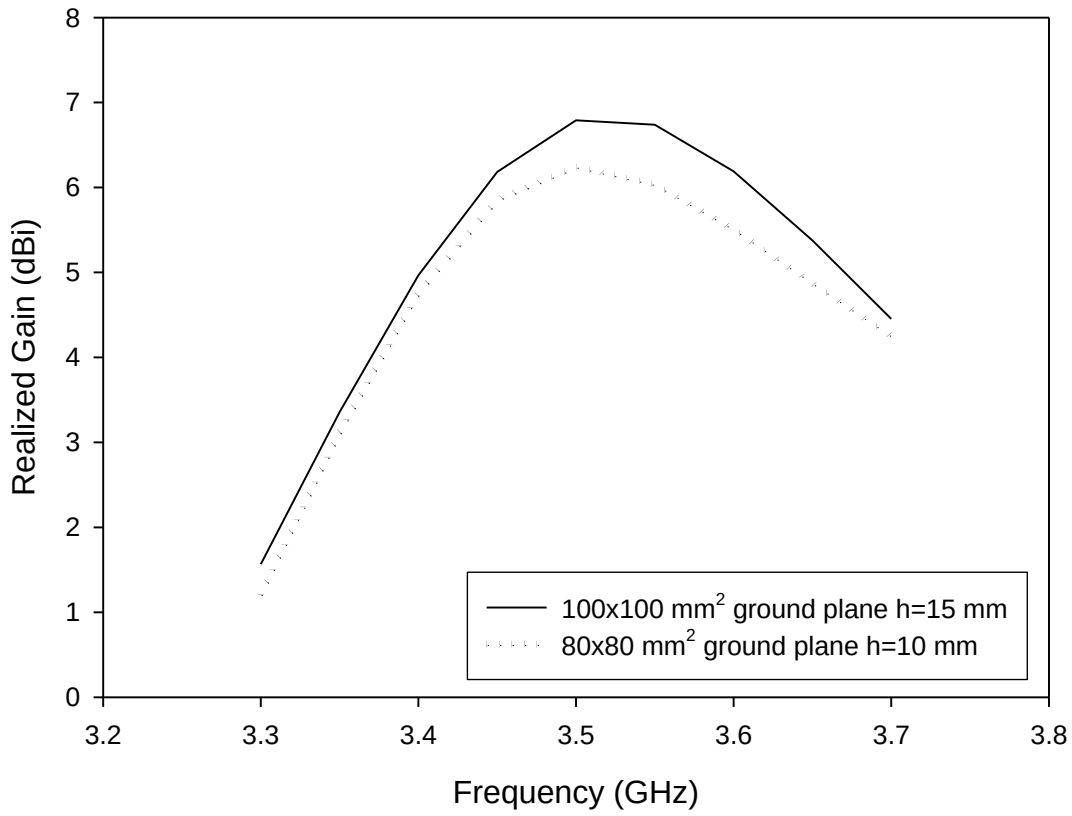

Figure 3.36 Comparison of the realized gains of the patch antennas, on different ground planes.

3.6.6 Effect of the Size of the Parasitic Patch on the Realized Gain for 80×80 mm^2 Ground Plane

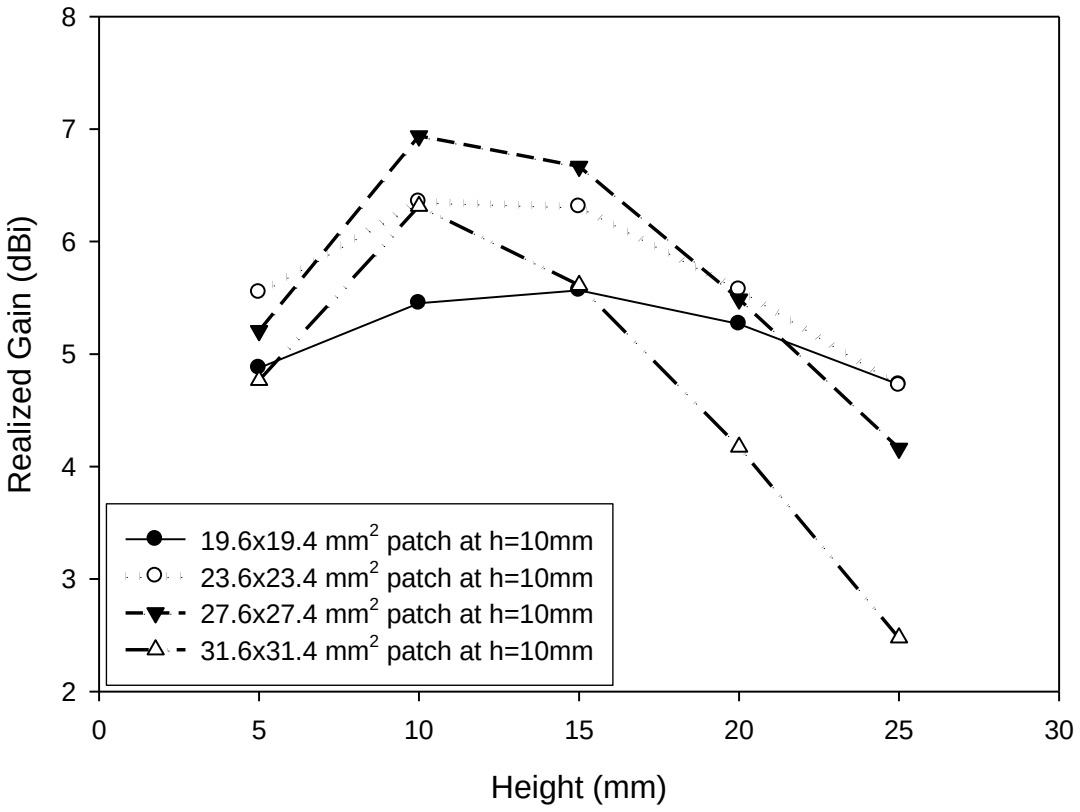

Figure 3.37 Comparison of realized gains for different size parasitic patches.

Similar to Figure 3.21 the effect of the size of the parasitic patch on the realized gain has also been studied and the results are shown in Figure 3.37. The patch sizes and the realized gains have been listed in Table 3.2.

When the parasitic patch size is 23.6×23.4 mm^2 (this is the reference parasitic patch), the realized gain is 6.36 dBi. When the reference patch size is increased 4 mm in x and y directions (the 27.6×27.4 mm^2 parasitic patch), the realized gain becomes about 6.94 dBi. When the reference patch size is increased 8 mm in x and y directions (the 31.6×31.4 mm^2 parasitic patch), a realized gain of 6.32 dBi is obtained. If the size of the reference patch is decreased by 4 mm in x and y directions, the realized gain becomes about 5.45 dBi.

Table 3.2 Parasitic patch is at $h = 10$ mm and ground plane is 80×80 mm^2.

Patch size (mm^2)	Realized Gain (dBi)
23.6×23.4 (ref. design)	6.36
27.6×27.4 (+4 mm)	6.94
31.6×31.4 (+8 mm)	6.32
19.6×19.4 (-4 mm)	5.45

It can be seen that the maximum realized gain is achieved when the patch size is 27.6×27.4 mm^2 . The realized gain is about 7 dBi for this case.

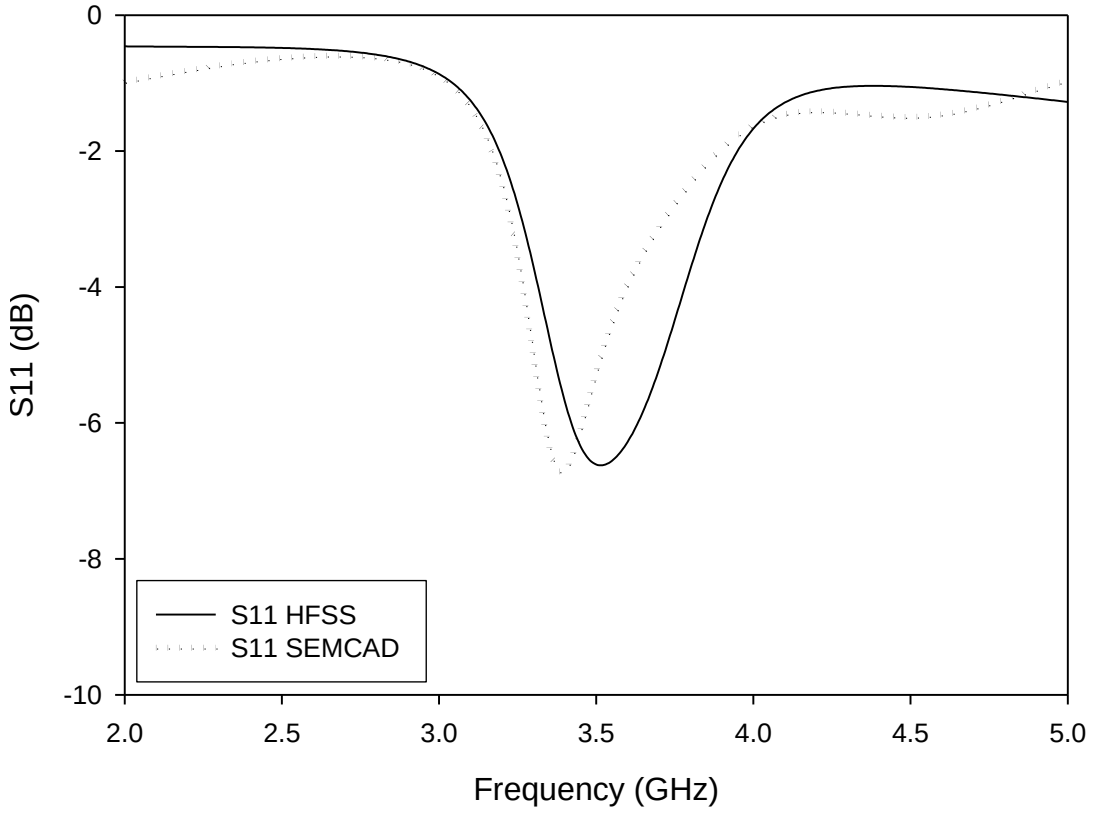

Figure 3.38 S11 of the patch antenna for $h = 10$ mm and parasitic patch size is 27.6×27.4 mm^2.

Figure 3.38 shows HFSS and SEMCAD simulated S11 of the patch antenna for $h = 10$ mm and when the parasitic patch size is 27.6×27.4 mm^2. It can be seen that the agreement between HFSS and SEMCAD simulations is very good.

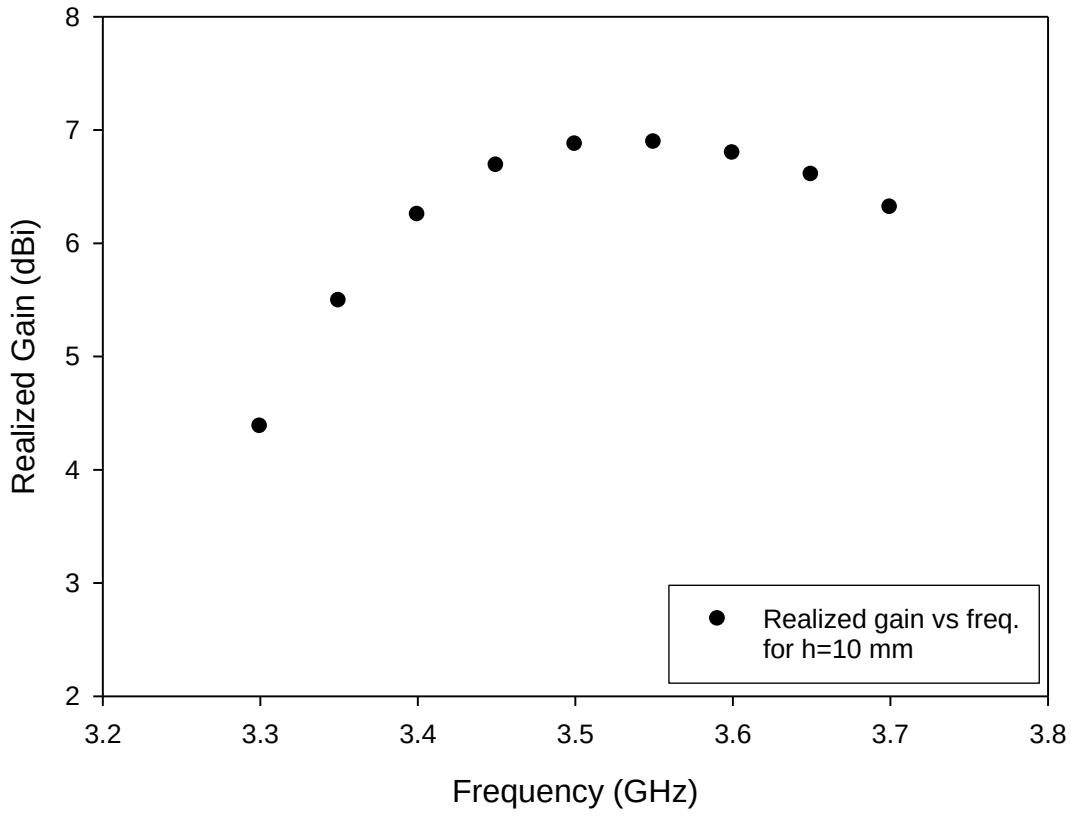

Figure 3.39 Realized gain as function of the frequency when the parasitic patch is 10 mm above the main patch and parasitic patch size is 27.6×27.4 mm^2.

As seen in Figure 3.39 the realized gain simulations for the parasitic patch at $h = 10$ mm give the best result at 3.5 GHz. At this frequency the value of the realized gain is about 7 dBi.

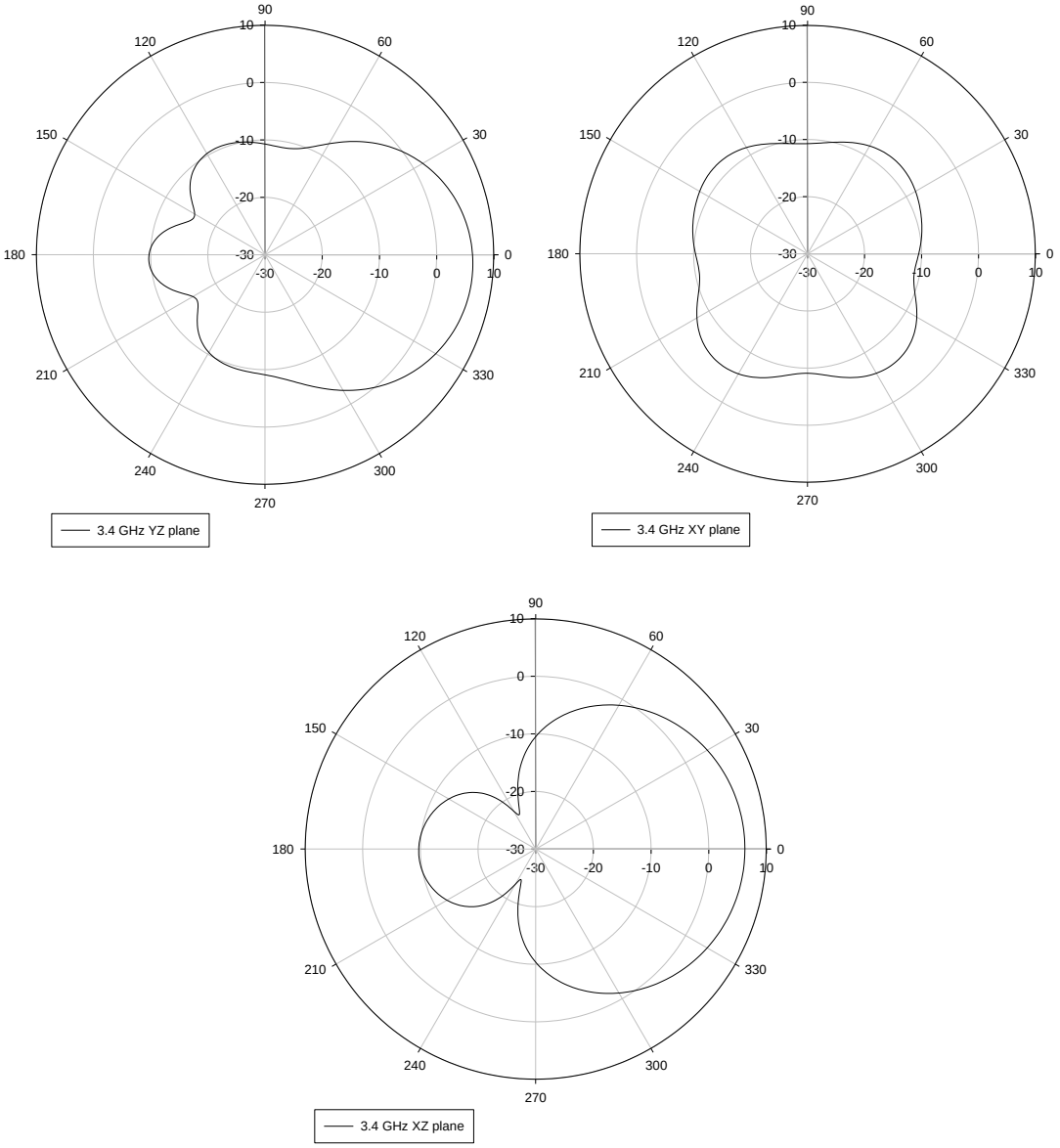

Figure 3.40 Radiation patterns at *yz*, *xy*, and *xz* planes 3.4 GHz.

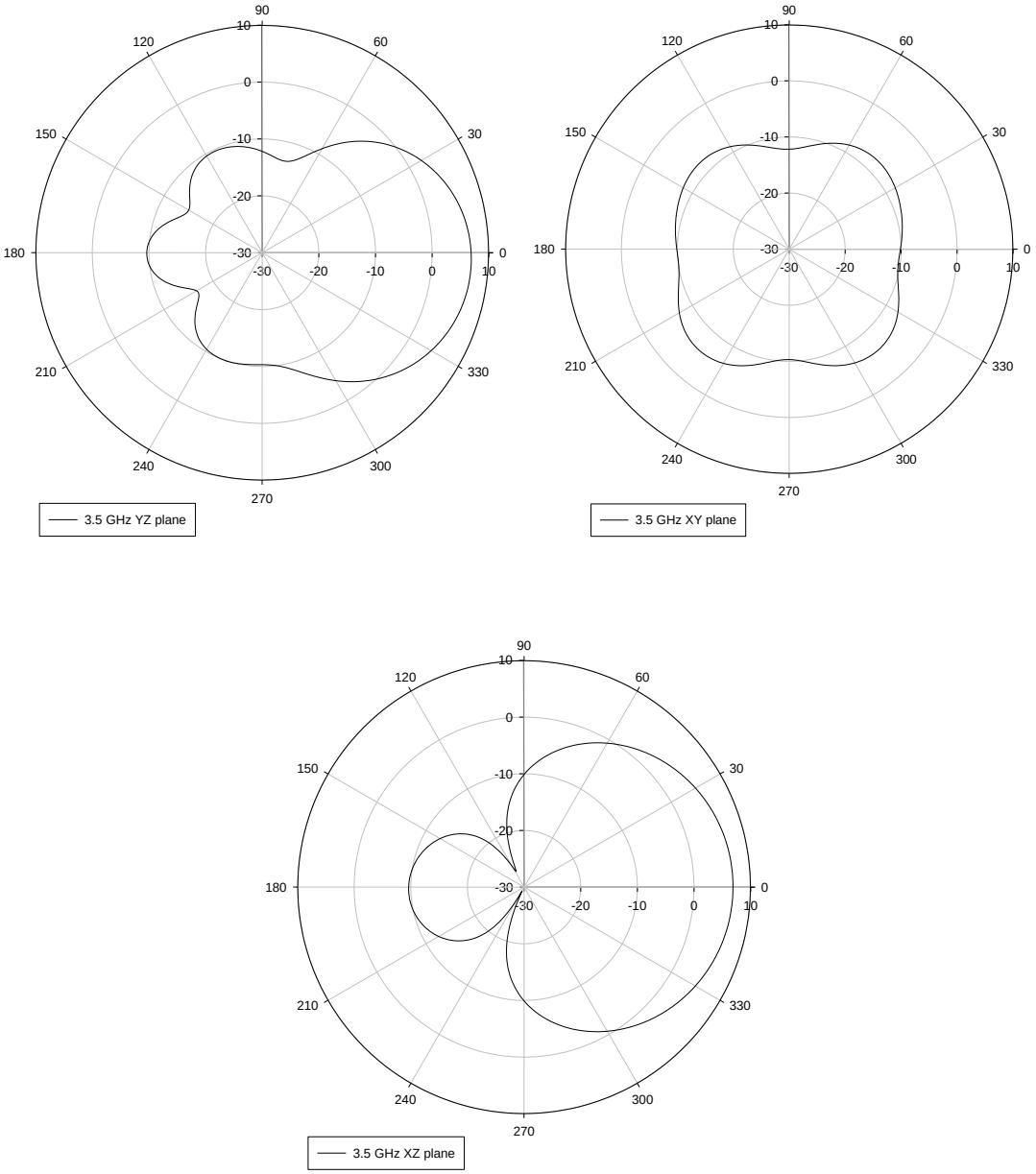

Figure 3.41 Radiation patterns at *yz*, *xy*, and *xz* planes 3.5 GHz.

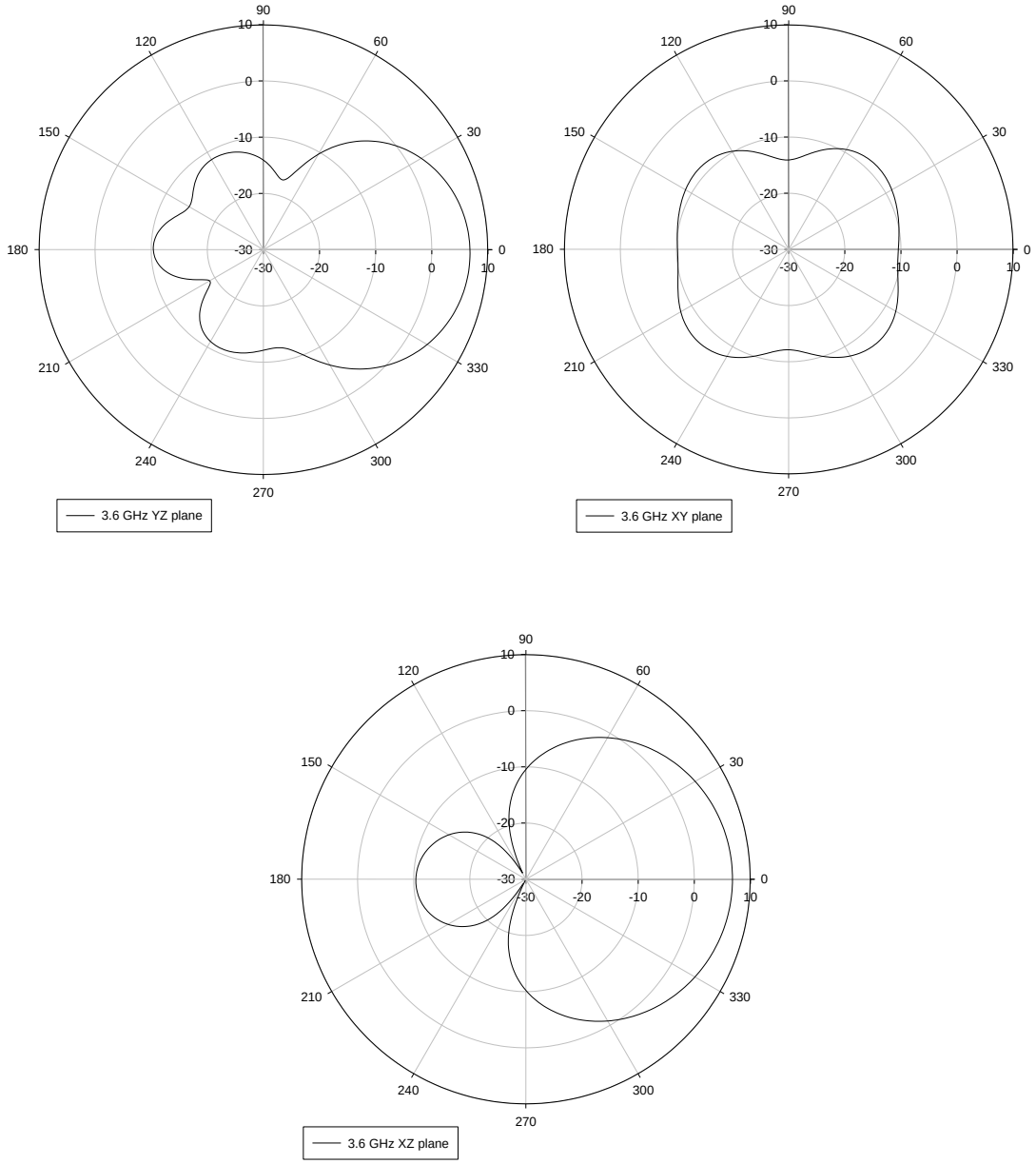

Figure 3.42 Radiation patterns at *yz*, *xy*, and *xz* planes 3.6 GHz.

As can be seen from Figs. 3.40, 3.41 and 3.42, the antenna has almost the peak gain at 3.5 GHz when the elevation angle is zero degrees. The radiation patterns do not vary significantly when the frequency is varied from 3.4 GHz to 3.6 GHz. There is not much radiation behind the ground plane.

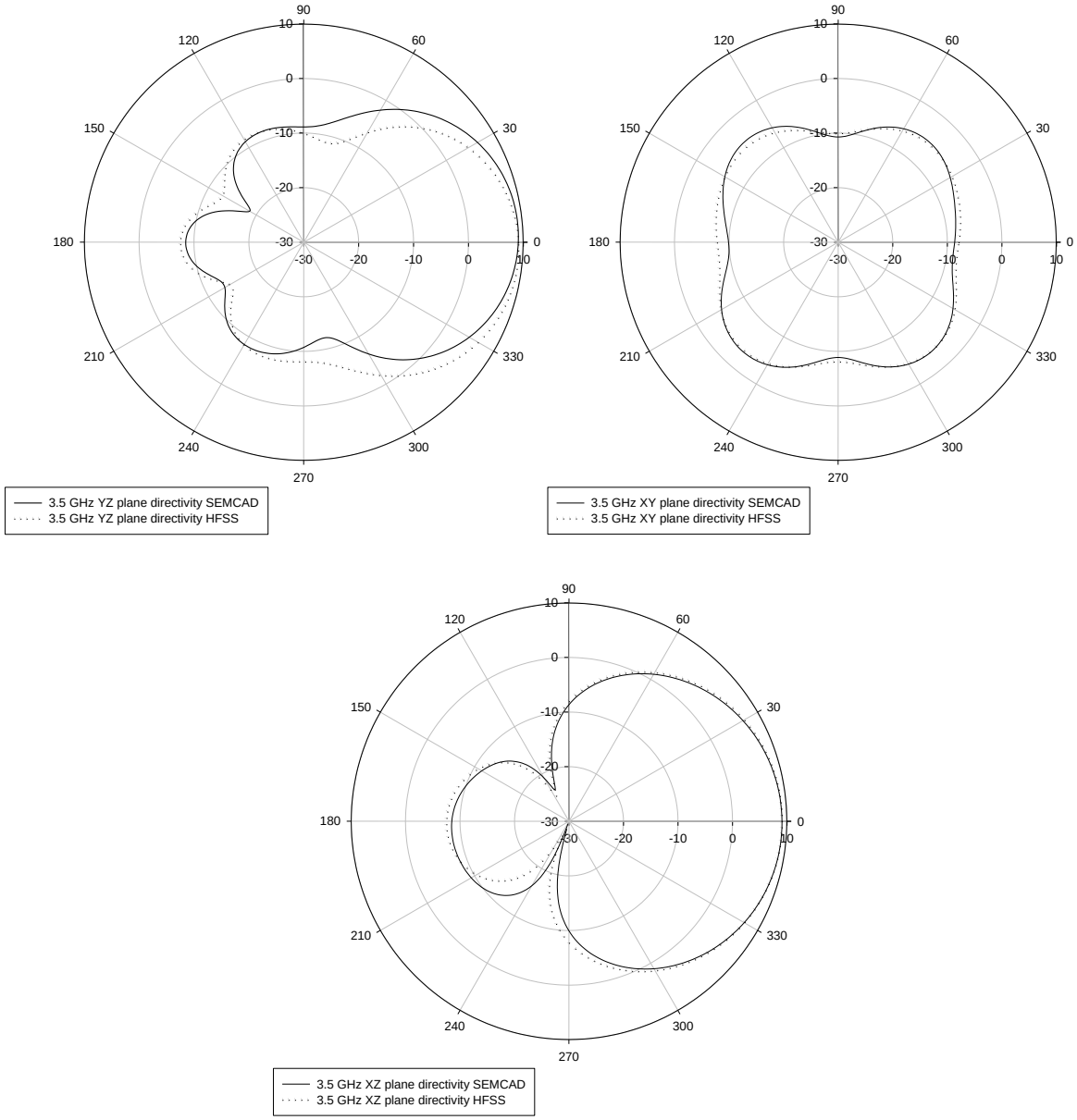

Figure 3.43 Directive pattern of the patch antenna for $h = 10$ mm and parasitic patch size is 27.6×27.4 mm^2 at 3.5 GHz**.**

Figure 3.43 shows that directive pattern of the patch antenna at 3.5 GHz, for $h = 10$ mm and 27.6×27.4 mm^2 parasitic patch size. It can be seen from the Figure 3.43 that SEMCAD and HFSS simulations are in excellent agreement.

3.6.7 The Patch Antenna with Side Walls (Right and Left)

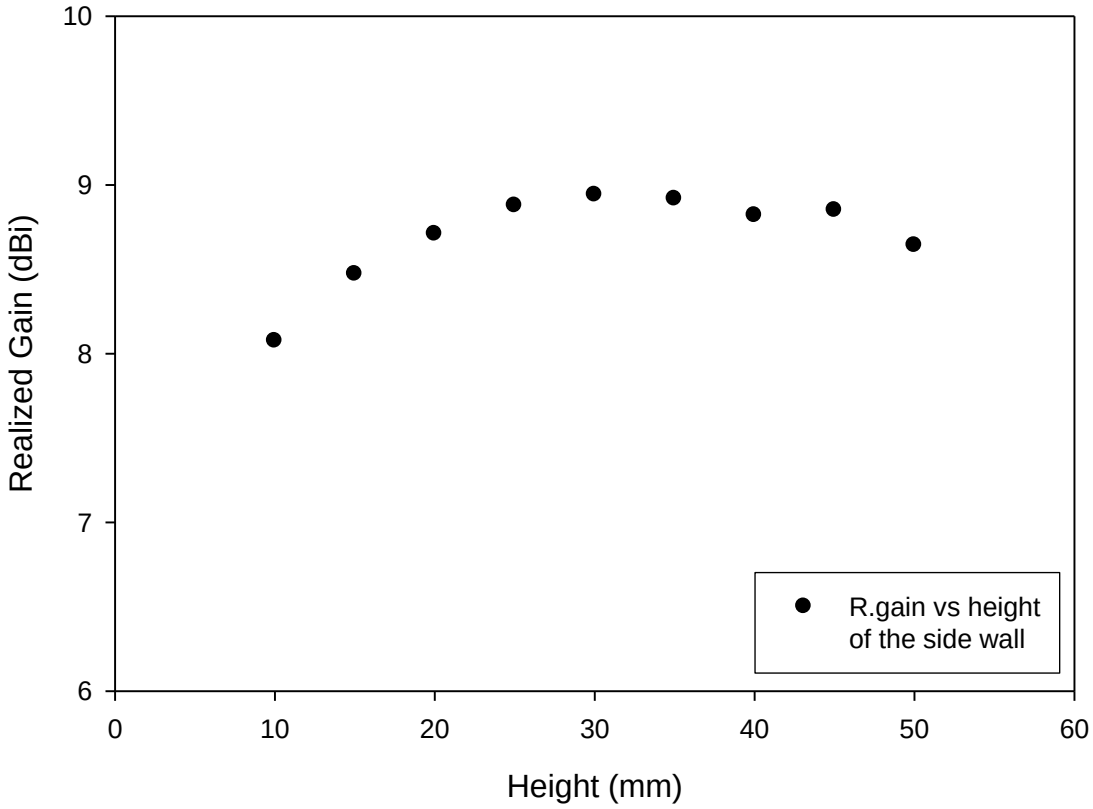

Figure 3.44 Realized gain of the patch antenna when the height of the side walls is varied.

Previously it was observed that the maximum realized gain occurs when the size of the parasitic patch is selected as 27.6×27.4 mm^2, when it is placed 15 mm above the main patch, and when the RF ground plane dimensions are 100×100 mm^2. In this section the effect of the side walls have been investigated. For this purpose, two side walls have been placed as shown in Figure 3.45.

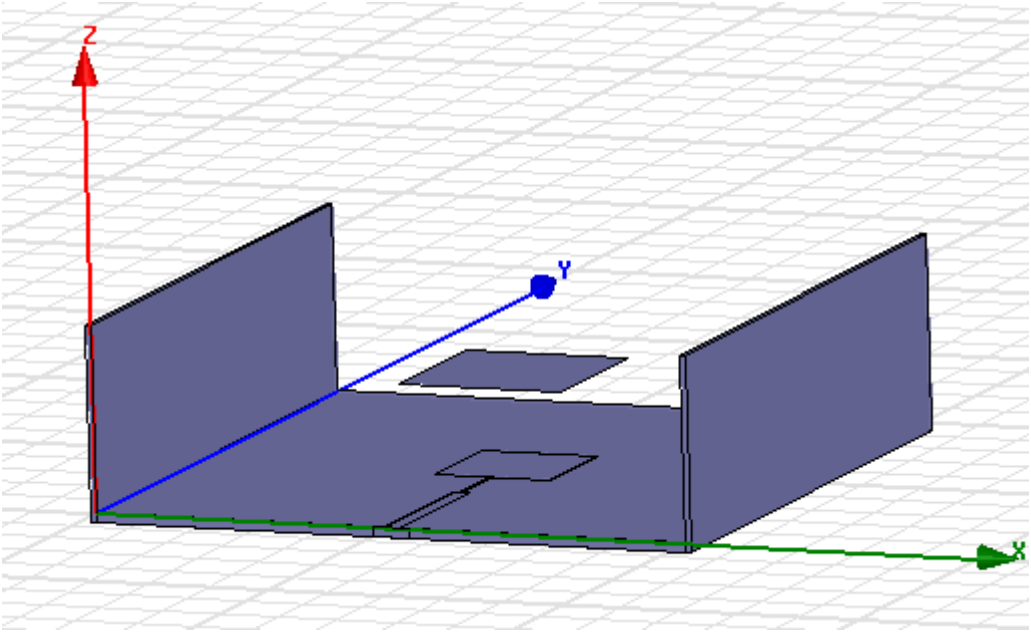

Figure 3.45 The antenna with left and right side walls.

When the height of the side walls is varied from 10 mm to 50 mm with 5 mm steps the realized gain varies as shown in Figure 3.44. The maximum realized gain is about 9 dBi when the height of the side walls is 30 mm.

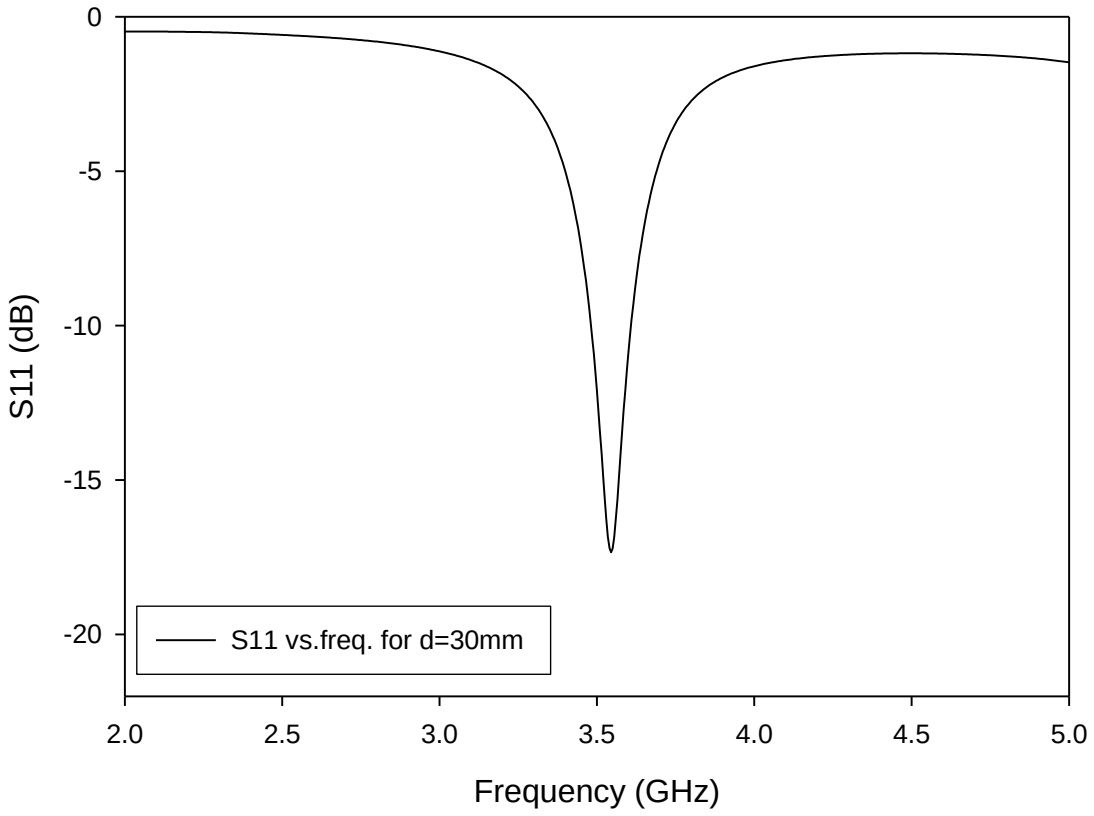

Figure 3.46 S11 of the patch antenna with side walls, height of the side walls.

S11 of the antenna for this case is shown in Figure 3.46. It can be seen that the antenna is well matched is 3.5 GHz in the presence of side walls except a slight shift in frequency.

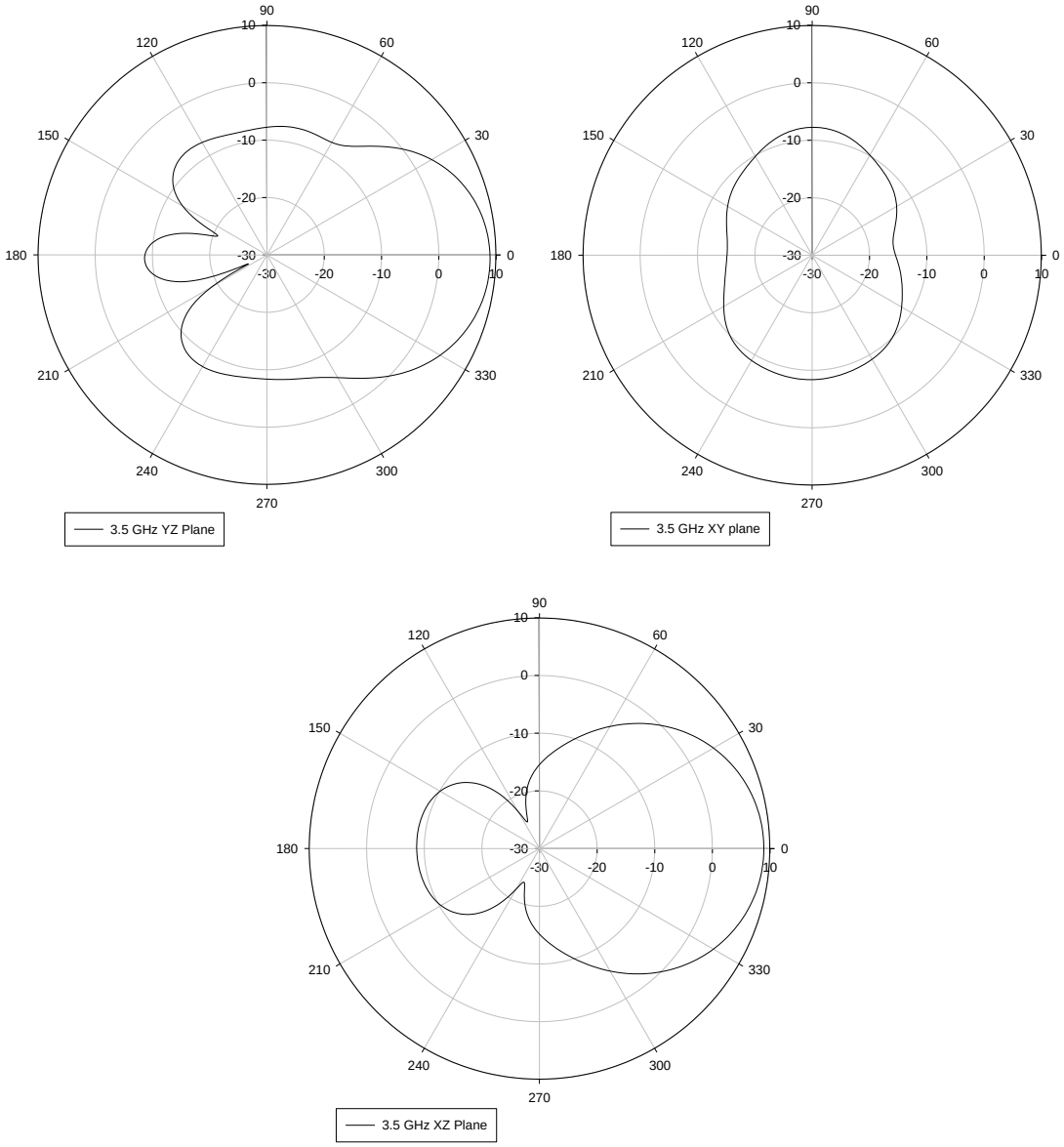

Figure 3.47 Radiation patterns at *yz*, *xy*, and *xz* planes 3.5 GHz**.**

As can be seen from Figs. 3.47 the antenna has a peak gain at 3.5 GHz when the elevation angle is zero degrees. There is not much radiation behind the ground plane. Beamwidth for 3.5 GHz is 51º in *xz* plane and 41º in *yz* plane.

3.6.8 The Patch Antenna with Three Side Walls (Right, Left and Behind)

In this section the effect of the three side walls have been investigated. For this purpose, a "behind" wall has been placed as shown in Figure 3.48.

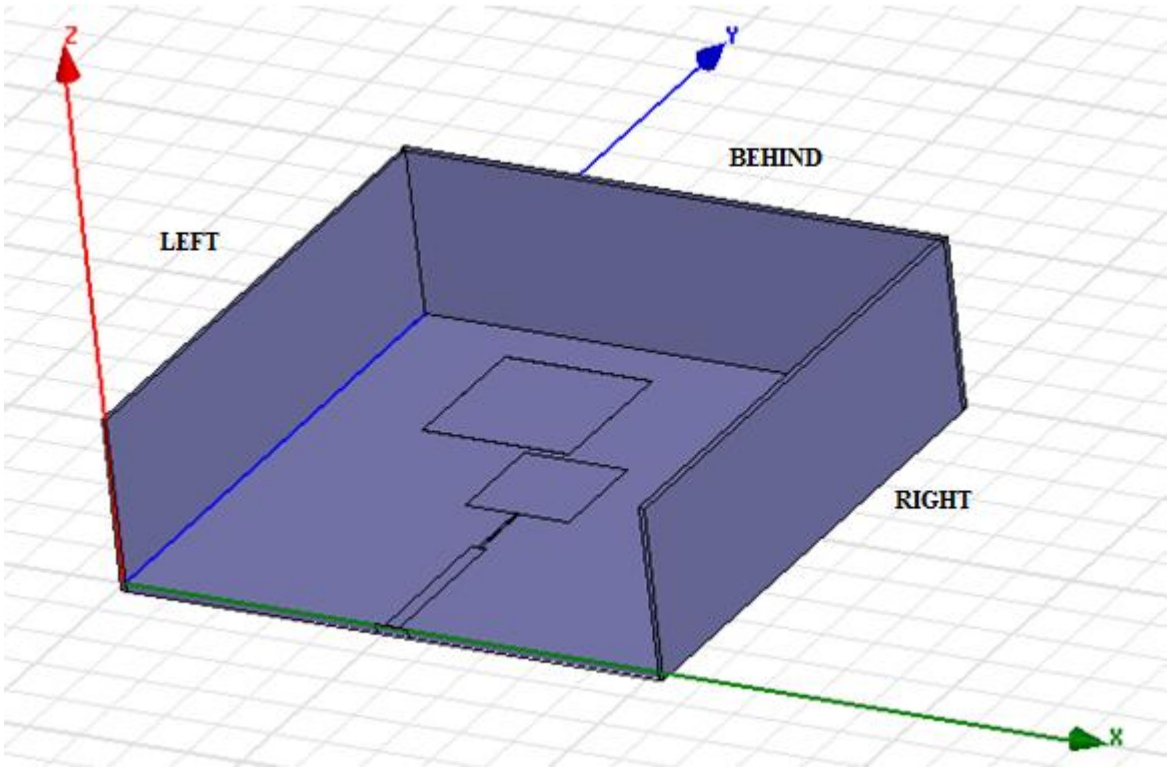

Figure 3.48 The antenna with left, right and behind walls.

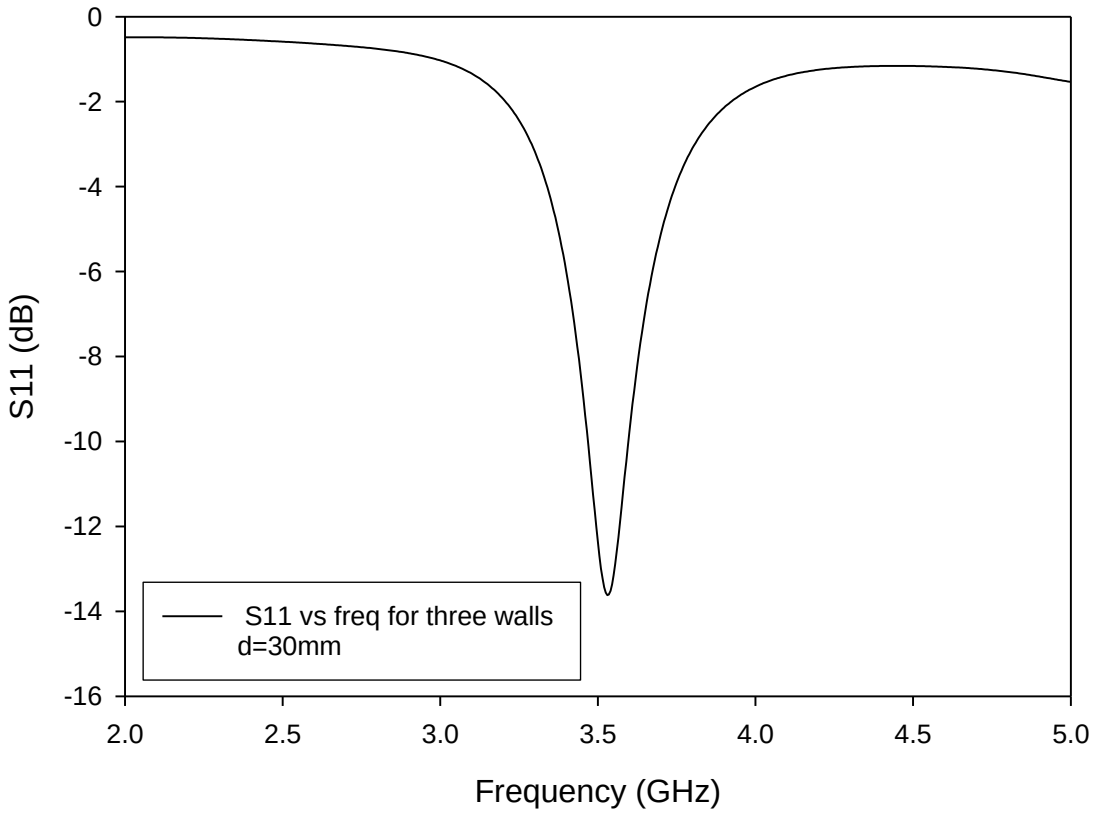

Figure 3.49 S11 of the patch antenna with side and behind walls.

S11 of the antenna with three walls case is shown in Figure 3.49. It can be seen that the antenna is well matched at 3.5 GHz in the presence of the side walls except a slight shift in frequency.

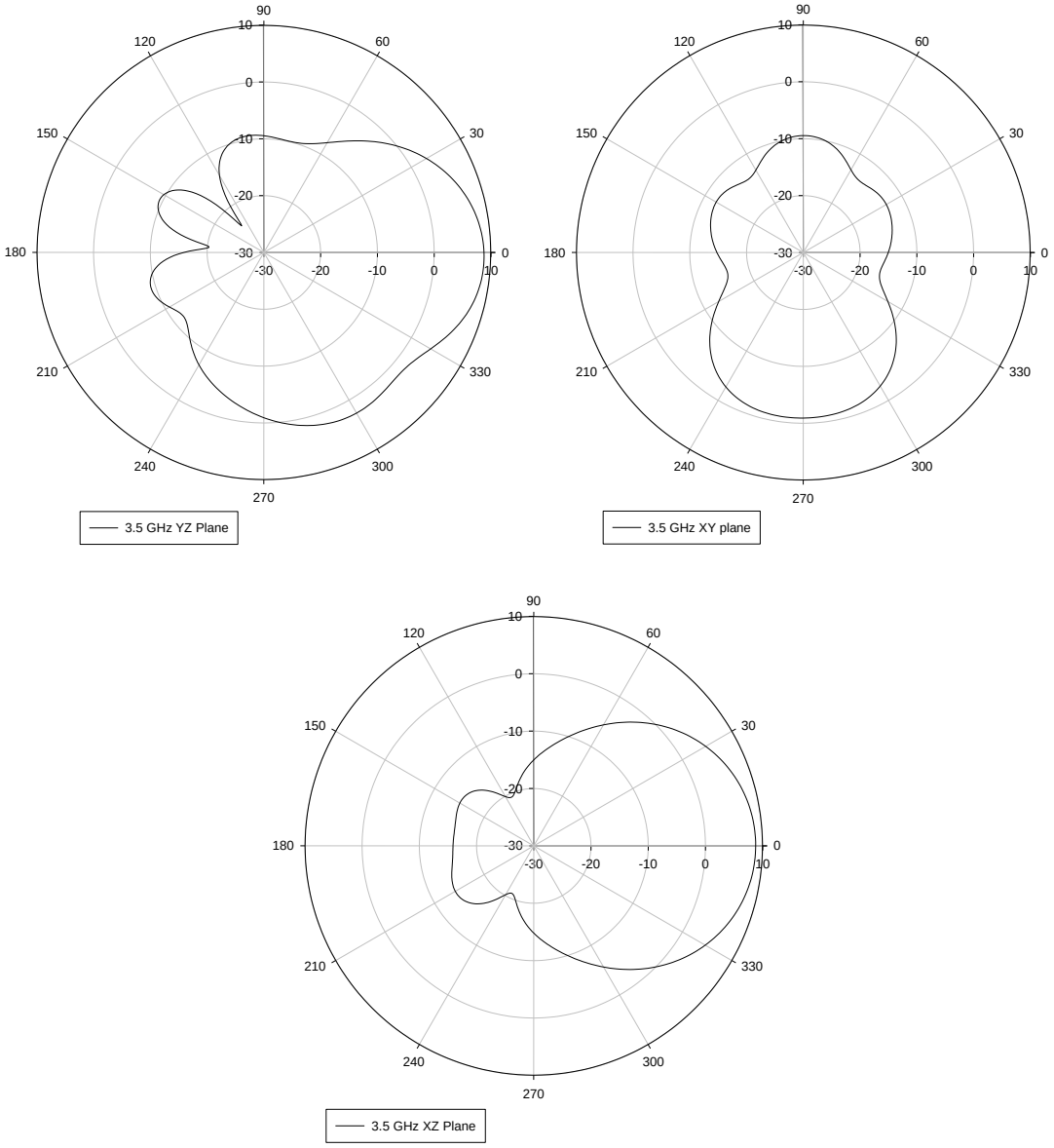

Figure 3.50 Radiation patterns at *yz*, *xy*, and *xz* planes 3.5 GHz.

When there is only the parasitic patch the main beam is directed in *z* direction. When the two side walls are added the antenna gain increases and the main beam still points the *z* direction. However when we add the third wall, a side lobe appears beside the main beam. For this reason, the antenna with three side walls is not a desirable design and the antenna with two side walls is selected for fabrication.

3.6.9 The Patch Antenna with Two Side Walls and an Upper Dielectric Layer

In the last section the effect of the right and left side walls and an upper dielectric layer on the antenna radiation pattern have been examined. For this purpose, an upper dielectric layer has been placed as shown in Figure 3.51.

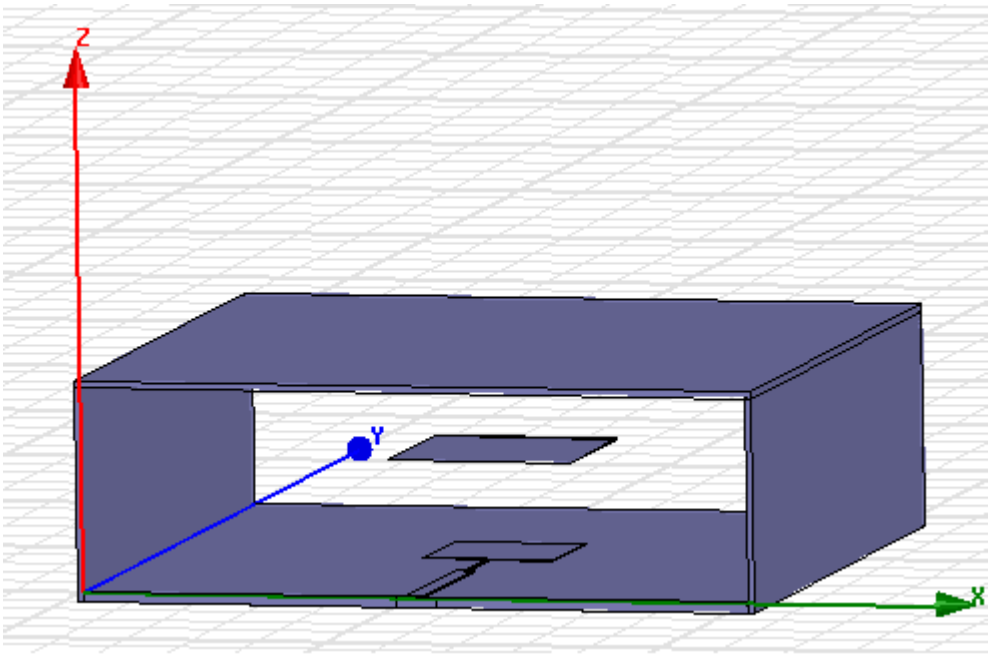

Figure 3.51 The antenna with left and right side walls, and upper dielectric layer.

This layer has been placed to protect the patch antenna and the parasitic radiator. The dimensions of the upper dielectric layer is 102×100 mm^2 and made of FR4-type easily available material. The thickness of the FR4 upper layer is 1 mm.

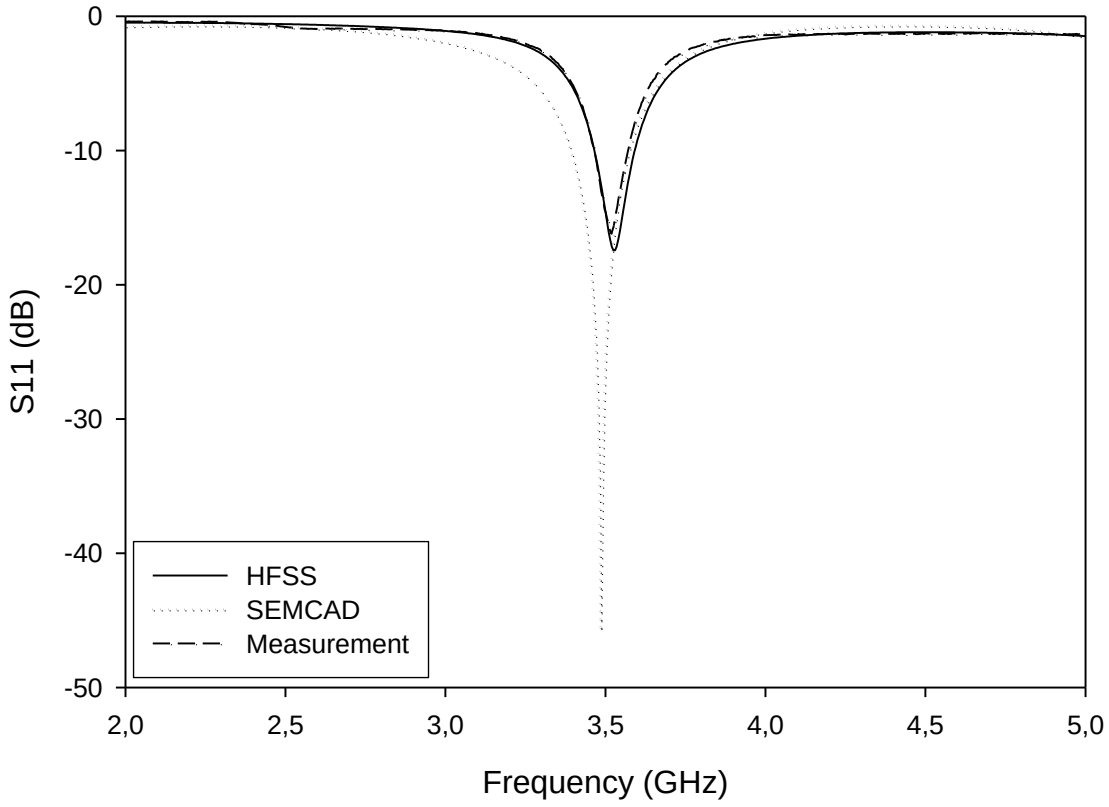

Figure 3.52 S11 of the patch antenna with two side walls and an upper FR4 layer.

S11 of the antenna for this case can be seen in Figure 3.52. The antenna is very well matched at 3.5 GHz in the presence of the side walls and upper FR4 layer. It can be seen from the Figure 3.52 that measurement and HFSS simulation are in excellent agreement. Antenna S11 measurements have been performed at Tübitak BİLGEM Electromagnetic and Antenna Systems Division using an Anritsu MS2037C/2 Vector Network Analyzer (VNA).

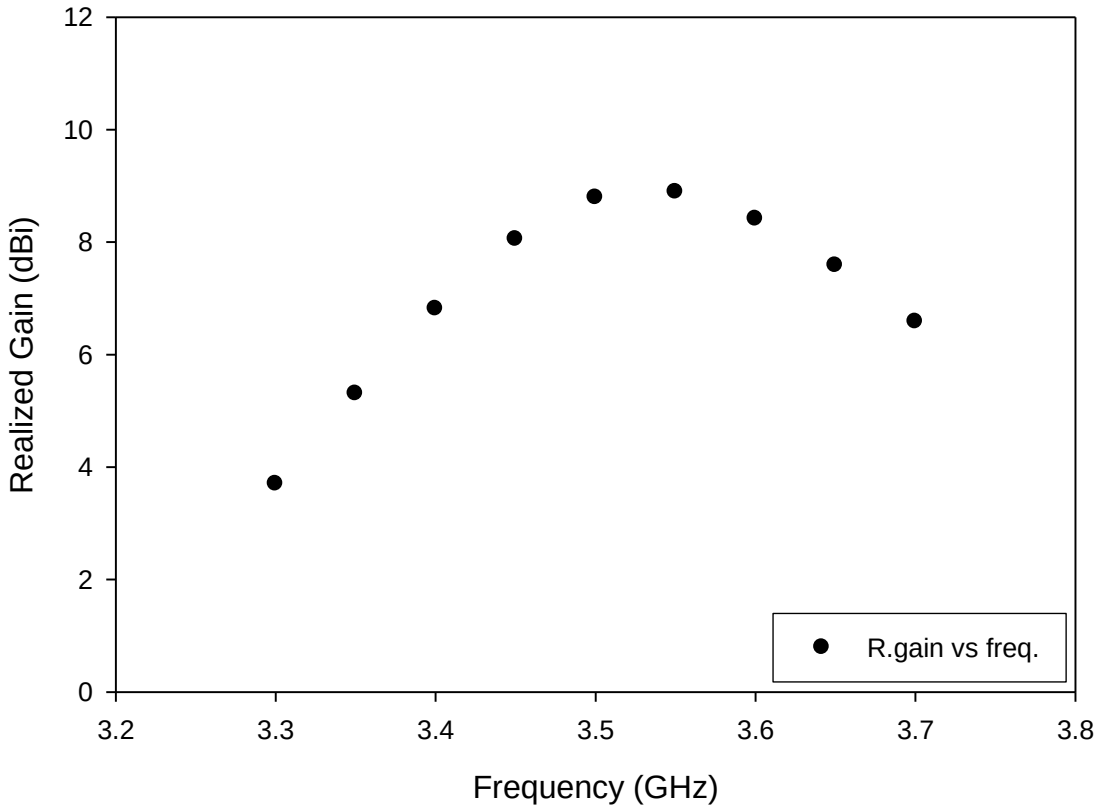

Figure 3.53 Realized gain versus frequency.

As seen in Figure 3.53 the realized gain simulations for the two side walls and upper dielectric layer give the best result at 3.5 GHz. At this frequency the value of the realized gain is approximately 9 dBi.

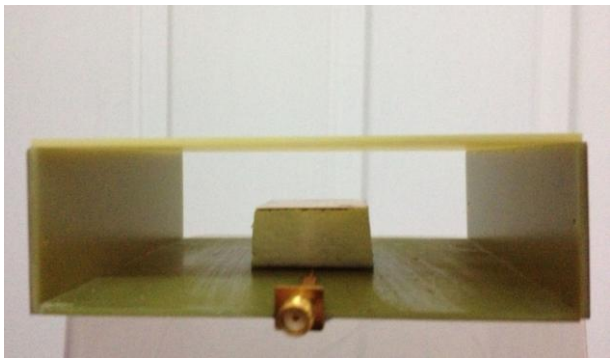

Figure 3.54 A photograph of the fabricated patch antenna with a parasitic patch, two side walls, and an upper dielectric layer.

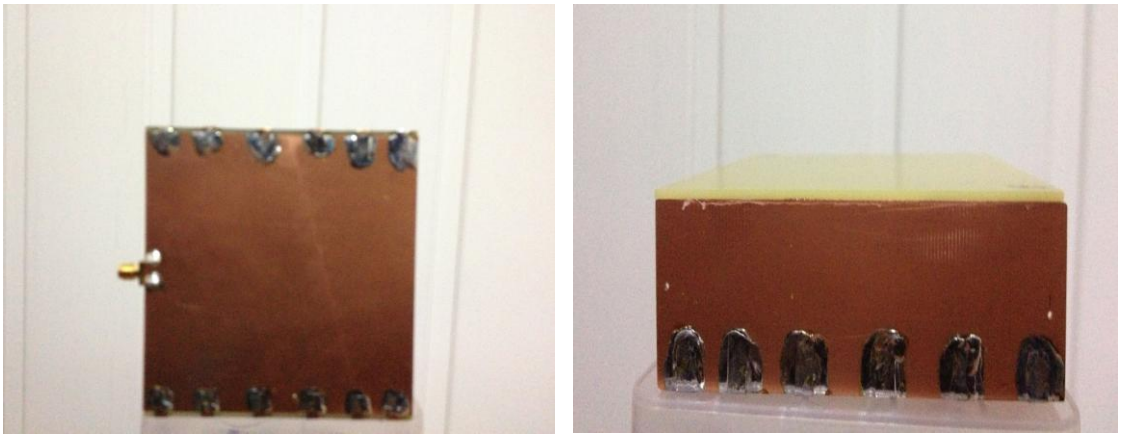

Figure 3.55 Photographs of the fabricated patch antenna with a parasitic patch, two side walls, an upper dielectric layer and SMA connector.

It can be seen from the Figure 3.54 and 3.55, the two side walls have been connected to RF ground by soldering narrow copper sheets at multiple points for better RF grounding.

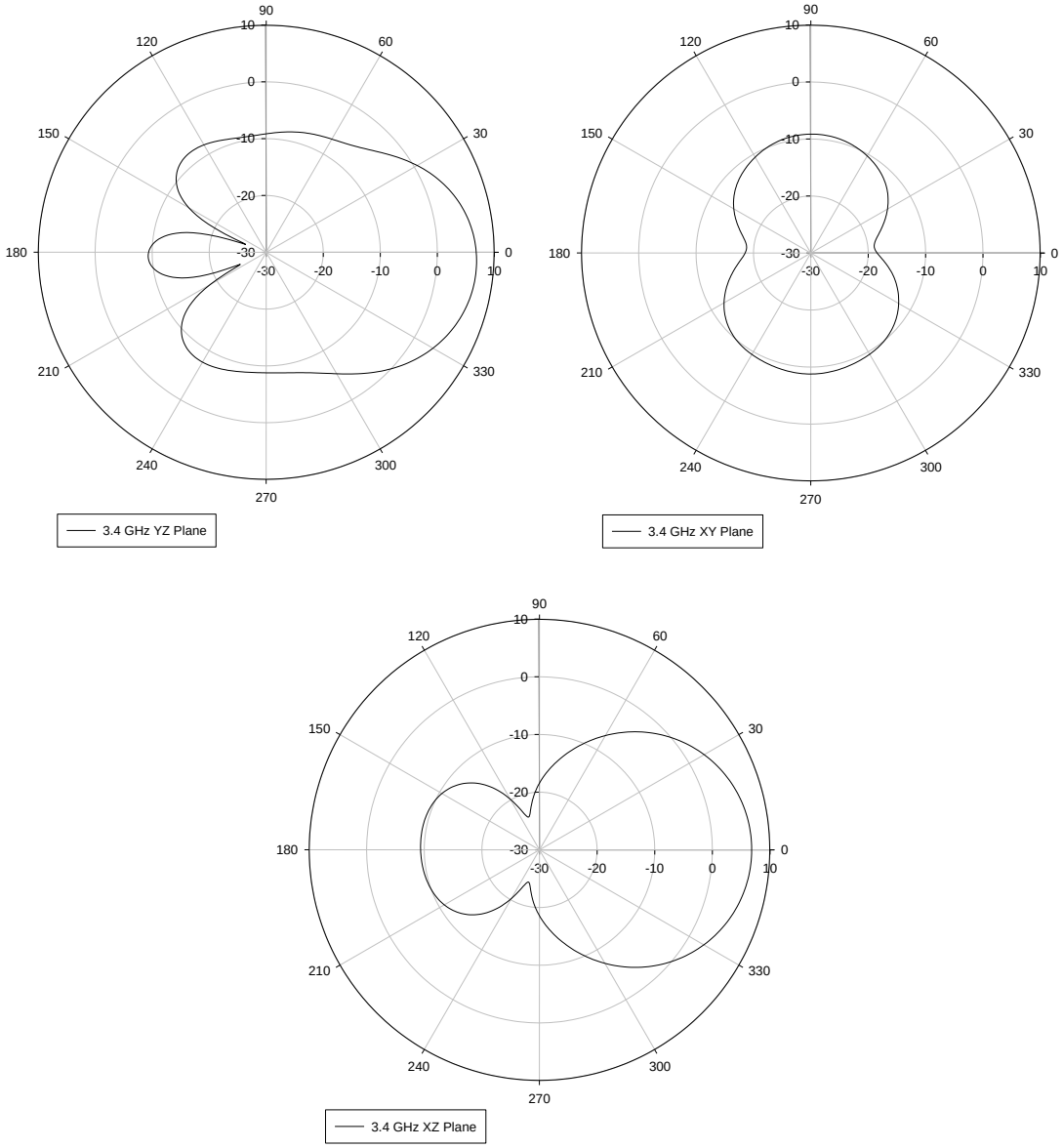

Figure 3.56 Radiation patterns at *yz*, *xy*, and *xz* planes 3.4 GHz.

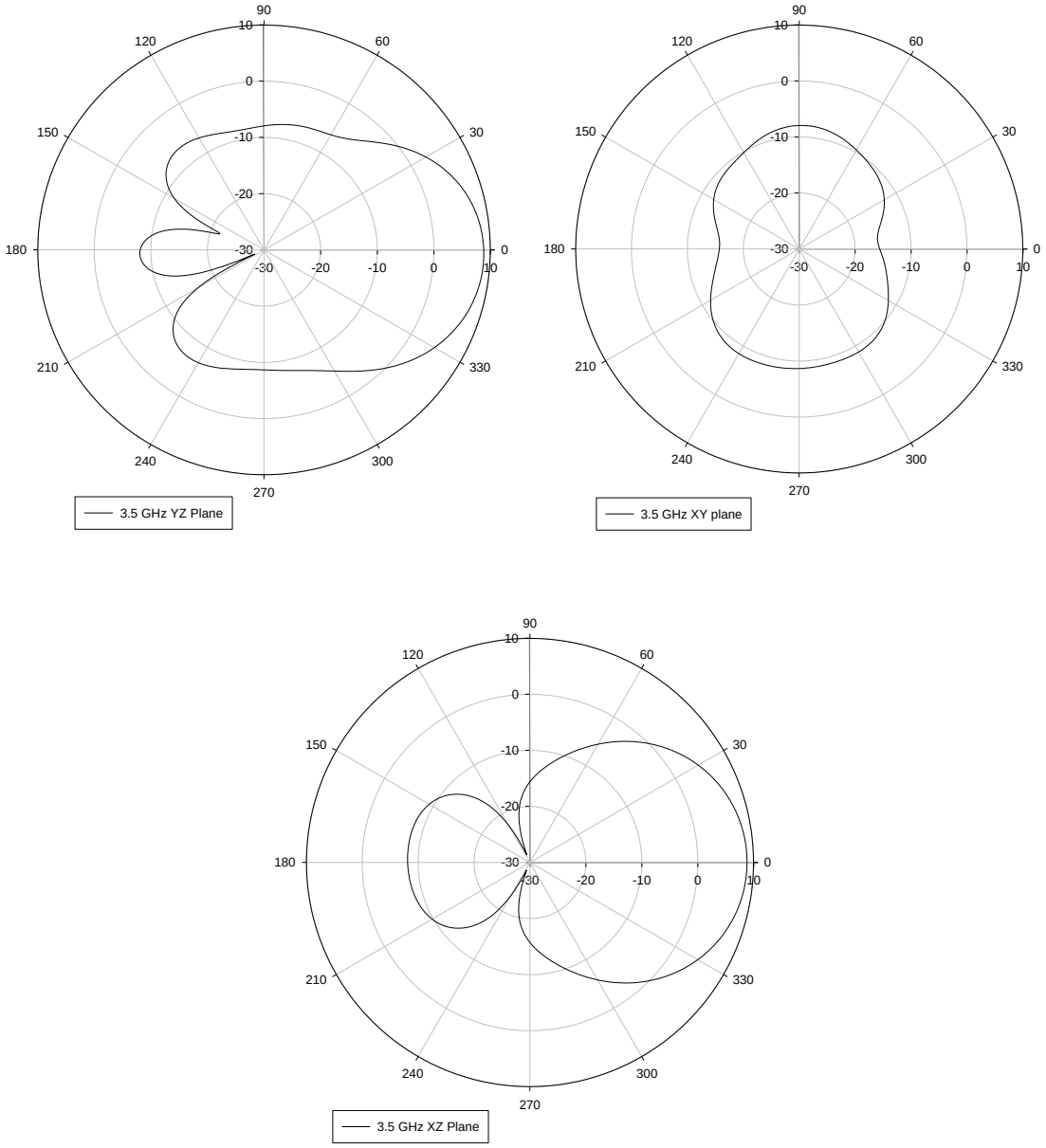

Figure 3.57 Radiation patterns at *yz*, *xy*, and *xz* planes 3.5 GHz.

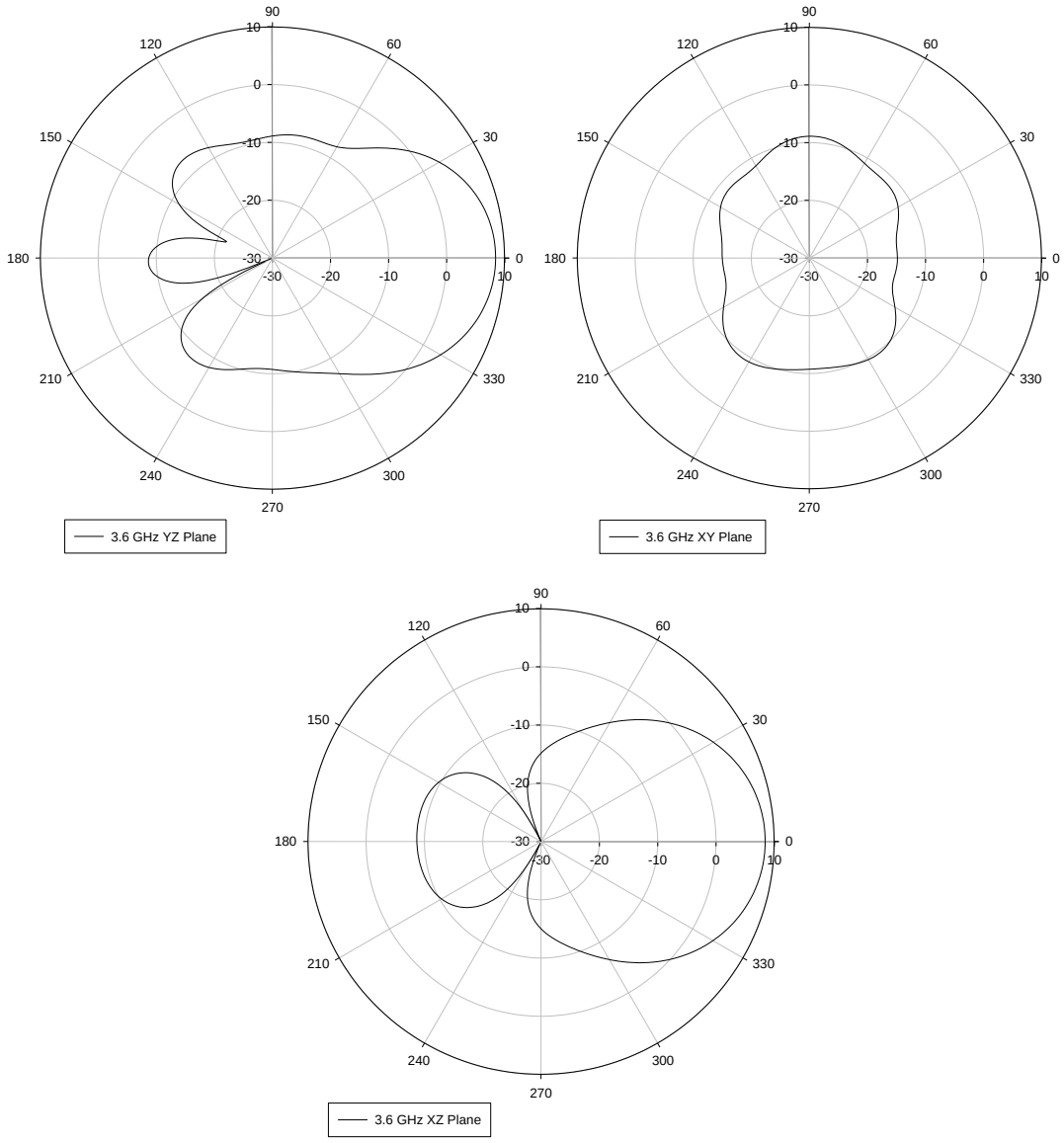

Figure 3.58 Radiation patterns at *yz*, *xy*, and *xz* planes 3.6 GHz.

As can be seen from Figs. 3.56, 3.57 and 3.58 the antenna has a peak gain at 3.5 GHz when the elevation angle is zero degrees. The radiation patterns do not vary significantly when the frequency is varied from 3.4 GHz to 3.6 GHz. There is not much radiation behind the ground plane. Beamwidth for 3.5 GHz is about 52º in *xz* plane and about 42º in *yz* plane.

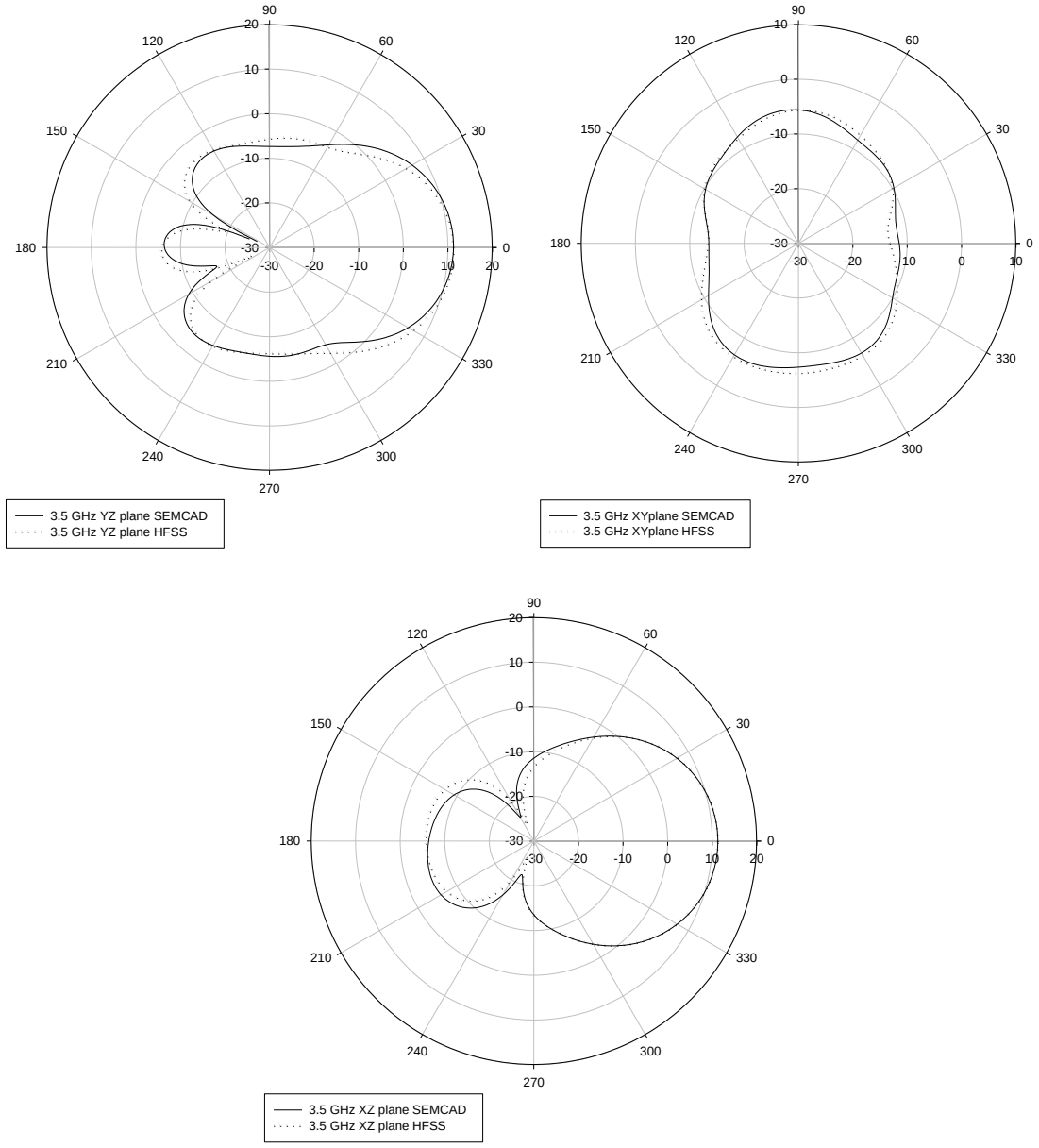

Figure 3.59 Directive pattern of the patch antenna for $h = 15$ mm and parasitic patch size is 27.6×27.4 mm^2 at 3.5 GHz**.**

It can be seen from the Figure 3.59 that SEMCAD and HFSS directive pattern simulations are in excellent agreement. Finally the patch antenna with a parasitic patch at $h = 15$ mm and a parasitic patch size of 27.6×27.4 mm^2 is selected for fabrication. Also RF ground dimensions are selected 100×100 mm^2. S11 measurements of various designs have been added to this thesis.

4. CONCLUSION

A new and simple technique of improving the gain of a microstrip patch-type WiMAX antenna operating at 3.5 GHz using a nearly square shaped parasitic radiator and a raised ground plane is presented in this thesis. To increase the antenna gain, a parasitic radiator is placed on top of the patch antenna. The patch antenna has been built on low-cost and easily available 1.6 mm thick FR4-type substrate with a relative permittivity of 4.4 and a loss tangent of 0.02. Moreover, 100×100 mm^2 and 80×80 mm^2 RF ground planes have been examined for this process. It was observed that the gain increase is maximum when the distance between the parasitic patch and the main patch is about 15 mm for a 100×100 mm^2 RF ground plane, and when the parasitic patch has a size of 27.6×27.4 mm^2. A gain improvement of about 3 dB has been obtained for this case. Additional gain improvement in the order of 1-2 dB has been achieved by adding left and right metallic side walls that are shorted to RF ground. The effect of the different heights of the two side walls on the antenna performance has been examined. The best result has been obtained at 30 mm. The behind wall has not been placed because of an undesirable effect on the radiation pattern of the antenna. Finally an FR4 layer has been placed on top to protect the patch antenna and the parasitic radiator from impacts. The thickness of the FR4 upper dielectric layer is 1 mm. With this technique, a gain improvement of about 5.2 dB has been achieved without the need of an RF amplifier.

The patch antenna is driven by a 50-Ω microstrip line. Impedance matching between the driving port (SMA connected port) and the antenna has been realized using a quarter-wave long transformer. Antenna VSWR is about 1.2 dB at the operating frequency of 3.5 GHz. A foam-type material whose relative permittivity is very close to that of the air has been placed between the patch and the parasitic layer as a mechanical support. Finally a prototype of the proposed antenna operating in the 3.5 GHz WiMAX band has been constructed on FR4 substrate.

It has been shown that the gain of a conventional microstrip patch antenna can be increased from 3.6 dBi to 8.8 dBi corresponding to about 5.2 dB enhancement in gain. The impedance and radiation performances of the proposed antenna were theoretically studied showing a good agreement between theoretical results and simulations. Antenna S11

measurements have also been added and it is shown that HFSS simulations and measurements are in excellent agreement. Given the simplicity of the technique presented in this thesis, this technique can be easily combined with other gain enhancement methods to provide even higher improvement in gain, which can be very useful for applications requiring higher gain values.

This thesis has been composed of four chapters. The first chapter includes some general introduction about antennas, WiMAX frequencies, literature review and about the antenna design. The second chapter includes general information about antenna design parameters, equations and simulation tools, HFSS and SEMCAD. Chapter 3 is the design chapter which involves the theoretical calculations about the microstrip antenna at 3.5 GHz frequency. Moreover design of the patch antenna with HFSS and SEMCAD simulations, and antenna S11 measurements have been included in this chapter. The last chapter which is chapter 4 is about conclusion.

REFERENCES

[1] Andrews, J., G., Ghosh, A., Muhamed, R., (2007), *Fundamentals of WiMAX*, Prentice Hall, February.

[2] Güngör, M., Tekin, M., A., Yılmaz, R., (2009), "WiMAX: Diğer Genişbant Telsiz Erişim (GTE) Teknolojileri ile Karşılaştırılması" *Bilgi Teknolojileri ve İletişim Kurumu Sektörel Araştırma ve Stratejiler Dairesi Başkanlığı.*

[3] Benedetto, S., Biglieri, E., (1999), *Principles of Digital Transmission: With Wireless Applications*, Springer, ISBN 0-306-45753-9.

[4] Chen, K., C., Marca, R., B., (2008), *Mobile WiMAX*, London: John Wiley & Sons.

[5] http://www.radio-electronics.com/info/wireless/wimax/frequencies-spectrum.php (07.01.2014)

[6] Hector, L., G., Schultz, H., L., (1936), "The Dielectric Constant of Air at Radiofrequencies", *Physics*, 7(4). pp. 133–136.

[7] *3D EM-Field Simulation for High Performance Electronic Design*, Pittsburgh: Ansoft Corporation, Ansoft HFSS version 11.

[8] *3D EM-Field Simulation SEMCAD, Zürich:* Schmid & Partner Engineering AG, SEMCAD version 1.8.

[9] Balanis, C., A., (2005), *Antenna Theory, Analysis and Design*, 3rd ed., New York: John Wiley & Sons.

[10] Deschamps, G., A., (1953), "Microstrip Microwave Antennas", *3rd USAR Symposium on Antennas,*

[11] Gutton, H., and G., Baissinot, (1955), "Flat Aerial for Ultra High Frequencies", *French Patent No. 703113.*

[12] Munson, R., E., (1973), "Single Slot Cavity Antennas Assembly", *U.S. Patent No.3713162*, January 23.

[13] Munson, R., E., (1972), "Microstrip Phased Array Antennas", *Proc. of Twenty-Second Symp. on USAF Antenna Research and Development Program*, October.

[14] Munson, R., E., (1974), "Conformal Microstrip Antennas and Microstrip Phased Arrays", *IEEE Transactions on Antennas and Propagation*, 22(1), 74–78.

[15] Howell, J., Q., (1975), "Microstrip Antennas", *IEEE Trans. on Antennas and Propagation*, 90-93, January.

[16] Bahl, I., (1982), "Design of microstrip antennas covered with a dielectric layer", *IEEE Transactions on Antennas and Propagation*, 30(2), 314–318, March.

[17] Garg, R., Bhartia, P., Bahl, I., Ittipiboon, A., (2001), *Microstrip Antenna Design Handbook*, Boston-London: Artech House Antennas & Propagation Library.

[18] James, J,. R., (1981), *Microstrip Antenna Theory and Design*, London and New York: Peter Peregrinus Ltd.

[19] James, J., R., and Hall, P., S., (1989), *Handbook of Microstrip Antennas*, Vols. 1 and 2, London: Peter Peregrinus Ltd.

[20] "Workshop on Printed Circuit Antenna Technology" , *Paper 31*, New Mexico State University, Las Cruces, October 1979, pp. 480.

[21] Yildirim, B., Cetiner, B., A., (2008), "Enhanced Gain Patch Antenna With a Rectangular Loop Shaped Parasitic Radiator", *IEEE Antennas and Wireless Propagation Letters*, 7.

[22] Wu, A., Guan, B., Zhang, Z., (2006), "A Novel WiMAX Patch Antenna", *Proceedings of Wireless, Mobile and Multimedia Networks, IET International Conference*, November 6-9, Hangzhou, China.

[23] Stutzman, W., L., and Thiele, G., A., (1998), *Antenna Theory and Design*, 2nd ed., New York: John Wiley.

[24] Balanis, C., A., (2008), *Modern Antenna Handbook*, New York: John Wiley & Sons.

[25] Volakis, J., L., (2007), *Antenna Engineering Handbook*, McGraw Hill Companies.

[26] Pozar, D., M., and Schaubert, D., H., (1995), *Microstrip Antenna Design*, Piscataway, New Jersey: IEEE Press.

[27] http://www.ansoft.com, "User"s guide – High Frequency Structure Simulator", Version 11, (7 December 2012).

[28] Johnson, R., C., (1993), *Antenna Engineering Handbook*, 3rd ed., Atlanta: McGraw Hill Companies.

[29] Pozar, D., M., (1992), "Microstrip Antennas", *Proc. IEEE*, 80(1), 79–81, January

[30] *Smith Software*, Burgdorf: Berne University and Applied Science, *Smith Software* version 2.03.

[31] *3D EM-Field Simulation for High Performance Electronic Design*, Pittsburgh: Ansoft Corporation, Ansoft Designer version 3.5.

BIOGRAPHY

Name-Surname: Funda Cırık

Birth place and date: Karabük, 16.09.1987

Graduated University: Kocaeli Üniversitesi, Elektronik ve Haberleşme Mühendisliği Bölümü, 2010.